Distribution Agreement

In presenting this thesis or dissertation as a partial fulfillment of the requirements for an advanced degree from Emory University, I hereby grant to Emory University and its agents the non-exclusive license to archive, make accessible, and display my thesis or dissertation in whole or in part in all forms of media, now or hereafter known, including display on the world wide web. I understand that I may select some access restrictions as part of the online submission of this thesis or dissertation. I retain all ownership rights to the copyright of the thesis or dissertation. I also retain the right to use in future works (such as articles or books) all or part of this thesis or dissertation.

Signature:

_____ _____

Eric H. Armstrong Date

The Role of Fatty Acid Binding Protein 5 (FABP5) in Peroxisome Proliferator-Activated Receptor β/δ (PPARβ/δ)-Mediated Fatty Acid and Retinoic Acid Signaling: A Structural Perspective

By

Eric H. Armstrong
Doctor of Philosophy

Graduate Division of Biological and Biomedical Science
Molecular and Systems Pharmacology

_____

Eric A. Ortlund, Ph.D.
Advisor

_____

Christine M. Dunham, Ph.D.
Committee Member

_____

Edward T. Morgan, Ph.D.
Committee Member

_____

T.J. Murphy, Ph.D.
Committee Member

Accepted:

_____

Lisa A. Tedesco, Ph.D.
Dean of the James T. Laney School of Graduate Studies

_____

Date

The Role of Fatty Acid Binding Protein 5 (FABP5) in Peroxisome Proliferator-Activated Receptor β/δ (PPARβ/δ)-Mediated Fatty Acid and Retinoic Acid Signaling: A Structural Perspective

By

Eric H. Armstrong
B. S., Vanderbilt University, 2007

Advisor: Eric A. Ortlund, Ph.D.

An abstract of
A dissertation submitted to the Faculty of the
James T. Laney School of Graduate Studies of Emory University
in partial fulfillment of the requirements for the degree of
Doctor of Philosophy

Graduate Division of Biological and Biomedical Science
Molecular and Systems Pharmacology
2014

Abstract

The fatty acid binding proteins (FABPs) are a group of intracellular lipid-binding proteins (iLBPs) found throughout the animal kingdom, nine of which have been characterized in mammals, including humans. Consisting of a 10-stranded β-barrel capped by two α-helices, these ~15 kDa calycins were initially believed to assist in the solubilization of their lipid ligands. More recent studies, however, have expanded the role of certain FABPs as specific mediators of vital signaling pathways. FABP5, like its family members, displays a promiscuous binding profile, being able to form a complex with numerous long chain fatty acids of varying degrees of saturation, as well as fatty acid metabolites, retinoids, and synthetic probes and drugs. Interestingly, only a portion of those tested, such as the ω-6 polyunsaturated linoleic acid and the Vitamin A metabolite all-*trans* retinoic acid (atRA), had been demonstrated as "activators," whose binding results in the protein's translocation from the cytoplasm to the nucleus, where it is then able to deliver its cargo to the nuclear peroxisome proliferator-activated receptor β/δ (PPARβ/δ), thereby enhancing the receptor's target gene transcription. However, the molecular mechanisms underlying both FABP5's nuclear import as well as its activating ligand selectivity remained unclear.

The work contained herein has established the existence of a tertiary nuclear localization signal (NLS) located within the α-helical cap of FABP5. Formation of the NLS has been found to be dependent upon the interplay between the protein's α2 helix and β2 loop. These dynamics are in turn governed by the conformation of complexed fatty acid, in which a higher degree of alkyl tail curvature within the protein's binding pocket results in FABP5's adoption of the activated state. This model implicates *cis* bonded polyunsaturated fatty acids as an entire class of potential FABP5 activating ligands. In contrast, the highly planar atRA was not found to bind appreciably to either FABP5 or PPARβ/δ *in vitro*. Thus, it is proposed that one or more of RA's *cis* isomers might actually be responsible for the FABP5, PPARβ/δ-mediated retinoid signaling pathway.

The Role of Fatty Acid Binding Protein 5 (FABP5) in Peroxisome Proliferator-Activated Receptor β/δ (PPARβ/δ)-Mediated Fatty Acid and Retinoic Acid Signaling: A Structural Perspective

By

Eric H. Armstrong
B. S., Vanderbilt University, 2007

Advisor: Eric A. Ortlund, Ph.D.

A dissertation submitted to the Faculty of the
James T. Laney School of Graduate Studies of Emory University
in partial fulfillment of the requirements for the degree of
Doctor of Philosophy

Graduate Division of Biological and Biomedical Science
Molecular and Systems Pharmacology
2014

Acknowledgements

If the pursuit of postgraduate education can be compared to a race, the Ph.D. is most certainly a marathon. As a longtime sufferer of asthma, I can say with confidence that there are those without whom I would not have been able to cross the finish line.

To my parents and in-laws, thank you for the words of encouragement, and frequent reminders to eat. Frances, it was easy to do so when the meals came from your kitchen. Kurt, having someone else around who had gone through the process was invaluable. Thank you for never offering an opinion unless it was asked for, but always having a pertinent story to share, all with the lesson that getting a Ph.D. is hard. Misery loves company, but it also loves validation. Mom and Dad, thank you for the assurance that tomorrow is a new day.

To my recently graduated friends in the Neuroscience program, thank you for keeping research fresh, exciting, and full of promise…and also for the beer.

To the fellow graduate students, post-docs, and former lab technician of the Ortlund Lab, I count myself fortunate that even when the work itself was not going well, it was at least carried out in the company of friends.

Many, many words of thanks and appreciation to my patient and faithful committee. T.J., I still remember our ligand binding study discussion, which gave me the needed confidence that I was in the right, but also the direction to take to be absolutely sure. Eddie and Christine, thank you for always going through my data with a fine toothed comb- from my first committee report to my dissertation, you have both assured that the conclusions that I have drawn are the correct ones. Eric, thank you for taking a chance on me. Whether it was inviting me aboard after my sixth rotation, or sending me

on the trip to Cleveland that actually changed everything, or accommodating my less than ideal graduation timeline, you have proven to be both a great scientist and mentor, and will always have my utmost gratitude and respect.

Finally, Kate, you have been running alongside me since the very beginning, and have helped me see it through to the end. I am just as honored today as I was four years ago when we made our team official, and I can’t wait to continue running with you to see what lies beyond the next horizon.

Table of Contents

Figure Index

Table Index

List of Abbreviations

(±)8-HEPE: 8-hydroxyeicosapentaenoic acid
1,8-ANS: 1-anilinonaphthalene-8-sulfonic acid
2-AG: 2-arachidonoylglycerol
2-AGE: 2-arachidonyl glyceryl ether
4-HDHA: 4-hydroxydocosahexaenoic acid
4-HNE: 4-hydroxynonenal
4-oxoDHA: 4-oxodocosahexaenoic acid
5-HEPA: 5-hydroxyeicosatetraenoic acid
6-oxoOTE: 6-oxooctadecatrienoic acid
8-(S)-HETE: 8-(S)-hydroxyeicosatetraenoic acid
9,13dcRA: 9,13-di-*cis*-retinoic acid
9-(S)-HODE: 9-(S)-hydroxyoctadecadienoic acid
11cRA: 11-*cis*-retinoic acid
11cRAL: 11-*cis*-retinal(dehyde)
13-(S)-HODE: 13-(S)-hydroxyoctadecadienoic acid
15-HETE: 15-hydroxyeicosatetraenoic acid
15-HETE-G: 15-hydroxyeicosatetraenoic acid glyceryl ester
15d-PGJ2: 15-deoxy-Δ-12,14-prostaglandin J2
16:0/18:1-GPC: 1-palmitoyl-2-oleoyl-sn-glycerol-3-phosphocholine
A-FABP: adipocyte fatty acid binding protein
AA: arachidonic acid
aa: amino acid
ABCA1: ATP-binding cassette transporter A1
ACBP: acyl-CoA-binding protein
ADH: alcohol dehydrogenase
AEA: *N*-arachidonoylethanolamine (anandamide)
AF: activation function
ALA: α-linoleic acid
ALBP: adipocyte lipid-binding protein
ALDH: aldehyde dehydrogenase
ANOVA: analysis of variance
atRA: all-*trans* retinoic acid
atRAL: all-*trans* retinal(dehyde)
atROH: all-*trans* retinol
B-FABP: brain fatty acid binding protein
BA: bile acid
BCMO1: β-carotene-15,15'-monooxygenase
BLBP: brain lipid-binding protein
BME: β-mercaptoethanol
BPL-B: brush-border phospholipase B
BS^3: bis(sulfosuccinimidyl)suberate
BSDL: bile-salt dependent lipase
CBD: cannabidiol
CD8: cluster of differentiation 8

CM: chylomicron
CMR: chylomicron remnant
CoA: coenzyme A
CRABP: cellular retinoic-acid binding protein
CRBP: cellular retinol-binding protein
CTE: C-terminal extension
D2R: dopamine receptor D_2
DAPI: 4'6-diamidino-2-phenylindole
DBD: DNA binding domain
DHA: docosahexaenoic acid
DMEM: Dulbecco's modified eagle medium
DMSO: dimethyl sulfoxide
DSm: double switch mutant
DTT: dithiothreitol
E: embryonic day
E-FABP: epidermal fatty acid binding protein
EGFP: enhanced green fluorescent protein
EPA: eicosapentanoic acid
ER: endoplasmic reticulum
EtOH: ethanol
FA: fatty acid
FABP: fatty acid binding protein
FAS: fatty acid synthase
FBS: fetal bovine serum
FDP: farnesyl diphosphate
FMP: farnesyl monophosphate
FPP: farnesyl pyrophosphate
gFABP: gut fatty acid binding protein
GnHCl: guanidinium hydrochloride
H: helix (α-helix)
H-FABP: heart fatty acid binding protein
hCRABP: human cellular retinoic acid-binding protein
HDX: hydrogen deuterium exchange mass spectroscopy
HEPES: 4-(2-hydroxyethyl)-1-piperazineethanesulfonic acid
HIC: hydrophobic interaction chromatography
hKPNA2: human karyopherin-α2
HNF: hepatic nuclear factor
HPLC: high-performance liquid chromatography
HSC: hepatic stellate cell
HSD: honestly significant difference
I-BABP: intestinal bile acid-binding protein
I-FABP: intestinal fatty acid binding protein
IBB: importin β binding domain
IPTG: isopropyl β-D-1-thiogalactopyranoside
IFN-γ: interferon γ
Il-FABP: ileal fatty acid binding protein

iLBP: intracellular lipid-binding protein
ILLBP: ileal lipid-binding protein
ITC: isothermal titration calorimetry
KFABP: keratinocyte-type fatty acid binding protein
L-FABP: liver fatty acid binding protein
LA: linoleic acid
LBD: ligand binding domain
LCFA: long-chain fatty acid
LCUFA: long-chain unsaturated fatty acid
LDL: low density lipoprotein
LPA: lysophosphatidic acid
LpL: lipoprotein lipase
LRAT: lecithin:retinol acetyltransferase
LRP: LDL-receptor related protein
M-FABP: muscle fatty acid binding protein OR myelin fatty acid binding protein
MA: myristic acid
MBP: maltose binding protein
MCFA: medium-chain fatty acid
MDGI: mammary-derived growth inhibitor
MDR: medium-chain dehydrogenase/reductase
MetS: metabolic syndrome
MW: molecular weight
N.D.: not detected
NADA: *N*-arachidonoyl-dopamine
NAE: N-acylethanolamine
NES: nuclear export signal
NESm: nuclear export signal mutant
NLS: nuclear localization signal
NLSm: nuclear localization signal mutant
NR: nuclear receptor
NTD: N-terminal domain
***O*-AEA**: *O*-arachidonoyl ethanolamine
OA: oleic acid
OD: optical density
OEA: oleoylethanolamide
PA: palmitic acid
PA-FABP: psoriasis associated-fatty acid binding protein
PAGE: polyacrylamide gel electrophoresis
PBS: phosphate buffered saline
PDB: protein data bank
PDK1: 3-phosphoinositide-dependent kinase 1
PEA: palmitoylethanolamide
PEG: polyethylene glycol
PEI: polyethlyenimine
PES: polyethersulfone
PGA1: prostaglandin A1

PGA2: prostaglandin A2
PGB2: prostaglandin B2
PGC1-α: PPARγ coactivator 1α
PGD2: prostaglandin D2
PGG2: prostaglandin G2
PGH1: prostaglandin H1
PGH2: prostaglandin H2
PGI2: prostaglandin I2 (prostacyclin)
PLRP-2: pancreatic lipase-related protein 2
PMP2: peripheral myelin protein 2
PoA: palmitoleic acid
PPAR: peroxisome proliferator-activated receptor
PPRE: PPAR response element
PTL: pancreatic triglyceride lipase
Pu: purine
PUFA: polyunsaturated fatty acid
RA: retinoic acid
RAR: retinoic acid receptor
RALDH: retinaldehyde dehydrogenase
RARE: RAR response element
RBP: retinol-binding protein
RDH: retinol dehydrogenase
RE: retinyl ester
REH: retinyl ester hydrolase
RMS: root mean square
ROH: retinol
ROR: RAR-related orphan receptor
RXR: retinoid X receptor
S: strand (β-strand)
SA: stearic acid
SCD: stearoyl-CoA desaturase
SCP-2: sterol carrier protein 2
SDR: short-chain dehydrogenase/reductase
SDS: sodium dodecylsulfate
S.E.: standard error
SER-CAT: Southeast Region Collaborative Access Team
SpA: sapienic acid
SR-BI: scavenger receptor class B, type I
SRP1p: yeast importin α
STRA6: stimulated by retinoic acid 6
SUMO: small ubiquitin-related modifier
T-FABP: testis fatty acid binding protein
TB: terrific broth
TEV: tobacco etch virus
TFA: trifluoroacetic acid
THC: tetrahydrocannabinol

TIF2: transcriptional mediators/intermediary factor 2
TLBP: testis lipid-binding protein
TNF-α: tumor necrosis factor α
TTR: transthyretin
VAD: vitamin A deficient
VLCFA: very long chain fatty acid
VLDL: very low-density lipoprotein
WT: wild type

CHAPTER 1 : GENERAL INTRODUCTION

1.1 Introduction

One of the most fundamental aspects of life is its ability to communicate. At the cellular and sub-cellular level, this is achieved with an interactive network of signaling pathways. The chemical messengers used in these pathways can be as simple as ions, or as intricate as entire protein complexes. Naturally, many of these messengers are hydrophilic, which enable them to diffuse freely throughout the aqueous environment of the cell. However, the water insolubility of numerous lipid signaling molecules is simply too great to allow their free-form presence in appreciable quantities within the cytosol. This is certainly the case for two particular lipid subsets, the long-chain fatty acids (LCFAs) and retinoids, a problem which nature has seen fit to address with the intracellular lipid binding proteins (iLBPs).

1.1.1 Intracellular Lipid Binding Proteins

The iLBPs, along with the avidins and lipocalins, form one of the three major branches which constitute the calycin superfamily of proteins (1; 2). Their presence within numerous multi-cellular eukaryotes throughout the animal kingdom points to their ancient origin, with the first iLBP gene duplication event believed to have occurred ~ 930 million years ago (3-5). Such an ample window of time has since allowed for considerable diversification. Currently, there are 15 known orthologs in humans, which fall into two main groups: the retinoid binding proteins and the fatty acid binding proteins (FABPs) (5). Their corresponding genes are found over nine different chromosomes, and exist as four exons alternating with three introns, a format common to all vertebrate iLBPs (Table 1-1) (5). Each member exhibits unique tissue specific expression levels,

	Other Names	Tissue/Cell Expression	Known Ligands	Gene Locus	Length (aas)
CRABP-I	RBP5	Ubiquitous: esp. in brain, skin, and testis	atRA	15q24	137
CRABP-II	RBP6	Skin, mammary glands, uterus, kidneys, prostate, olfactory epithelium	atRA	1q21.3	138
CRBP-I	RBP1	Ubiquitous: brain, spinal cord, heart, colon, bladder, uterus, prostate, stomach, testis, ovaries, pancreas, adrenal glands, thyroid, mammary glands, kidneys, liver, small intestine, spleen, lymph nodes, appendix, lungs, trachea, placenta	atROH	3q23	135
CRBP-II	RBP2	Small intestine, kidneys	atROH, atRAL	3q23	134
CRBP-III	RBP5, HRBPiso	Kidneys, liver, spleen, lymph nodes, appendix	atROH	12pter-p13.31	135
CRBP-IV	RBP7	Ubiquitous: brain, heart, esophagus, stomach, small intestine, appendix, colon, rectum, kidneys, skeletal muscle, spleen, thymus, lymph nodes, bone marrow, trachea, lung, placenta, bladder, uterus, prostate, testis, ovaries, liver, pancreas, adrenal glands, salivary glands	atROH	1p36.22	134
FABP1	Liver FABP (L-FABP), Z protein, Hepatic FABP, Heme-binding protein	Liver, intestine, pancreas, kidneys, lungs, stomach	LCFAs, acyl-CoA, eicosanoids, lysophospholipids bilirubin, bile salts, cholesterol, heme	2p11	127
FABP2	Intestinal FABP (I-FABP), Gut FABP (gFABP)	Intestine, liver	LCFAs	4q28-q31	132
FABP3	Heart FABP (H-FABP), Muscle FABP (M-FABP), Mammary-derived growth inhibitor (MDGI), O-FABP, FABP11	Cardiac muscle, skeletal muscle, brain, kidneys, lung, stomach, testis, adrenal glands, mammary glands, placenta, ovaries, brown adipose tissue	LCFAs, non-prostenoid oxygenated fatty acids	1p33-p32	133

FABP4	Adipocyte FABP (A-FABP), aP2, ALBP	Adipose tissue, macrophages, dendritic cells, skeletal muscle	LCFAs, atRA, 4-hydroxynonenal (4-HNE)	8q21	132
FABP5	Epidermal FABP (E-FABP), Keratinocyte-type FABP (KFABP), Psoriasis-associated-FABP (PA-FABP)	Ubiquitous: skin, tongue, adipose, macrophages, dendritic cells, mammary glands, brain, stomach, intestine, kidneys, liver, lungs, heart, skeletal muscle, testis, retina, lens, spleen, placenta	LCFAs, medium-chain fatty acids (MCFAs), eicosanoids, 4-HNE, endocannabinoids atRA?	8q21.13	135
FABP6	Ileal FABP (Il-FABP), Ileal lipid-binding protein (ILLBP), Intestinal bile acid-binding protein (I-BABP), Gastrophin	Ileum, ovaries, adrenal glands, stomach	LCFAs, bile acids (BAs)	5q33.3-q34	128
FABP7	Brain FABP (B-FABP), Brain lipid-binding protein (BLBP), MRG	Brain, retina, mammary glands	LCFAs, very long chain fatty acids (VLCFAs), endocannabinoids ?	6q22-q23	132
FABP8	Myelin FABP (M-FABP), Peripheral myelin protein 2 (PMP2)	Peripheral nervous system, Schwann cells	LCFAs, cholesterol?	8q21.3-q22.1	132
FABP9	Testis FABP (T-FABP), Testis lipid-binding protein (TLBP), PERF, PERF 15	Testis, salivary glands, mammary glands	LCFAs?	8q21.13	132

1-1. Common characteristics of the iLBPs

protein-protein interactions and ligand binding abilities, with the family as a whole displaying a wide range of amino acid sequence identity (20-77% for humans) (Table 1-2) (5-10).

Multiple sequence alignment as well as phylogenetic analysis of iLBPs across species results in a clustering of the proteins into four subfamilies that reflect their ligand preferences (8; 11). Subfamily I is composed of the retinoid binding proteins - cellular retinoic acid-binding proteins (CRABP) I and II and cellular retinol-binding proteins (CRBP) I-IV, which bind their eponymous ligands with both high selectivity and affinity (9; 10; 12; 13). Subfamilies II-IV lie within the FABP group, with subfamily II comprised of FABPs 1 and 6, which in addition to LCFAs are able to form complexes with bulkier ligands such as bile salts, cholesterol, bilirubin, and heme (14-16). FABP2 is the lone constituent of subfamily III, due to its inability to bind ligands other than LCFAs, while FABPs 3-5, and 7-9 together form subfamily IV, characterized by its members' overall promiscuity in binding fatty acids of more variable length in addition to various FA metabolites and retinoids (Table 1-1) (5; 6; 8; 17; 18).

Despite such broad phylogeny, sequence similarity, and ligand binding capability, all iLBPs share a remarkably similar tertiary structure (11). Every member adopts a fold consisting of 10 β-strands, forming two five-stranded β-sheets positioned nearly at right angles to each other. All strands are connected by turns, with the exception of strands A and B, in between which a helix-turn-helix, or Schellman, motif lies, and strands G and H, whose turn is substituted by an Ω loop (19) that varies in length. The orthogonally oriented β-sheets are in close proximity at the end of the protein opposite to the Schellman motif, in effect creating a variation of a β-barrel known as a β-clam. Inter-

	CRABP I	CRABP II	CRBP I	CRBP II	CRBP III	CRBP IV	FABP 1	FABP 2	FABP 3	FABP 4	FABP 5	FABP 6	FABP 7	FABP 8
CRABP I														
CRABP II	77.2													
CRBP I	40.8	44.6												
CRBP II	36.2	39.2	54.9											
CRBP III	35.4	39.2	55.2	50.4										
CRBP IV	36.9	40.0	56.4	58.7	48.9									
FABP 1	29.4	31.0	26.4	29.6	24.0	28.0								
FABP 2	30.5	28.2	28.7	24.8	20.2	23.3	20.6							
FABP 3	42.3	42.3	32.6	39.7	34.9	38.2	28.0	31.0						
FABP 4	39.2	37.7	35.1	38.2	28.2	38.9	24.0	31.8	64.1					
FABP 5	36.9	33.1	28.8	25.2	28.8	28.2	23.2	24.8	49.2	52.7				
FABP 6	25.6	28.0	26.4	31.5	25.6	25.0	36.8	24.8	27.2	26.6	21.6			
FABP 7	39.2	40.8	38.2	36.6	26.7	37.4	30.4	33.3	66.4	56.5	45.0	25.0		
FABP 8	43.1	39.2	36.6	35.1	34.4	37.4	24.8	28.7	62.6	66.4	56.5	21.0	58.8	
FABP 9	37.7	36.2	33.6	35.1	30.5	37.4	24.0	27.9	55.0	63.4	51.2	21.0	52.7	67.2

1-2. Amino acid identity percentages of the human iLBPs

strand hydrogen bonding helps to maintain overall shape, which is aided by ordered waters that fill the conserved gap between strands D and E (20). Together, the β2 and β4 turns and the α helical cap constitute the portal domain, whereby ligand is hypothesized to enter the ~1200 $Å^3$ interior (Figure 1-1) (21). In the case of FAs and all-*trans* retinoic acid (atRA), an active metabolite of all-*trans* retinol (atROH, Vitamin A), binding occurs via hydrogen bond coordination between the ligands' carboxylic acid headgroup and Arg-112, Arg-133, and Tyr-135 (hCRABP-II numbering), a trio of amino acids conserved in all CRABPs and FABPs, while the ligands' lipophilic carbon tails engage in hydrophobic interactions with a variety of non-polar residues within the binding pocket (11; 22).

Although such binding does result in ligand solubilization, the role of iLBPs has steadily grown from that of indistinct lipid shuttlers to critical components of specific signaling pathways (6). In general, this is accomplished in one of two ways. The first, and more indirect, is by iLBP presentation of its cargo to metabolic enzymes, allowing for the enhanced formation of a metabolite which is necessary for propagation of a particular signal (7; 23). The second, more direct method is through the ability of certain iLBPs to facilitate the activation of two families of nuclear receptors, the retinoic acid receptors (RAR) and the peroxisome proliferator-activated receptors (PPAR) (24-26). It is the purpose of this chapter to provide an overview of iLBP-mediated atRA and LCFA nuclear receptor signaling through the lens of the CRABP-II-RAR and FABP5-PPARβ/δ pathways.

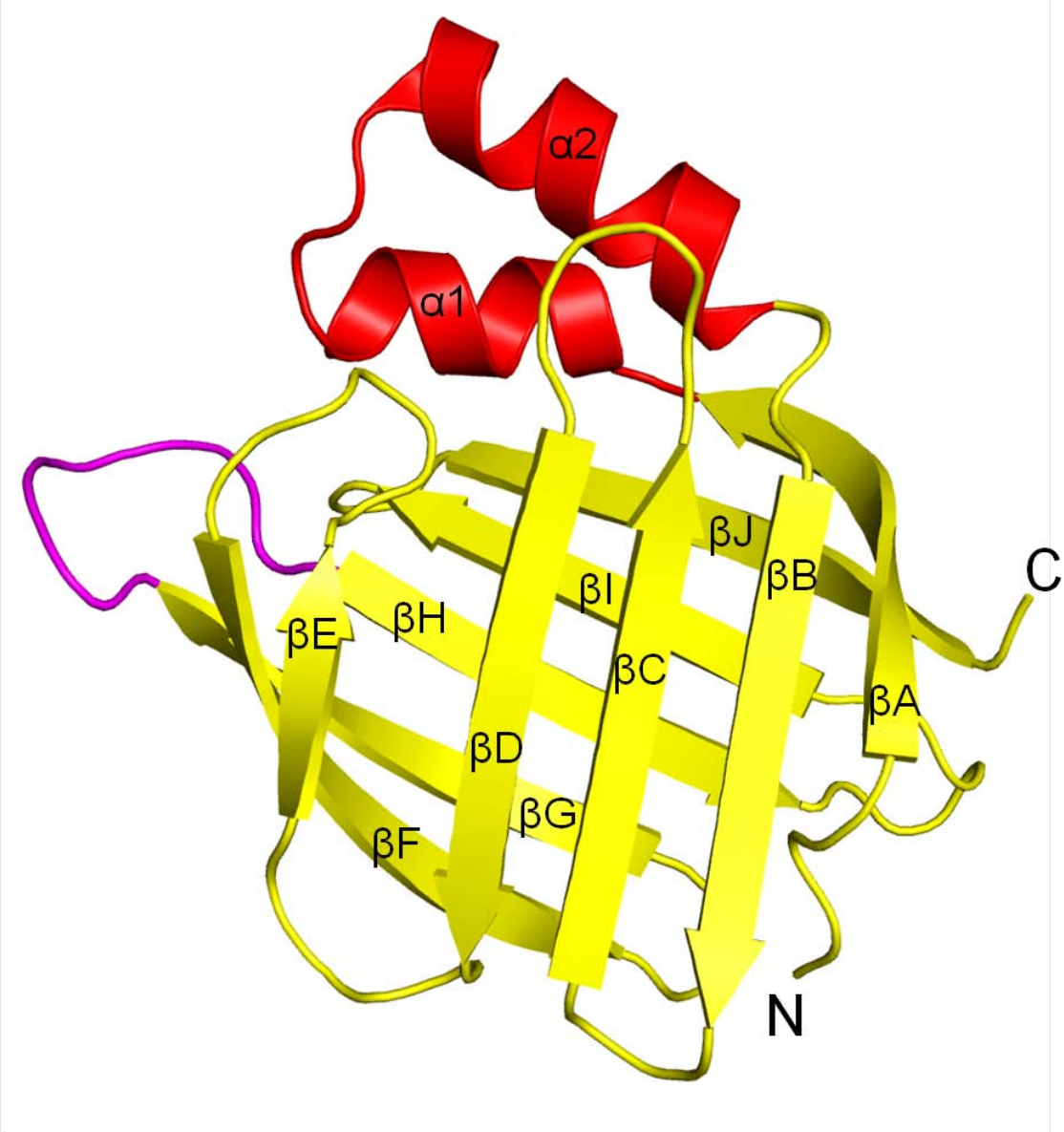

1-1. Representative three dimensional structure of the iLBP protein family

CRABP-II (PDB code: 2FR3) (27) adopts the classic iLBP tertiary fold of a β-clam (yellow) capped by a Schellman motif (red) and harboring an Ω-loop (purple) between its G and H β-strands. The ordered waters necessary for hydrogen bonding between βD and βE are not shown.

1.2 The CRABP-II-RAR Signaling Pathway

1.2.1 Metabolism of Vitamin A

Vitamin A was first discovered and recognized as being necessary for growth in 1913 by McCollum and Davis (28). In the century that has followed, research has dramatically expanded its importance. Today, it is known as a vital nutrient for vertebrates as well as tunicates and lancelets, playing a role throughout the chordate life cycle from embryogenesis and development, to tissue regulation, vision, circadian clock entrainment, immune response, and reproduction (23; 24). However most, if not all, of these functions are not the direct result of the parent molecule itself, but rather its numerous retinoid metabolites produced across multiple cell types. The three best characterized of these are 11-*cis* retinal (11cRAL), all-*trans* retinal (atRAL) and atRA (Figure 1-2). The retinal isomers have long been recognized as the chromophores used by the opsin protein family for photon signal transduction, with several decades having passed since they were first implicated in processes ranging from vision in animals (29) to phototaxis in algae (30) and energy production in Archaea (31). Though relatively newer advances in the field have even further expanded the use of these chromophores to bacteria (32), this large and active field of study ultimately lies outside the scope of this review. Instead, we will focus on Vitamin A's eventual conversion to atRA, the metabolite responsible for retinoid signaling at the gene transcription level via activation of the RARs (Figure 1-3).

The retinoid parent atROH is composed of four isoprene units joined head to tail, and possesses three major domains: a β-ionone ring, a polyene side chain, and a primary alcohol functional group (Figure 1-2). The conjugated five carbon-carbon double bond

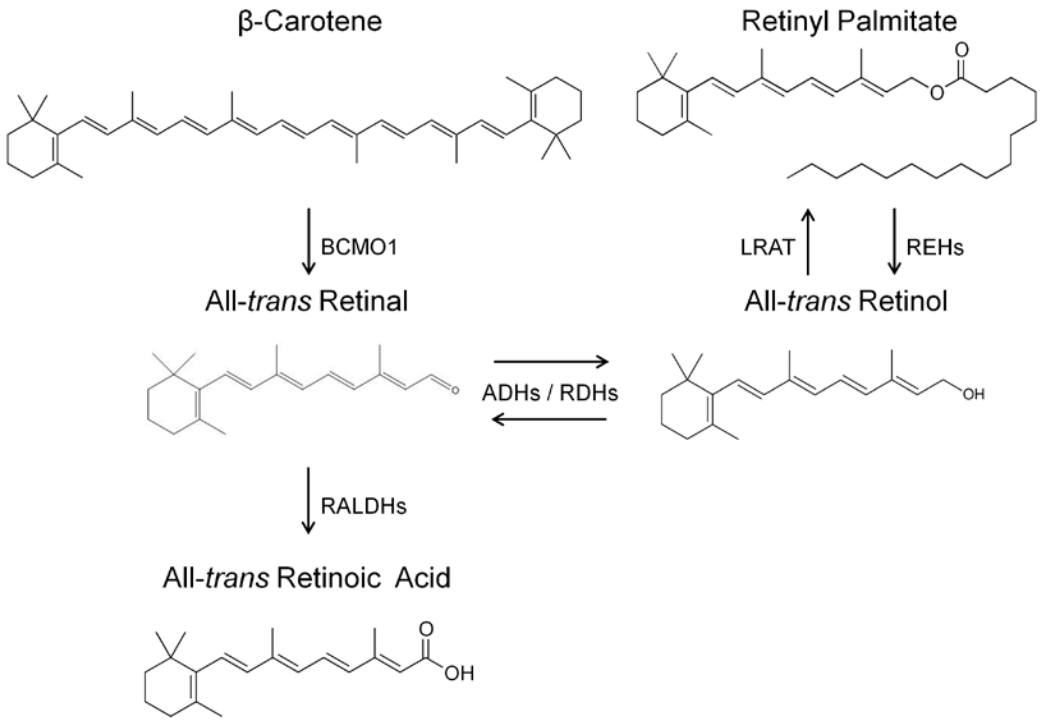

1-2. Common metabolites along the atRA synthesis pathway

Animals must obtain atRA from their diet, the majority of which is in the form of carotenoid (plant) or retinyl ester (animals) precursors. Arrows that point in opposite directions indicate reversible reactions. BCMO1: β-carotene-15,15'-monooxygenase (the second atRAL generated is not shown), LRAT: lecithin:retinol acetyltransferase, REH: retinyl ester hydrolase, ADH: alcohol dehydrogenase, RDH: retinol dehydrogenase, RALDH: retinaldehyde dehydrogenase

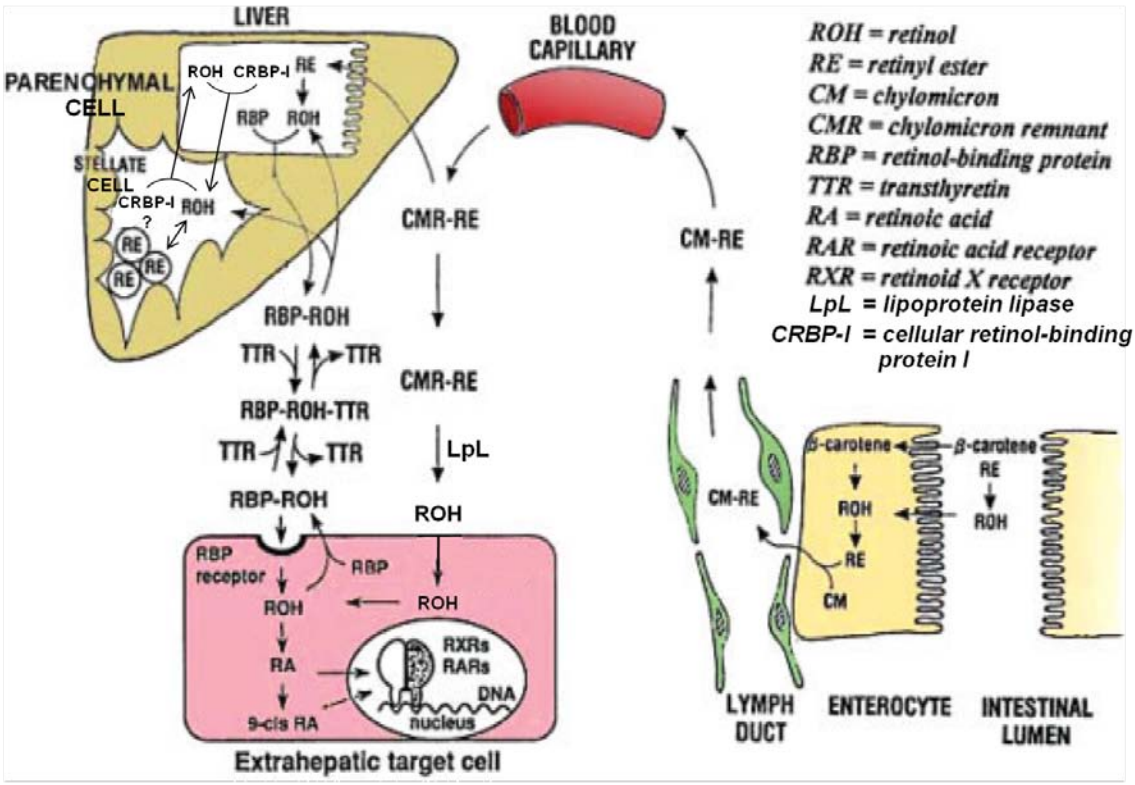

1-3. Schematic of atRA metabolism from ingestion to RAR activation

Cells throughout the body can receive Vitamin A in several fashions, such as in the form of retinyl esters attached to chylomicron remnants, or as retinol bound to RBP. The much smaller presence of atRA bound to plasma albumin is not shown. Figure is adapted with permission from: Blomhoff R, Blomhoff HK. 2006. Overview of retinoid metabolism and function. *Journal of neurobiology* 66:606-30

system within the acyclic portion of atROH underlies the molecule's extreme sensitivity to both light and oxidation. Consequently, very little of Vitamin A and its metabolites are found in their free form within the body, instead being bound to proteins that offer both increased solubility and protection (7; 22; 23; 33; 34).

Animals are unable to synthesize atROH *de novo*; therefore, they must acquire it from their diet. Plants, algae, fungi, and some bacteria produce a class of compounds called carotenoids, which are largely responsible for the red, orange, yellow, and purple pigmentation observed within these organisms (35). Their consumption exposes animals to these carotenoids, three of which, α-carotene, β-carotene (Figure 1-2), and β-cryptoxanthin, are well-characterized proretinoids. Alternatively, animals' consumption of other animals gives them access to the stored Vitamin A in their tissues, often in the form of retinyl esters such as retinyl-palmitate (Figure 1-2), stearate, oleate, or linoleate (36). Regardless of exposure method, retinoid metabolism largely begins in the proximal section of the small intestine, with important processes occurring both within the lumen and intestinal walls (37-40). Carotenoids undergo scavenger receptor class B, type I (SR-BI)-mediated uptake into the enterocyte (41-45), where the proretinoids are then symmetrically cleaved at the double bond located centrally within their polyene linker by β-carotene-15,15'-monooxygenase (BCMO1) (46-50), yielding either one (in the case of α-carotene and β-cryptoxanthin) or two (in the case of β-carotene) molecules of atRAL. This is in contrast to the retinyl esters, whose hydrolysis to atROH and LCFA in the lumen by pancreatic triglyceride lipase (PTL) (51) and pancreatic lipase-related protein 2 (PLRP2) (52), and in the brush border by brush-border phospholipase B (BPL-B) (53), must occur prior to retinoid absorption by the enterocyte. In both cases, however, the

small intestine-specific iLBP CRBP-II binds and solubilizes the retinoid products, allowing atRAL to be converted to atROH by reductases before delivering its Vitamin A cargo to lecithin:retinol acetyltransferase (LRAT) (54), where it is re-esterified and packaged into nascent chylomicrons for distribution throughout the organism (55). In this way, CRBP-II is important for optimizing retinoid absorption from the diet, and is crucial for survival of the fetus when retinoid conditions are limiting (56).

The nascent chylomicrons, semi-ordered apolipoprotein-containing lipid aggregates ranging from 100-2000 nm in diameter, are secreted from enterocytes into lacteals, lymphatic vessels that surround the small intestine (7; 57). From there, they are able to reach the general circulation, where they eventually mature via a combination of apolipoprotein exchange and lipoprotein lipase (LPL)-induced triglyceride hydrolysis (7; 23). The resulting chylomicron remnants, still containing a large majority of their retinyl esters (57), are one of the major avenues by which organs throughout the body are introduced to retinoid; nevertheless, the liver alone is able to clear up to three quarters of these remnants from the blood (58; 59). This is accomplished through hepatocyte uptake, which is itself coordinated by the binding of the remnants to low density lipoprotein (LDL) receptor, LDL-receptor related protein (LRP), or SR-BI on the hepatocyte cell surface prior to internalization (60; 61). Once inside, the retinyl esters undergo immediate hydrolysis by any of an array of enzymes broadly characterized as retinyl ester hydrolases (REHs), made up of constituents from either the carboxylesterase or lipase groups (62). A member of the latter, bile-salt dependent lipase (BSDL) has been shown to undergo enhanced activity in the presence of *apo* CRBP-I (63). This iLBP is thought to then be the principle vehicle of transfer for the atROH hydrolyzed product from

hepatocytes to the hepatic stellate cells (HSCs) (64). Once there, 50-80 % of total body retinol is stored in cytoplasmic lipid droplets as retinyl esters produced by *holo* CRBP-I-assisted LRAT esterification(65-67).

Hepatic storage and controlled release of atROH counteracts the natural, diet-induced fluctuations in retinoid exposure, resulting in a steady plasma retinol concentration of 1-2 μM (23). Expression of the lipocalin retinol binding-protein (RBP) is essential for mobilization of atROH from hepatocytes (68). Localized in the endoplasmic reticulum (ER) in its *apo* state, RBP translocates to the Golgi upon binding atROH, before being secreted into the circulation (69; 70). Mobilization of Vitamin A from HSCs is less well studied. Due to their lack of RBP expression (36), as well as their relatively small size and abundance within the liver as compared to hepatocytes (71-73), it is assumed that their hydrolyzed retinoid stores are first mobilized back to parenchymal liver cells prior to secretion (7), though the necessary transport protein(s) have not yet been elucidated. Once released, RBP-atROH associates with transthyretin (TTR) in a 1:1 ratio (74), forming a complex whose ~75 kDa size prevents glomerular filtration of plasma retinol (75).

Over 95 % of plasma retinol is bound to RBP in the fasting state (7; 76), although there are two other main methods of retinoid exposure whereby cells are able to obtain atRA. The most direct is via the assumed diffusion of atRA from the plasma, where it is bound to albumin at concentrations of 5-10 nM (77), through the phospholipid bilayer of the cell. The second, and primary exposure method in the post-prandial state, is through the retinyl ester chylomicron remnants that are able to bypass the liver (40). Although the extrahepatic tissue cells studied, with the exception of the placenta (78), have not been

shown to absorb the remnants in a lipoprotein receptor-mediated fashion, it is thought that LPL serves to adequately hydrolyze the remnant-associated retinyl esters, allowing for subsequent atROH passage through the plasma membrane (79; 80). In contrast, RBP-atROH binds stimulated by retinoic acid 6 (STRA6), a transmembrane RBP receptor present in many retinoid metabolizing tissues, whereby atROH is channeled from RBP directly into the cell (81). Interestingly, while influx of atROH from *holo* RBP via STRA6 is coupled strongly with intracellular LRAT and CRBP-I expression, efflux of the ligand to plasma *apo* RBP via STRA6 is coupled with intracellular CRBP-I and II (82).

Once inside the cell, the first step for the oxidation of atROH to atRA is retinol's conversion to atRAL. The two best characterized groups of enzymes responsible for this reversible reaction are the cytosolic alcohol dehydrogenases (ADHs) belonging to the medium-chain dehydrogenase/reductase superfamily (MDR), and the microsomal retinol dehydrogenases (RDHs) of the short-chain dehydrogenase/reductase superfamily (SDR) (83). While ADH1 and likely ADH2 are involved in liver retinol detoxification brought about by retinol excess (84; 85), ADH3 and 4 participate in the generation of atRA in various tissues (86), with both shown to be vital for the survival of newborn mice under Vitamin A-limiting conditions (87; 88). Similarly, the NAD^+ and $NADP^+$-dependent SDRs have been proven to play important roles in the visual cycle (RDH5, RDH12) (89-92), retinoid homeostasis (RDH1) (93), and embryogenesis (RDH10) (94). Although there is some evidence to suggest ligand shuttling between CRBP-I and the RDHs (33; 95; 96), all of these enzymes have been shown to bind both retinol and retinal in their free forms (97; 98), suggesting instead a role for CRBP-I in sequestering atROH from these oxidoreductases for esterification (83).

Finally, the irreversible oxidation of atRAL to atRA is catalyzed by a group within the aldehyde dehydrogenase (ALDH) family, the retinaldehyde dehydrogenases (RALDHs). Studies conducted at both the gene and protein levels as well as knockout mouse models for each have yielded a wealth of information regarding the function of these enzymes, and their retinoid product, throughout the animal's lifespan (99). *Raldh1*, first expressed in the dorsal retina of the embryo (100; 101), is found throughout epithelial tissues in the adult, and is especially present in the liver (102), where it is postulated to work in concert with ADH1 to prevent hepatic retinol toxicity (99; 103). RALDH2 is the first of the enzyme group to be expressed; consequently, it is the sole source for atRA signaling from embryonic day (E) 7.5-E8.5, and its absence in the *Raldh2*$^{-/-}$ mouse line is devastating, halting development of the embryo at E8.75, with death occurring by E9.5-E10.5 (104; 105). Expression of *Raldh3* begins in the optic vesicle and nasal placode, later moving to the ventral retina, nasal pit, otic vesicle, and mesonephros, and at last to the ventral telencephalon (106; 107). While *Raldh3*$^{-/-}$ fetuses do not seem to bear any striking external defects, this belies defects of their forebrain (108), eyes (109; 110), kidneys (111), and nasal passages, the latter of which results in death soon after birth (112). While these observations of the single gene knockouts have illuminated the intricate spatial and temporal profile of atRA within RALDH-expressing tissues, the *Raldh1*$^{-/-}$, *Raldh3*$^{-/-}$ mouse line has also revealed the molecule's paracrine signaling ability during embryogenesis (109; 110). Together, these investigations of the RALDHs provide direct and elegant affirmation of atRA's role as a powerful morphogen whose levels must also be tightly regulated into adulthood.

1.2.2 The Retinoic Acid Receptors

Though the far-reaching effects of Vitamin A had been well documented, largely through observation of the consequences of its deficiency in both animals and humans, it was not until 1960 that Dowling and Wald (113), building off of previous research conducted by Arens and Van Dorp (114-116), characterized the ability of retinoic acid to ameliorate all non-retina pathologies in Vitamin A deficient (VAD) rats. Study of the "wider and wholly obscure phenomena" (113) attributed to atRA took a quantum leap forward with the joint discovery of the first retinoic acid receptor in 1987 (117; 118). In the 25 years since, the atRA and 9-*cis* retinoic acid (9cRA)-binding family has expanded to include three isotypes, RAR α, β, and γ, each encoded by separate genes (119). RARs belong to class II of the superfamily of ligand regulated transcription factors known as nuclear receptors (NRs). As such, their functional unit consists of a heterodimer with the 9cRA-binding nuclear receptor, retinoid X receptor (RXR), with the complex thought to remain bound to nuclear DNA, where it forgoes transcription of target genes in the absence of activation by the retinoic acid isomers (120; 121). Although both receptors are able to bind 9cRA, the importance of atRA cannot be understated, since RXR has been shown to play a subordinate role in complex activation (122), and the extremely chemically sensitive 9cRA is only detectable in low amounts in limited cell types (123), making the status of this elusive isomer as an endogenous ligand for either receptor an ongoing matter of debate (124; 125).

RARs adopt the modular structure characteristic of nuclear receptors, consisting of six regions, labeled A-F, that exhibit homology at the tertiary and functional levels (Figure 1-4) (121; 125). Region E, also known as the ligand binding domain (LBD),

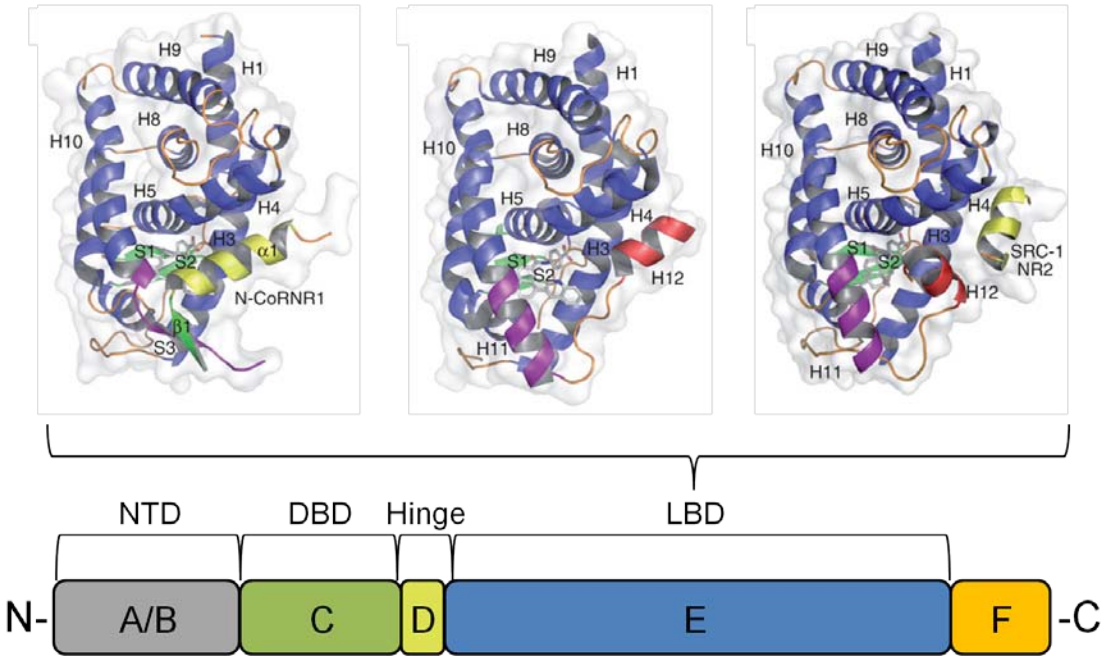

1-4. RARs assume the multidomain structure common to all nuclear receptors

Shown at bottom is a representation of the primary amino acid sequence of RARα1, with the delineation of functional tertiary domains drawn to scale. The ligand binding domain of RARα in three separate activation states is displayed at top. In the proposed *apo* intermediate state, H12 (red) occupies the co-regulator binding cleft, a conformation that can be stabilized by a synthetic antagonist (PDB code: 1DKF). When bound to an agonist, movement of H12 enables the receptor LBD to form a complex with the SRC-1 NR2 co-activator peptide fragment (right, PDB code: 3KMR). Binding of an inverse agonist drives the LBD into its fully inactivated conformation (left), with disorder in H12 and the transition of H11 to a β-strand (S3) providing the necessary space and topography for complex formation with the extended motif of the N-CoRNR1 co-repressor peptide fragment (yellow) (PDB code: 3KMZ). Figure is adapted with permission from: le Maire A, Teyssier C, Erb C, Grimaldi M, Alvarez S, et al. 2010. A unique secondary-structure switch controls constitutive gene repression by retinoic acid receptor. *Nature structural & molecular biology* 17:801-7.

assumes the familiar globular motif observed in all NR LBDs that have been crystallized to date: 12 α-helices, the first 11 of which arranged are in three antiparallel sheets, commonly referred to as an α-helical sandwich. When bound to an agonist such as atRA, the highly flexible helix 12, also known as the activation function 2 (AF-2) helix, packs up against the LBD, where it is stabilized by helices 3 and 4 (126). This creates a hydrophobic cleft on the LBD's surface suitable in size for binding to the LxxLL-interaction motifs of various coactivator proteins, which in turn leads to recruitment of the transcriptional machinery (125). Although no published *apo* RAR structures currently exist, it is believed that in the absence of ligand, AF-2 displaces the LxxLL motif within the cleft, leading to release of coactivator, a conformational state that can be stabilized by synthetic antagonists (127). Intriguingly, the LBD of RARα has been shown to form an additional, more explicitly repressive conformation that can be stabilized by synthetic inverse agonists. This is accomplished by the transition of AF-2 to a more disordered state located farther from the helical sandwich, enlarging the surface pocket that is now only enclosed by helices 3 and 4, while simultaneously destroying the charge clamp that helped to secure the LxxLL helical motif in place (127). Coactivator protein is then released, with the cleft now able to bind the extended motifs of corepressors (128; 129), which serve as the scaffolds for the protein complexes responsible for remodeling of chromatin into its more condensed, transcriptionally hindered state (125). Assays conducted *in vitro* correlate these structural conclusions, with RARα shown to be far more capable of binding to corepressors than either RARβ or RARγ in the absence of ligand (130-132).

RARs interact with DNA through region C, appropriately termed the DNA binding domain (DBD). It consists of two non-equivalent zinc-fingers, two α-helices oriented perpendicular to each other, and a C-terminal extension (CTE) (125). While the more C-terminal helix (helix 2) stabilizes overall protein structure, helix 1 makes base-specific contacts within the major groove of the DNA strand (121). RARs bind with RXRs as asymmetrically-oriented heterodimers to RA response elements (RAREs), which are composed of direct repeats of the PuG(G/T)TCA core sequence (125). In the classical RAREs, these repeats are separated by 5 bp (DR5), and have been found in the promoter regions of genes encoding CYP26A1 (an atRA oxidizing enzyme) (133), several homeodomain and hepatic nuclear factor (HNF) proteins (transcription factors essential for embryogenesis and metabolic homeostasis, respectively) (134; 135), and the RARβ2 isoform (136). The discovery of additional DR2 and DR1 RAREs has further expanded the RAR target gene repertoire to include CRBPs I (137) and II (138), while providing proof of alternate binding modes between the RAR-RXR heterodimer and DNA (139; 140) that affect corepressor association and receptor activation (141).

The remaining regions of RAR, as with all other NRs, are thought to be naturally disordered, yet undoubtedly functional (125). Regions A and B together comprise the N-terminal domain (NTD). Region A is poorly conserved across isotypes, and indeed its various truncations due to differential promoter usage and alternative splicing results in the formation of the eight major isoforms (α1-2, β1-4, γ1-2) (119). Additionally, region A/B serves as the activation function 1 (AF-1), due to its involvement in ligand-independent modulation of receptor-driven gene transcription, likely via protein-protein interaction governed by post-translational modifications (119; 125; 141). The hinge

region (region D) connecting the DNA and ligand binding domains, in addition to harboring nuclear localization signals, provides the conformational flexibility necessary for the DBD rotation relative to LBD required in RAR-RXR heterodimer binding to DR1 RAREs vs. DR 2 and 5 RAREs (125). The final region, F, is not found within all NRs, and its length and sequence are variable even within the RAR family (125). However, it is known to be phosphorylated in various positions (142; 143), is capable of binding mRNA (144), and has been proposed in RARα to stabilize H12 when the receptor is unbound to ligand (145), providing an additional driving force for heightened RARα repression.

The high degree of conservation among orthologs, combined with their unique expression profile in both the embryo and adult, led Chambon et al. to first propose over 20 years ago that the RAR isotypes could perform separate functions (146). As with the atROH and atRAL oxidizing enzymes, studies conducted with knockout mouse models have proven indispensable in validation of this hypothesis. In general, RARα is expressed ubiquitously, while RARβ and RARγ are confined to select cell types (147). *Rara*-, *Rarb*-, and *Rarg*-null mutants all survive into adulthood with overlapping abnormalities, while *Rara/b*, *Rara/g*, and *Rarb/g* double knockouts die *in utero* or at birth, reflecting a degree of functional redundancy between the RAR isotypes (122). Nevertheless, the results of numerous subtly different experiments together have provided an expansive body of nuanced data necessary to isolate the specific isotype primarily responsible for a particular facet of organogenesis. RARα largely governs heart, urogenital, and respiratory system formation, while RARγ signaling drives skeletal and ocular development, with RARβ playing an important secondary role in the latter (122). Viability of single RAR

isotype knockout mice, in combination with the development of spatio-temporally controlled somatic mutagenesis of RAR isotypes, has expanded our knowledge of RAR signaling to the adult as well (148). Target gene transcription or active repression by agonist-bound or *apo* RARα, respectively, has been found to either drive or prevent differentiation of myeloblasts into neutrophils (149). Both RARα and RARβ have been shown to contribute to neurotransmission in the striatum through their transcriptional regulation of the dopamine receptor D_2 (D2R) (150). RARγ signaling regulates the maintenance of the hematopoietic stem cell pool in the bone marrow (151) and is required for CD8+ T cell and macrophage response and cytotoxicity (152; 153), while the receptor's presence in suprabasal keratinocytes is involved in atRA-induced hyperproliferation of basal layer keratinocytes via paracrine signaling (154). Finally, the intricacies of RAR function are further magnified in light of the fact that its physiological partner, RXR, is also expressed as three distinct isotypes (α, β, and γ), consisting of two isoforms each. In effect, this could result in up to 48 different heterodimers with which to transduce the atRA signal (119).

1.2.3 Cellular Retinoic Acid-Binding Protein II

Interestingly, it was during the search for the retinoid binding nuclear receptors in the 1970s that the presence of ~15 kDa cytoplasmic retinoic acid binding proteins was first discovered (155; 156). Within four years of discovery, CRABP-I had been specifically purified and partly characterized (12; 157), with CRABP-II following a decade later (13). As previously mentioned, both proteins adopt the characteristic iLBP fold, and bind with a high preference to atRA. The ligand affinity of CRABP-I is approximately five times higher than that for CRABP-II (158), which results in CRABP-

I's ability to sequester atRA from CRABP-II in purified protein preparations and likely *in vivo* (159; 160). This is surprising from a structural perspective, as the proteins share a high level of similarity within their binding cavities. Both harbor a water accessible volume of ~280 $Å^3$ that is more than sufficient to accommodate the ~15 Å long retinoid in a largely planar conformation, with the β-ionone double bond oriented nearly *cis* to the polyene chain and the carboxylic group rotated being the only substituent out of plane, by ~55° (161). However, it is hypothesized that the conserved substitutions of Met10→Ile10 and Phe123→Met124 from CRABP-I to CRABP-II drive slight differences in the conformation of Arg132/133 and Tyr134/135, which in turn alter hydrogen bonding with the carboxylate of the retinoid and result in ligand affinity reduction (161).

Expression of CRABP-II begins at the early stages of embryogenesis, being first detectable at E3 in the chick (162) and already present at maximum levels by E9.5 in the mouse (163). Its expression profile is unique from that of CRABP-I, both in terms of its spatiotemporal patterning and its upregulation in response to atRA (164), the result of DR1, DR2, and DR5 RAREs within its gene promoter region (165; 166). Though the mRNA transcripts from both are found to overlap to varying degrees across numerous embryonic tissues and regions, in general, CRABP-II expression is more widespread (167). This trend is reversed by adulthood, however, with the presence of CRABP-II found to be mainly limited to mammalian tissue systems that undergo continual differentiation and renewal, such as the epidermis (168), endometrium (169), corpus luteum (170), and olfactory epithelium (171).

The high level of CRABP interspecies amino acid sequence identity compared to that within the same species, in conjunction with their separate expression patterns, has

long suggested that these proteins serve distinct and evolutionarily conserved functions (172). Indeed, while it is largely agreed that CRABP-I facilitates the catabolism of atRA into various oxidized derivatives (172-175), CRABP-II has been shown to play an intermediary role in the atRA-RAR signaling pathway (Figure 1-5). Confined to the ER in its *apo* state, binding of atRA stabilizes CRABP-II's interaction with the small ubiquitin-related modifier (SUMO) E2 ligase Ubc9, which SUMOylates CRABP-II on Lys-102, thereby allowing for its release into the cytoplasm (176). Presumably, the same ligand-induced conformational shift responsible for Ubc-9 interaction also drives formation of a tertiary nuclear localization signal (NLS), consisting of Lys-21, Arg-30, and Lys-31, within the protein's alpha helical cap (177). This, in turn, results in recognition by importin α, and ensuing nuclear translocation. Once localized to the nucleus, CRABP-II is hypothesized to be released from its pentameric SUMO moiety before interacting directly with the LBD of RAR, since Lys-102, along with Gln-75 and Pro-81, has also been shown to mediate receptor complex formation (178). This allows for the channeling of atRA from CRABP-II into RAR's binding pocket, activating the receptor while CRABP-II leaves the nucleus to begin the cycle anew (179). This pathway likely plays a minor role in embryogenesis, as the only aberrant phenotype presented by CRABP-II knockout mice is the presence of an extra postaxial digit on the forelimb, which occurs with 10-50 % penetrance and is strain dependent (180; 181). However, upregulation of CRABP-II has been observed in cell proliferation-based pathologies such as psoriasis (182; 183), with high levels of protein expression positively correlated to atRA-based chemotherapy response in certain cancers (24).

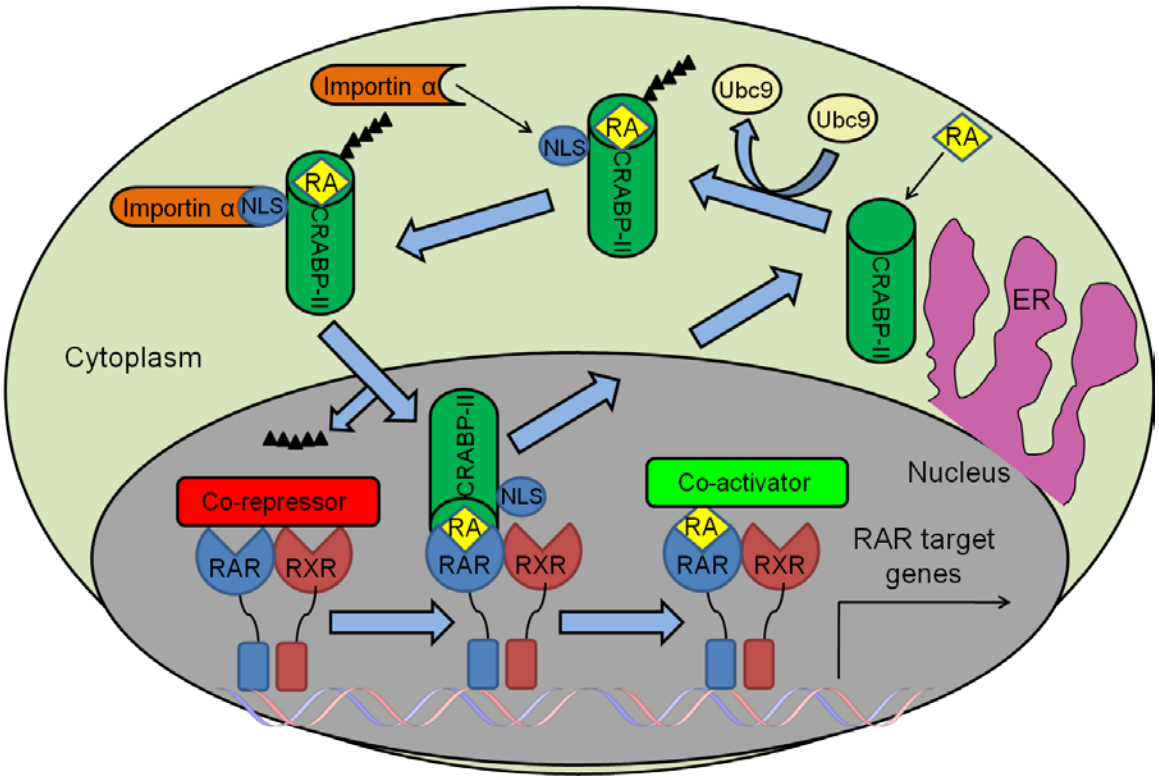

1-5. The CRABP-II-RAR signaling pathway

Both SUMOylation by Ubc9 as well as nuclear import by importin α are integral to the CRABP-II mediated enhanced signaling of RAR. ER: endoplasmic reticulum, Black triangle: single copy of SUMO protein.

1.3 The FABP5-PPARβ/δ Signaling Pathway

1.3.1 Long-Chain Fatty Acids

The importance of LCFAs to all cellular life forms is difficult to overestimate. Encompassing fatty acids with alkyl tail lengths spanning 14-20 carbons, LCFAs are an essential component of the phospholipids that form all major biological membranes, a major metabolic fuel source, and precursors to entire classes of signaling molecules. Predominantly in the form of triacylglycerols when obtained from the diet, these fatty acids must first be hydrolyzed to their free form by pancreatic lipase in the jejunum before crossing the enterocyte membrane (184). Once within the cell, they are re-packaged into neutral fats and assembled into chylomicrons, which are then excreted to be distributed throughout the body. Processing of the chylomicron remnants in the liver results in the production of very low-density lipoprotein (VLDL), which in the circulation can undergo triglyceride lipolysis by hepatic lipase and/ or endothelial lipase, accompanied by cholesteryl ester and phospholipid transfer, to become low-density lipoprotein (LDL) (185). Unlike the chylomicrons and VLDL, LDL does not deliver its fatty acid cargo to target cells via LPL-mediated hydrolysis of its triaclyglycerol components (see section 1.2.1 for a fuller description of the process as it relates to atROH), but is able to bind to LDL receptors on the cell's surface, where it is subsequently endocytosed (185; 186). In addition to lipoprotein-mediated triglyceride transport, fatty acids are also found within the plasma bound to albumin, largely the result of their initial free form release by adipocytes (185-187). This process is responsive to the energy needs of the individual, and is able to elevate circulating fatty acid levels from 200-600 μM to 1 mM in the fasting state (26; 186; 188).

The solubility of many LCFAs, especially those which are saturated or monounsaturated, is less than 10 μM at physiological pH. However the levels of LCFA-coenzyme A (CoA) esters, considered to be the "active" form of LCFAs used by the cell for its metabolic processes, have been measured at concentrations of up to 164 μM in rat liver (189), and 258 μM in the mitochondria of rat adipocytes (190). The discrepancy in these values is due to the presence of various lipid transport proteins, such as acyl-CoA-binding protein (ACBP), sterol carrier protein 2 (SCP2), and the FABPs, the latter of which have been shown to constitute as much as 2-5 % of all cytosolic protein in select cell types (26; 186; 189). Through LCFA solubilization, these lipid shuttlers have been proposed to increase the cellular membrane: cytosol equilibrium partition coefficient (186), as evidenced by FABPs' ability to drive relocation of 38 % and 50 % of model membrane and microsomal membrane-bound fatty acids, respectively, into the surrounding aqueous environment (186; 191-194). This leads to enhanced cellular fatty acid uptake as well as intracellular diffusion rates, thereby increasing the efficiency of all LCFA-related functions (186; 195).

Although the majority of fatty acids are provided by the diet, they can also be made *de novo*, primarily within the liver and adipose tissue. This is accomplished with fatty acid synthase (FAS), a cytoplasmic complex which in animals consists of two identical 273 kDa polypeptides arranged in an X-shaped dimer that can carry out seven different enzymatic reactions in two catalytic centers (196-198). Fatty acid synthesis begins with an acetyl-CoA primer, which is subsequently elongated two carbon units at a time via a condensation reaction with malonyl-CoA, with each step requiring NADPH as a reductase. After seven rounds have been completed, the 16 carbon long saturated

palmitic acid (PA) is released. Additional modification of PA, as well as any other LCFA, is made in the ER by a chain of four enzymes that together perform the function of FAS, i.e. the further elongation of LCFAs to lengths of 18-26 carbons using LCFA-CoA, malonyl-CoA, and NADPH as substrates (196). Regulation of the process occurs at the first, rate limiting step, which is performed by a family of enzymes called the fatty acid elongases, of which each member showcases a distinct expression profile and fatty acid substrate preference.

Fatty acid elongation often occurs in conjunction with desaturation, a process mediated in mammals exclusively by the acyl-CoA desaturases (199). Humans are currently known to express three of these enzymes (199; 200). The first is stearoyl-CoA desaturase (SCD), a Δ-9 desaturase that places a double bond beginning at the ninth carbon counting from the carboxyl in saturated fatty acids spanning 12-19 carbon units, thus forming monounsaturated fatty acids (201). The remaining two are Δ-6 and Δ-5 desaturases, which are able to add additional double bonds located between the one previously made by SCD and the fatty acid carboxyl head group, resulting in the formation of polyunsaturated fatty acids (PUFAs) (199; 200). As humans lack both a Δ-12 and ω-3 desaturase, ω-6 and ω-3 PUFAs must be obtained from the diet (199). Since linoleic acid (LA) and α-linolenic acid (ALA) are the only precursors required from which humans can synthesize all other necessary ω-6 and ω-3 fatty acids, respectively, they have been termed essential fatty acids. Much interest has been devoted to these omega classes, as their primary function lies not in their ability to serve as fuel or regulators of membrane fluidity, but as specific signaling molecules that help direct

cellular response (199). At the transcriptional level, this is largely due to their activation of the PPARs (202).

1.3.2 The Peroxisome Proliferator-Activated Receptors

Peroxisomes are cytoplasmic organelles found in nearly all eukaryotic cells that play a role in numerous and wide-ranging metabolic functions, including oxidation of very long chain fatty acids (VLCFAs) and branched chain fatty acids, H_2O_2 based respiration, catabolism of amino acids, purines, and polyamines, and synthesis of bile acids and plasmologens (203; 204). For over four decades, it has been known that administration of a wide variety of synthetic and natural compounds, ranging from phthalate ester plasticizers and fibrates to dehydroepiandrosterone, to rats and mice resulted in increased peroxisome formation within parenchymal cells (205; 206). However, it was Reddy and Rao who first proposed that the effects of these peroxisome proliferators could be attributed to a specific receptor binding event (206; 207). This receptor, PPARα, was cloned in 1990 (208), and the entire family, consisting of PPARα, PPARβ/δ, and PPARγ, was isolated in Xenopus two years later (209).

As nuclear receptors, the PPARs possess the same functional domain organization as the RARs, with the exception that they lack the C-terminal region F. Thus, they are composed of a disordered N-terminal AF-1, followed by a DBD consisting of two highly conserved zinc-finger motifs, a flexible hinge region, and a C-terminal LBD (121; 210). Also like the RARs, they are class II hormone receptors, remaining localized in the nucleus where they are bound as heterodimers with RXR to hormone response elements that consist of two direct PuGGTCA (or variants thereof) core sequence repeats (121). As noted previously, while these repeats can be separated by either one, two, or five base

pairs in RAREs, the classical PPAR response elements (PPREs) have either a single spacing nucleotide (DR1), or to a much lesser extent two nucleotide spacers (DR2), as well as an extended 5'-half site that confers both PPRE affinity as well as PPAR isotype specificity (211; 212). The LBD is composed of a helical sandwich with a four stranded β-sheet, surrounding a tripartite binding pocket (213). All agonists bind such that their polar headgroup lies inside the arm of the pocket that is capped by helix 12 (Arm I-see Figure 3-6), which allows the moiety to engage in hydrogen bonding with a conserved H12 tyrosine that is necessary to stabilize the AF-2 in the activated position. Conversely, the absence of this hydrogen bond frees the AF-2 to move farther away from the ligand, resulting in partial agonism or antagonism of the receptor (214). Although binding pocket topology dictates ligand specificity for each receptor isotype, all family members share a similar pocket volume of ~1300 $Å^3$, one of the largest within the NR superfamily (213). Therefore, it is not surprising that the PPARs are capable of binding to a wide array of naturally occuring hydrophobic ligands in addition to saturated and unsaturated long chain fatty acids (215), such as various steroid precursor metabolites (216), eicosanoids (217-219), and phospholipids (220) (Figure 1-6). Such a degree of promiscuity, coupled with their affinity for transcribing gene targets involved in metabolism, suggests that these receptors serve as "lipid sensors" (221), able to modulate energy homeostasis in accordance with the metabolic profile of the organism. To this end, both PPARα and PPARγ have been pharmaceutically targeted via the fibrates and thiazolidinediones (glitazones) to combat dyslipidemia and diabetes, respectively (222; 223); however, PPARβ/δ remains less well characterized.

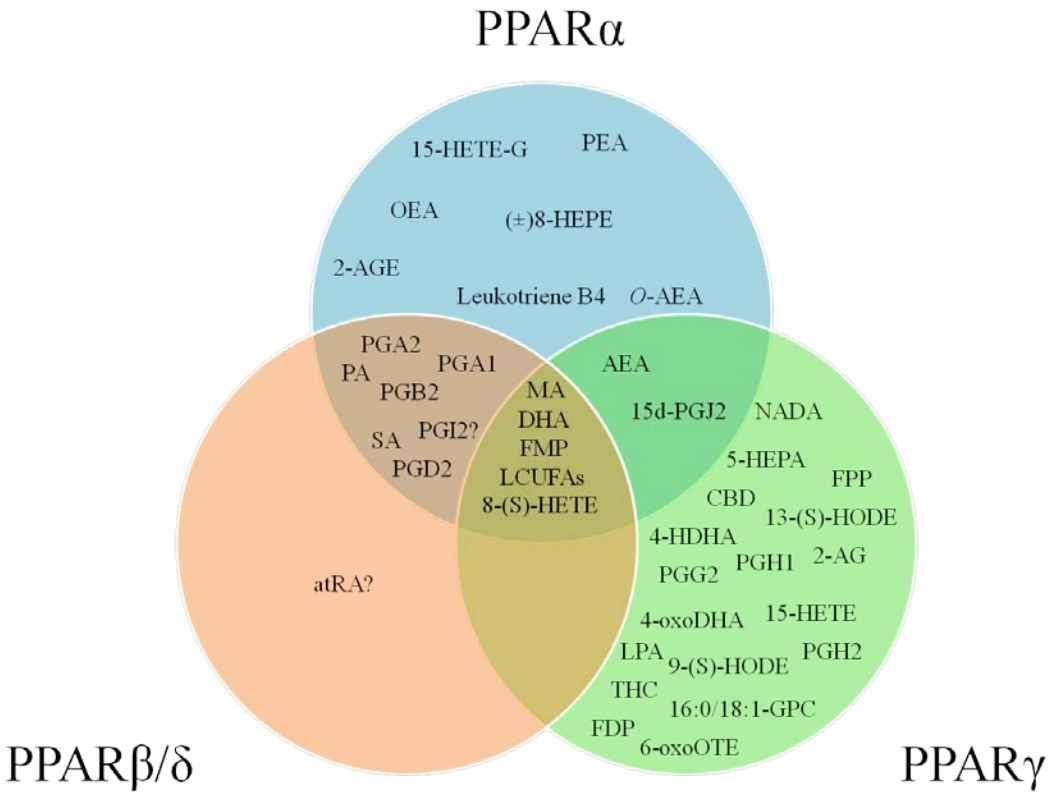

1-6. Endogenous PPAR ligands

A large array of lipids has been shown to bind and/or activate one or more PPAR isotypes. However, their intracellular concentration, coupled with their receptor binding affinity, has resulted in continuing debate concerning many of these candidates' physiological relevance. Additionally, many of the ligands shown have not been tested for all three PPAR family members. Therefore, their distribution is more a reflection of research focus than isotype specificity. PEA: palmitoylethanolamide, 15-HETE-G: 15-hydroxyeicosatetraenoic acid glyceryl ester, OEA: oleoylethanolamide, (±)8-HEPE: 8-hydroxyeicosapentaenoic acid, 2-AGE: 2-arachidonyl glyceryl ether, *O*-AEA: *O*-arachidonoyl ethanolamine, PGA1: prostaglandin A1, PGA2: prostaglandin A2, PA: palmitic acid, PGB2: prostaglandin B2, PGI2: prostaglandin I2 (prostacyclin), SA: stearic

acid, PGD2: prostaglandin G2, MA: myristic acid, DHA: docosahexaenoic acid, FMP: farnesyl monophosphate, LCUFA: long-chain unsaturated fatty acid, 8-(S)-HETE: 8-(S)-hydroxyeicosatetraenoic acid, AEA: *N*-arachidonoylethanolamine, 15d-PGJ2: 15-deoxy-Δ-12,14-prostaglandin J2, atRA: all-*trans* retinoic acid, NADA: *N*-arachidonoyl-dopamine, 5-HEPA: 5-hydroxyeicosatetraenoic acid, FPP: farnesyl pyrophosphate, CBD: cannabidiol, 13-(S)-HODE: 13-(S)-hydroxyoctadecadienoic acid, 4-HDHA: 4-hydroxydocosahexaenoic acid, 2-AG: 2-arachidonoylglycerol, PGH1: prostaglandin H1, PGG2: prostaglandin G2, 4-oxoDHA: 4-oxodocosahexaenoic acid, 15-HETE: 15-hydroxyeicosatetraenoic acid, LPA: lysophosphatidic acid, PGH2: prostaglandin H2, 9-(S)-HODE: 9-(S)-hydroxyoctadecadienoic acid, THC: tetrahydrocannabinol, 16:0/18:1-GPC: 1-palmitoyl-2-oleoyl-sn-glycerol-3-phosphocholine, FDP: farnesyl diphosphate, 6-oxoOTE: 6-oxooctadecatrienoic acid. The figure is a compendium of refs. (211; 219; 220; 224-232).

1.3.3 PPARβ/δ

PPARβ/δ, despite being the least conserved of the PPAR isotypes across species, is ubiquitously expressed in the adult (202; 203), and consequently implicated in a broad range of cellular functions. Like its family members, it has been shown to be involved in various aspects of the metabolic syndrome (MetS), a compendium of obesity-related disorders clinically characterized by elevated waist circumference, triglyceride levels, blood pressure, and fasting glucose levels combined with lower levels of HDL cholesterol, which correlate with a heightened risk for cardiovascular disease and type II diabetes (233). PPARβ/δ agonists have been successful in increasing plasma level HDL concentrations and improving overall serum lipid profiles in both $Lepr^{db/db}$ (insulin resistant) mice as well as obese rhesus monkeys (234; 235). Although the exact mechanisms behind the observed physiology remain unclear, the receptor has been tentatively correlated with raised HDL levels in humans via increased expression of ATP-binding cassette transporter A1 (ABCA1) in macrophages, fibroblasts, and intestinal cells, driving their higher cholesterol efflux (235; 236). Knockout of PPARβ/δ in mice is often embryonic lethal, with those that survive displaying an interesting pathology. While these mice have ~3-fold reduction in adiposity across all types of fat tissue, they are less metabolically active, glucose-intolerant, and are more susceptible to developing dyslipidemia, likely the result of greater hepatic VLDL production exacerbated by lowered LPL activity (237-239).

PPARβ/δ is also known to play a significant role in biological processes that are tangential to MetS. It is the predominant isotype in both rodent and human skeletal muscle (240), being especially prevalent in the oxidative type I fibers (241), and has been

demonstrated to be a powerful regulator of muscle metabolism adaptation to external stimuli. Upregulation of both the receptor and its target genes occurs in response to either fasting or endurance exercise, resulting in increased fatty acid uptake and mitochondrial transport and consequently a greater muscle reliance on LCFA catabolism vs. carbohydrate oxidation for energy (202; 242). While a muscle specific PPARβ/δ KO mouse model displayed decreased levels of type I fibers in the tibialis and prevalence towards obesity (243), overexpression of the receptor in muscle increased the level of these oxidative fibers compared to wild type (244). More drastically, muscle specific expression of a constitutively active PPARβ/δ mutant resulted in mitochondrial biogenesis, an increase in the oxidative type I: glycolytic type II muscle fiber ratio, and increased running endurance in untrained mice (241). Recently, research has indicated that PPARβ/δ, in addition to PPARs α and γ, is able to modulate inflammation (242; 245). Agonism of the receptor has been attributed to inhibition of chemokine production and adhesion molecule expression in vascular endothelium (246-248), providing a possible avenue to combat atherosclerosis. Attenuation of the inflammatory response via PPARβ/δ activation has also been observed in multiple other tissues and cell types in rodents, including the testis (249), heart (250; 251), adipose tissue (252), and astrocytes (253).

Finally, PPARβ/δ engages in processes unrelated to metabolism or MetS. As mentioned above, the functionality of PPARβ/δ is crucial to embryo survival, in part due to its effect on placenta development. Transcription of one of its target genes, 3-phosphoinositide-dependent kinase 1 (PDK1), results in the eventual phosphorylation of Akt, necessary to promote the differentiation of Rcho-1 trophoblasts into giant cells (254). The same, or similar, pathway also helps to explain the role of PPARβ/δ in wound

healing. Upon skin injury, both tumor necrosis factor α (TNF-α) and interferon γ (IFN-γ) are released at/near the site of insult, leading to augmented expression of both PPARβ/δ and its endogenous ligand(s). The resulting increase in PDK1 →pAkt signal transduction not only accelerates the differentiation of keratinocytes, but also strengthens their resistance to apoptosis (255; 256). Lastly, the high level of PPARβ/δ expression in the developing neural tubes of rats, combined with its continued presence across most brain cell types tested in the adult rat and mouse, provided the first hints concerning a role for the receptor in brain function and development (257). In support of this, a study found that nearly half of the PPARβ/δ KO mice tested (3 of 5 females, 2 of 7 males) exhibited altered myelination within the corpus collosum compared to wild type controls (258). Although the complete underlying mechanism is still unclear, it is worth noting that the brains of female KO mice also exhibited significant changes in phospholipid and esterified FA levels (259).

1.3.4 FABP5

In 1991, the existence of a small (~14.5 kDa) cytosolic protein, located in rat, mouse, and human epidermis, and capable of binding with various affinities an array of MCFAs, LCFAs, FA metabolites, eicosanoids, and atRA was first reported (260). Following this, Madsen et al. were able to clone a protein that was highly upregulated in psoriatic skin, calling it psoriasis-associated fatty acid binding protein (PA-FABP) due to its sequence homology with known members of the FABP group (261), while an epidermal type FABP (E-FABP) was successfully cloned and characterized a year later (262). Soon, it became apparent that these were the same protein, which is now often referred to as FABP5.

Sequence and phylogenetic analysis places FABP5, along with FABPs 3, 4, and 7-9 in iLBP subfamily IV (5; 11), whose constituents share the defining characteristics of a promiscuous ligand binding profile as well as a 3_{10} helix located near their N-terminus (263). Nevertheless, FABP5 does showcase several distinguishing properties. In a urea denaturation assay, hFABP5 was found to be the least conformationally stable member in its subfamily (16). This result is surprising, as it harbors an unusually high number of cysteines, two of which (Cys-120 and Cys-127) participate in a disulphide bridge, the only instance of such a bond to be found throughout the entire family (264; 265). Additionally, though the protein was first discovered in skin, it has since been found throughout multiple tissue/cell types (see Table 1-1), and is considered to be the most widely expressed paralog within the FABP group (8).

The ubiquitous expression of FABP5 coupled with its overlapping ligand binding profile relative to other subfamily IV members have in general made attempts to delineate its specific physiological function(s) difficult. Nevertheless, 20 years of research has revealed FABP5's role as both a metabolic modulator and an arbiter of cell fate. Regarding the former, knockout of FABP5 yielded a mouse phenotype with lower circulating triglyceride, glucose, and cholesterol levels than wild type when fed a normal diet. Moreover, the transgenic mice were able to maintain greater insulin sensitivity and lowered plasma glucose than their wild type counterparts when challenged with obesity via two separate models (266). Similarly, a study conducted in a group of middle-aged Chinese subjects with approximately equal gender representation found that elevated plasma levels of FABP5 correlated positively with increased adiposity, adverse lipid profiles, and higher serum insulin levels, representing a novel circulating biomarker for

MetS (267). As regards the latter, it was discovered that FABP5 could also serve as a facilitator of PPARβ/δ specific signaling (25). The process was found to be similar to that previously detailed for CRABP-II and RAR, with FABP5 undergoing translocation to the nucleus, wherein via a direct protein-protein interaction it would presumably channel its cargo into PPARβ/δ's ligand binding pocket, thereby enhancing the nuclear receptor's activation. However, there was one crucial difference: while CRABP-II binds atRA with extremely high selectivity, FABP5 was able to bind all ligands tested, yet only known PPARβ/δ agonists could elicit its nuclear localization.

The scope of the FABP5-PPARβ/δ signaling pathway was considerably broadened when atRA was found not only to selectively bind and activate PPARβ/δ over PPARs α and γ (230), but also to drive nuclear import of FABP5 (268). A model was proposed in which the retinoid could undergo directed transport by either CRABP-II to RAR, or FABP5 to PPARβ/δ, with drastically different results (268). While the former, or "classical" signaling pathway led to RAR-mediated transcription of an array of genes related to differentiation, cell cycle arrest, and/or apoptosis, activation of PPARβ/δ through the "alternative" pathway turned on genes involved in survival and proliferation (Figure 1-6). Since the degree to which either path was used was demonstrated to be dependent on the expression level ratio of the transport proteins within those paths (ie CRABP-II: FABP5), the model provided not only an elegant explanation at the molecular level of the opposing cell-type dependent responses to atRA exposure, but a convenient method to predict, and if so desired, alter said response. Indeed, this method has been used, with success, on multiple RA-resistant cancer cell lines (268-273).

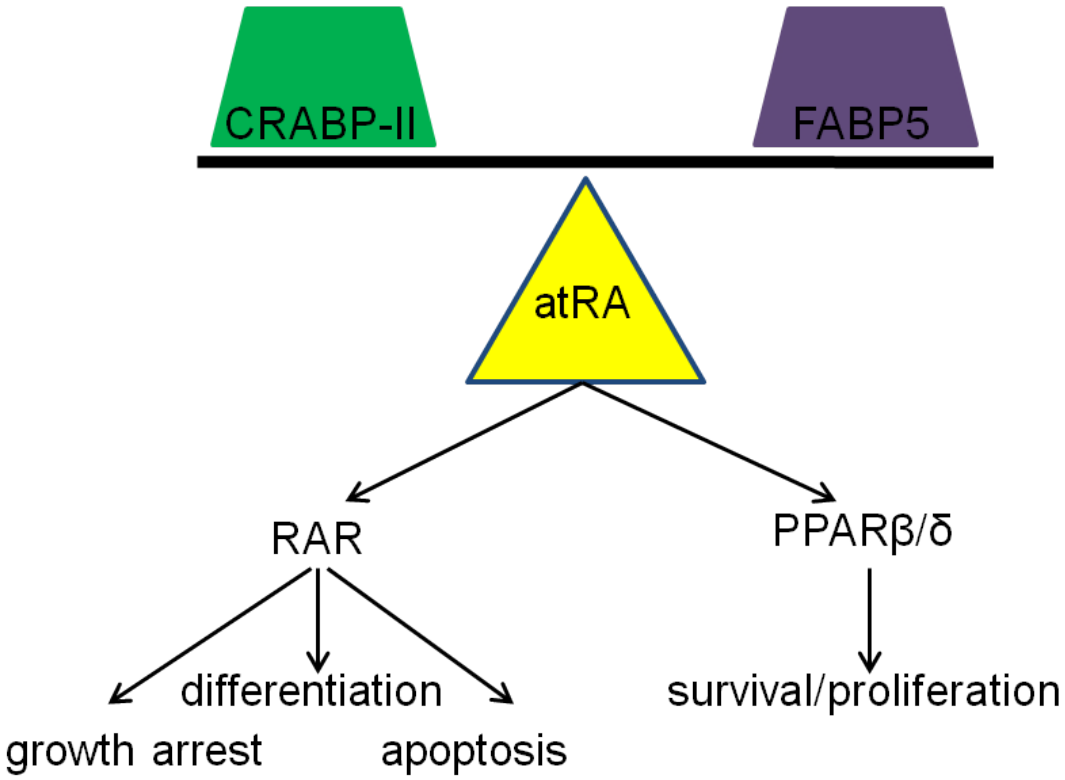

1-7. The ratio of CRABP-II to FABP5 determines cell response to atRA

It is not the expression levels of the nuclear receptors, but of their iLBP partners that dictates the signaling pathway taken by atRA upon introduction to a cell. While classical signal transduction results in RAR activation and often ensuing cell growth inhibition, the alternative pathway promotes cell survival response mechanisms stemming from PPARβ/δ target gene transcription.

1.4 Objectives of the Dissertation

Although FABP5 has been shown to undergo nuclear translocation in response to binding PPARβ/δ agonists, the method by which it does so is completely unknown. In addition, only two naturally occurring ligands, atRA and LA, have been tested thus far. Therefore, it is the purpose of Chapter 2 to elucidate, using a small array of commonly occurring LCFA's, the molecular mechanism underlying FABP5's activation state, i.e. the state in which it can be recognized for nuclear import. This chapter will also investigate the ability of FABP5 to distinguish between activating and non-activating fatty acids by analyzing the way in which complexed ligand is able to communicate its activation potential to the protein. Chapter 3 will then address the feasibility of pursuing a comprehensive structural analysis of the alternative RA signaling pathway. Taken together, it is the goal of this Dissertation to provide much needed biochemical and structural understanding of the powerful partnership between FABP5 and PPARβ/δ.

CHAPTER 2 : STRUCTURAL BASIS FOR LIGAND REGULATION OF THE FATTY ACID BINDING PROTEIN 5, PEROXISOME PROLIFERATOR-ACTIVATED RECEPTOR B/Δ (FABP5-PPARB/Δ) SIGNALING PATHWAY[1]

[1] This research was originally published in The Journal of Biological Chemistry. Armstrong EH, Goswami D, Griffin PR, Noy N, Ortlund EA. Structural basis for ligand regulation of the fatty acid-binding protein 5, peroxisome proliferator-activated receptor β/δ (FABP5-PPARβ/δ) signaling pathway. *J Biol Chem*. 2014; 289:14941-54. © the American Society for Biochemistry and Molecular Biology.

2.1 Introduction

LCFAs, in addition to serving as structural components and energy sources of the cell, participate in cellular signaling by modulating the activity of a group of nuclear receptors known as the peroxisome proliferation-activated receptors (PPARs) (215; 219; 226; 274-276). Due to the large number of target genes affected by this family of ligand-regulated transcription factors, LCFAs play a critical role in a variety of cellular processes and their related pathophysiologies, ranging from metabolic defects to cell differentiation and cancer progression (277; 278). However, the relative insolubility of these molecules makes them reliant upon a class of transport proteins, the FABPs, to exert their signaling effects (6; 8; 279).

There are nine known FABP members in mammals, each ~14-15 kDa in size with orthologs found throughout the animal kingdom (280). Though they exhibit a wide range of sequence identity (~20-70%), all form a twisted β-barrel, composed of 10 anti-parallel β-strands arranged into two orthogonal β-sheets, with a helix-turn-helix lid covering the ligand binding site (8; 279; 280). As members of the intracellular lipid binding protein (iLBP) family, they have traditionally been thought to be involved in the solubilization/ protection of their various hydrophobic cargoes, facilitating ligand movement via passive diffusion between the various compartments of the cell (281; 282). Increasingly, however, FABPs are emerging as specific mediators of precise signaling pathways. For instance, FABP1 facilitates the polyunsaturated fatty acid and fibrate-induced transactivation of PPARα, via direct interaction with the nuclear receptor's ligand binding domain (283-285). A similar role has been observed with FABP4, whereby its ligand-mediated

dimerization state governs nuclear import and subsequent ligand delivery to PPARγ (25; 286). Recent findings have even revealed FABPs to be the once enigmatic *N*-acylethanolamine (NAE) "transporter," responsible for endocannabinoid cellular uptake, hydrolysis, and PPARα activation (287; 288).

FABP5 (E-FABP, KFABP, mal1), first characterized over 20 years ago in keratinocytes, is one of the most ubiquitously expressed proteins in its class, and can be found across a broad spectrum of tissue/cell types such as the epidermis, adipose, macrophages, mammary glands, brain, kidney, liver, lung, heart, skeletal muscle, and testis (8; 261; 280). A member of iLBP subfamily IV, FABP5 binds a wide array of ligands in a 1:1 ratio, including fatty acids and fatty acid metabolites spanning 10-22 carbons in length with various saturation states, as well as the vitamin A metabolite all-*trans* retinoic acid and numerous synthetic drugs and probes (8; 11; 268; 289). It has also been found to be involved in a range of pathologies, including the Metabolic Syndrome (MetS) (266; 290), atherosclerosis (267), cancer (269-272; 291), and potentially certain neurodegenerative diseases (292).

Work conducted by *Tan et al.* demonstrated the ability of FABP5 to specifically enhance the transactivation of PPARβ/δ, whose known gene targets are involved in cellular glucose and lipid homeostasis (237-239), differentiation (254; 255), and resistance to apoptosis (255; 256). Despite FABP5's promiscuous binding profile, only a subset of fatty acids and other ligands have been shown to result in the protein's nuclear translocation, where it is thought to engage PPARβ/δ, allowing for the channeling of ligand into the nuclear receptor's binding pocket (25). Though previous structural studies have shed considerable light on the role of FABP4 in PPARγ signaling (286; 293), the

mechanism underlying select lipid activation (e.g. nuclear translocation) of FABP5 remain unknown. Using a combination of X-ray crystallography, hydrogen deuterium exchange mass spectroscopy (HDX), biochemical and cellular approaches, we have established the presence of a ligand-sensitive tertiary nuclear localization signal (NLS) located on the α1 and α2 helices of FABP5. Furthermore, we show that interaction of a bound ligand with FABP5's β2 loop relays conformational information to the NLS, thereby serving as the driving force for fatty acid-specific nuclear translocation.

2.2 Methods

Reagents – Chemicals were purchased from Sigma, Fisher, Polysciences, or Cayman, Inc. The pMCSG7-His plasmid was a gift from John Sondek (UNC, Chapel Hill), while pEGFP-N3 was graciously given by Anita Corbett (Emory University, Atlanta).

Cloning and Mutagenesis – Full-length, codon optimized wild-type human FABP5 (residues 1-135) was subcloned into pMCSG7-His, pCMV-Tag2B, and pEGFP-N3 expression vectors. The NLS-deficient mutant (hFABP5NLSm: Lys-24Ala, Lys-34Ala, Arg-33Ala) and "double-switch" mutant (hFABP5DSm: Met-35Ala, Leu-60Ala) were generated in the pMCSG7-His pCMV-Tag2B. hFABP5NLSm, hFABP5DSm and a nuclear export signal mutant (hFABP5NESm: Leu-69Ala, Leu-94Ala, Phe-89Ala) were generated in pEGFP-N3. All mutagenesis was performed using Quikchange II XL (Stratagene), and all constructs were sequenced for verification prior to use.

Protein Expression and Purification – Full-length human FABP5 in the pMCSG7 vector was transformed into *Escherichia coli* strain BL21(DE3) cells and expressed as a 6XHis fusion containing a Tobacco Etch Virus (TEV) protease cleavage site to facilitate tag removal. Cultures (1.3 L in TB) were grown to an OD_{600} of approximately 0.8 and induced with 1 mM isopropyl β-D-1-thiogalactopyranoside (IPTG) at 37 °C for 4 h. Cell mass was collected by centrifugation at 5 krpm for 15 min, lysed, and purified by nickel affinity chromatography. The His tag was cleaved by TEV protease at 4 °C overnight with simultaneous dialysis into a buffer containing 300 mM NaCl, 50 mM K_2HPO_4 (pH 7.4), and 5% glycerol, and purified to homogeneity by nickel affinity followed by gel filtration chromatography in phosphate buffered saline (PBS). To generate *apo* FABP5, pure protein was delipidated via chloroform/ methanol extraction according to the methods of Bligh and Dyer (294). Denatured protein was then solubilized in 4 mL buffer composed of 50 mM tris-HCl (pH 8.0), 6 M guanidinium chloride, and 2 mM DTT, and refolded by fast dilution at 4 °C in 500 mL of 20 mM tris-HCl (pH 8.5), 1.7 M urea, 4% glycerol, and 2 mM DTT. After adjusting the final concentration of urea to 2.0 M, refolded protein was concentrated by filter centrifugation and dialyzed against PBS at 4 °C overnight, before being purified via gel filtration chromatography.

Crystallization, Data Collection, Structural Refinement – Pure FABP5 was concentrated to 15 mg mL^{-1} via filter centrifugation in PBS buffer, and crystals of the *apo* protein were grown over two weeks via hanging drop vapor diffusion at 18 °C from solutions containing 2 μL FABP5 solution and 1 μL mother liquor (2 M ammonium sulfate, 300 mM Na/ K tartrate, 100 mM Na citrate, pH 5.6). Crystals were cryoprotected by immersion in mother liquor containing 15% glycerol and flash cooled in liquid

nitrogen. Data to a resolution of 1.67 Å were collected at 100K and a wavelength of 1.00 Å at the South East Regional Collaborative Access Team (SER-CAT) beamline (Advanced Photon Source, Argonne, IL), and processed using the HKL-2000 software (295). The structure was solved by molecular replacement using a previously determined structure (PDB code: 1B56) in PHASER (296). To obtain crystals of the FABP5-linoleic acid complex, *apo* FABP5 was exposed to LA at a 1:5 protein:ligand molar ratio in PBS, before being concentrated to 15 mg mL^{-1}. Crystals formed overnight at 4 °C via hanging drop vapor diffusion, using a crystallant consisting of 2.4 M ammonium sulfate, 200 mM Na/ K tartrate, and 100 mM Na citrate (pH 5.6). Crystals were cryoprotected with a 20% glycerol crystallant solution, and data to a resolution of 2.60 Å were collected at Emory University using a Rigaku MicroMax 007 HF generator with a Cu anode and a Saturn CCD detector, at a temperature of 100 K. Data indexing and phasing were carried out as described for *apo* FABP5. Model building and refinement for both structures were performed using COOT (297) and phenix.refine (298), respectively. Electrostatic surface potential maps of FABP5-LA were calculated by the PDB2PQR Server (299) and the Adaptive Poisson-Boltzmann Solver (300), while protein interior volumes were obtained with CASTp using a probe radius of 1.4 Å (301). Figures were generated using the PyMOL Molecular Graphics System (Schrodinger, LLC). Structure validation was performed with MolProbity, showing excellent overall model geometry as the *apo* and LA bound structures received scores in the 99^{th} and 100^{th} percentile, respectively (302). Final coordinates for *apo* FABP5 and FABP5-LA have been deposited into the PDB, under accession codes 4LKP and 4LKT.

Cell Localization Assay – COS-7 cells were grown on 10 cm plates in Dulbecco's modified eagle medium (DMEM) (Gibco) supplemented with 10% fetal bovine serum (FBS) at 37 °C and 5% CO_2. At ~60% confluency, polyethylenimine (PEI, Polysciences) was used to transfect cells with 5 μg pEGFP-N3 vector harboring full-length hFABP5WT, hFABP5NLSm, hFABP5NESm, or hFABP5DSm, with the DNA-PEI complex being removed 6-8 h after exposure. The following day, cells were checked for fluorescent protein expression, and then transferred to Lab-Tek II Chamber Slides (Thomas Scientific #154526) in DMEM buffer containing 5% charcoal-dextran stripped FBS. Twenty four hours post-transfer, cells were exposed to 10 μM fatty acid ligand solubilized in 0.1% ethanol for 30 min at 37 °C, washed 3X with ice cold PBS, fixed with 4% paraformaldehyde, and stained with 4'6-diamidino-2-phenylindole (DAPI). Slides were imaged using a Zeiss LSM510 META Upright confocal microscope (40x/1.3 Oil DIC objectives) employing Zeiss Zen2009 acquisition software, with both nuclear focusing and Enhanced Green Fluorescent Protein (EGFP) imaging conducted at an optical slice of 0.9 μm. Nuclear and cytoplasmic EGFP fusion protein fluorescence intensities were quantified using ImageJ, and the calculated nuclear: cytoplasm ratios were plotted in Prism 5 (GraphPad Inc., La Jolla, CA). Statistical significance was determined by one-factor ANOVA, with individual comparisons made with Tukey's honestly significant difference (HSD) post-hoc tests.

Ligand Binding Assays - Ligand binding was measured via competition of 1-anilinonaphthalene-8-sulfonic acid (1,8-ANS), which displays increased fluorescence when exposed to a hydrophobic environment (303). In brief, both wild-type and mutant hFABP5 were expressed and purified to homogeneity as described above, and dialyzed in

PBS (pH 8.2). Binding affinity (K_D) was derived by monitoring maximal fluorescence intensity of a constant concentration of 500 nM 1,8-ANS with increasing protein concentrations ranging from 20 nM-424 μM. Blank measurements obtained from protein only samples were subtracted at each protein concentration tested to obtain the final values. Competition assays were then performed in which protein was held at a constant concentration of 500 nM (1 μM for the FABP5NLSm palmitic acid competition), with 1,8-ANS also being held constant at either 5 μM (for hFABP5WT and hFABP5DSm) or 10 μM (for hFABP5NLSm) in the presence of increasing fatty acid concentrations from 10 nM-200 μM. Blanks consisting of 1,8-ANS and fatty acid in the absence of protein were subtracted at each ligand concentration tested. The resulting fluorescence values were used to calculate a K_i for the fatty acid of interest. Data were collected at 30 °C on a BioTek Synergy plate reader using an excitation filter of 380/20 nm and an emission filter of 460/40 nm, and processed in GraphPad Prism 5. Statistical significance was determined by one-factor ANOVA, and individual comparisons were made with Tukey's HSD post-hoc tests.

In-Cell Activation Assays - MCF-7 cells were transferred to 96 well plates, where they were grown and maintained in high glucose DMEM containing L-glutamine, Na pyruvate, and phenol red (Gibco), supplemented with 10% charcoal-dextran stripped FBS (Gibco) and 1% penicillin/streptomycin (Culture Buffer). One hundred ng $well^{-1}$ pSG5 vector harboring full-length mouse PPARβ/δ receptor, 100 ng $well^{-1}$ PPAR response element (PPRE)-driven firefly luciferase reporter (PPRE X3-TK-luc), and 20 ng $well^{-1}$ constitutive *Renilla* luciferase reporter (phRLtk) in the presence or absence of 25 ng $well^{-1}$ wild type or mutant variant human FABP5 cloned into the pCMV-Tag2B vector was

added to FuGENE HD in Opti-MEM (Invitrogen). This solution was diluted with Culture Buffer (-antibiotic) to a final concentration of 2.2-2.45 ng μL^{-1} total DNA. 100 µL $well^{-1}$ of this solution was used to transfect 70-90% confluent cells overnight. Cells were then treated in sextuplicate with 1-100 µM fatty acid ligand or vehicle (ethanol) in high glucose DMEM containing only L-glutamine and 1% penicillin/ streptomycin for 24 h (final working ethanol concentration 0.1%), and assayed with Dual-Glo luciferase substrate (Promega). Firefly activity was divided by *Renilla* activity to account for cell number, viability, and transfection efficiency, and graphs were generated in Graphpad Prism 5. Statistical significance was determined by either one or two-factor ANOVA, and individual comparisons were made with Tukey HSD or Bonferroni post-hoc tests.

Protein Unfolding Assay – Pure hFABP5WT and hFABP5NESm (1 µM, PBS) were exposed to increasing concentrations of guanidinium hydrochloride, and the resulting shift in peak intrinsic fluorescence intensity measured using a Shimadzu RF-5301PC spectrofluorophotometer at an excitation wavelength of 280 nm with a 5 nm spectral bandwidth. Values were fitted using a four parameter logistic equation, and the calculated fluorescence shift midpoints were compared via unpaired t-test with Welch's correction for unequal variances in Graphpad Prism 5.

Hydrogen-Deuterium Exchange Mass Spectroscopy (HDX) - Solution-phase amide HDX was carried out with a fully automated system as described previously (304). Briefly, 4 µl of sample consisting of 10 µM protein and 100 µM ligand in PBS, pH=7.4 was diluted to 20 µl with deuterium-containing HDX buffer and incubated at 25 °C for 10, 30, 60, 900, or 3,600 s. Following deuterium incorporation, the protein was denatured and back exchange minimized by dilution to 50 µL in an acidic buffer containing 0.1%

(v/v) trifluoroacetic acid (TFA) in 5 M urea (held at 1 °C). Samples were then passed across an immobilized pepsin column (prepared in house) at 50 µl min^{-1} (0.1% v/v TFA, 15 °C); the resulting peptides were trapped on a C8 trap cartridge (Hypersil Gold, Thermo Fisher). Peptides were then gradient-eluted with 4-40% (w/v) acetonitrile, 0.3% (w/v) formic acid over 5 min at 2 °C across a 1 mm × 50 mm C18 high-performance liquid chromatography (HPLC) column (Hypersil Gold, Thermo Fisher) and electrosprayed directly into an Orbitrap mass spectrometer (LTQ Orbitrap with ETD, Thermo Fisher). Peptide ion signals with a MASCOT score of >20 were used if they had no ambiguous hits using a decoy (reverse) sequence in a separate experiment using a 60 min gradient. The intensity weighted average m/z value (centroid) of each peptide's isotopic envelope was calculated with in-house developed software (305). Each envelope was corrected for back-exchange assuming 70% recovery and accounting for the known deuterium content of the on-exchange buffer. To quantify the difference in exchange rates, we calculated the average percent deuterium uptake for wild-type (WT) FABP5-palmitoleic acid (PoA) following 10, 30, 60, 900 and 3,600 s of exchange by averaging percent deuterium incorporation across all time points. From this value, we subtracted the average percent deuterium uptake measured at the same time points for the matching peptides of the FABP5WT-AA complex. Positive perturbation values indicate exchange rates are faster for these regions within FABP5WT in complex with PoA. To quantify the effects of the "double switch" mutant (DSm) we subtracted the percent deuterium uptake for FABP5WT-AA from FABP5DSm-AA, FABP5WT-PoA from FABP5DSm-PoA, and FABP5DSm-AA from FABP5DSm-PoA. The resulting differences in exchange were mapped on the structure of FABP5 and visualized with PyMOL (Schrödinger, LLC).

2.3 Results

2.3.1 Overall Structure and Oligomerization Status of Apo and Holo FABP5

To elucidate the molecular mechanisms driving ligand-specific FABP5 activation, we determined crystal structures of *apo* FABP5 and FABP5 in complex with LA, an ω-6 polyunsaturated pan-PPAR fatty acid agonist that has been shown to trigger FABP5's nuclear translocation (25). Since recombinant FABP5 co-purifies with *E. coli* LCFAs, delipidation/ denaturation of the protein followed by refolding was performed prior to LA exposure and subsequent crystallization (264; 294). The structure of *apo* FABP5 was solved in the $P4_32_12$ spacegroup at high resolution (1.67 Å), with the asymmetric unit comprised of a FABP5 monomer adopting the canonical iLBP fold (Figure 2-1a) (264; 265). Interestingly, crystals of the FABP5-LA complex grew only in the $P3_221$ spacegroup, with the resulting 2.6 Å structure revealing 4 copies of protein in the asymmetric unit (Table 2-1, Figure 2-1b). Since modulation of dimer interface is thought to account for the ligand-specific nuclear translocation of FABP4 (293), we tested whether fatty acid binding affects the oligomerization status of FABP5. Size exclusion chromatography of both *apo* protein (Bligh and Dyer delipidated and refolded) and FABP5 purified in the presence of saturating amounts of LA reveals that FABP5 is monomeric in both the liganded and unliganded state (Figure 2-1c). Additionally, dynamic light scattering conducted on untreated recombinant protein indicates that FABP5 exists solely in a monomeric population (data not shown), despite the presence of various bacterial LCFAs, suggesting that fatty acids do not alter the oligomerization state of the protein.

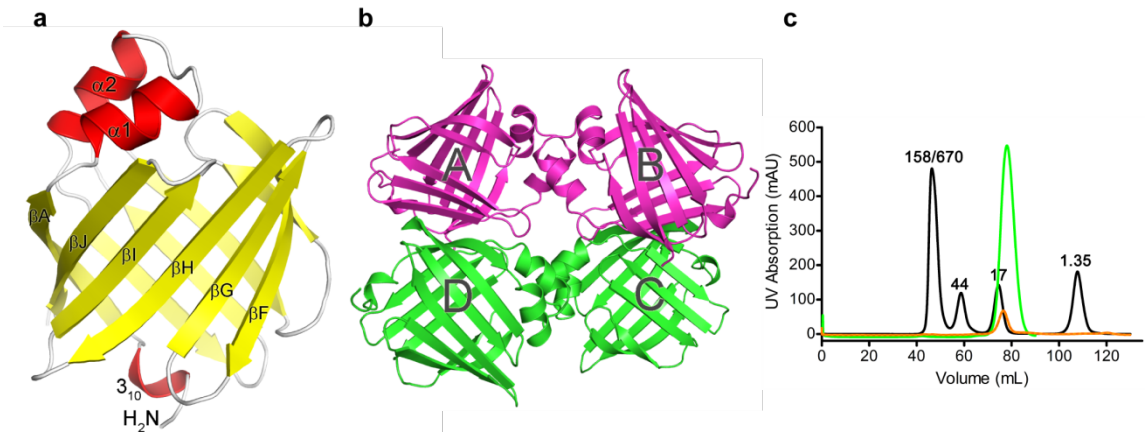

2-1. Structural overview of apo vs. LA-bound FABP5

a, tertiary structure of *apo* FABP5. Unbound protein adopts the familiar β-barrel fold capped by an α-helical lid, with a 3_{10} helix at the N-terminus. *b*, asymmetric unit of the FABP5-LA crystal, comprised of four copies of ligand bound protein. *c*, Overlay of size exclusion chromatographs for *apo* (orange) and LA-complexed (green) FABP5. Standard consisting of 1.35, 17, 44, 158, and 670 kDa markers is in black.

	Apo FABP5	FABP5-LA
Data collection		
Space group	$P4_32_12$	$P3_221$
Cell dimensions		
a, *b*, *c* (Å)	63.0, 63.0, 74.5	145.3, 145.3, 81.8
α, β, γ (°)	90.0, 90.0, 90.0	90.0, 90.0, 120.0
Resolution (Å)	1.67 (1.73 – 1.67)*	2.60 (2.69 – 2.60)*
R_{sym} or R_{merge}	4.2 (38.9)	12.0 (56.0)
I / σI	42.86 (4.45)	20.15 (3.03)
Completeness (%)	99.9 (99.4)	99.9 (99.9)
Redundancy	9.1 (6.8)	9.3 (7.5)
Refinement		
Resolution (Å)	1.67	2.60
No. reflections	18008	31542
R_{work} / R_{free}	18.1 / 21.5	20.5 / 25.9
No. atoms		
Protein	1095	4243
Ligand/ion	15	196
Water	111	69
B-factors		
Protein	19.8	46.7
Ligand/ion	28.3	63.8
Water	31.2	43.6
R.m.s. deviations		
Bond lengths (Å)	0.015	0.003
Bond angles (°)	1.825	0.624

2-1. Data collection and refinement statistics (molecular replacement)

* Data collected from a single crystal; values in parentheses are for highest-resolution shell.

2.3.2 Linoleic Acid Binds FABP5 In Two Distinct Conformations

The FABP5–LA interactions are in general very similar to those previously described by Hohoff *et al.* in their analysis of FABP5 complexed to an *E. coli* fatty acid (264). The carboxylic head group of LA forms a salt bridge with Arg-129, as well as a hydrogen bond with the hydroxyl moiety of Tyr-131. An additional hydrogen bond interaction is observed between LA and Arg-109 via an ordered water molecule (Figure 2-2a). The alkyl tail of the fatty acid is largely stabilized by Van der Waals interactions made with the hydrophobic sidechains of multiple amino acids that line the binding pocket, including Cys-120. Intriguingly, whereas all previous structural studies of FABP5 have shown this amino acid to participate in disulfide bond formation with Cys-127, electron density reveals the unequivocal presence of both amino acids in their sulfhydryl forms within all four monomers of LA-bound FABP5 (Figure 2-2b) (264; 265). In contrast, the *apo* protein contains a mixture of cysteine-cystine forms (Figure 2-2c). Since the *E. coli* fatty acid in the Hohoff *et al.* structure could only be modeled at 50% occupancy (264), we conclude that the absence of a disulfide bridge within FABP5-LA is the result of the ligand being fully bound, and likely helps to accommodate the ~191 $Å^3$ increase (averaged across all four FABP5-LA monomers) in ligand pocket volume as compared to *apo* protein (301).

Inspection of the water network within the binding pocket of the *apo* and LA *holo* proteins reveals a much higher number of ordered water molecules located within the top half of the β-barrel nearer the α-helix lid than in the bottom half nearer the proteins' termini. Though the presence of ligand is responsible for partial rearrangement of this network, waters 2, 7, 15, 31, 38, and 82 in *apo* FABP5 remain virtually unaltered

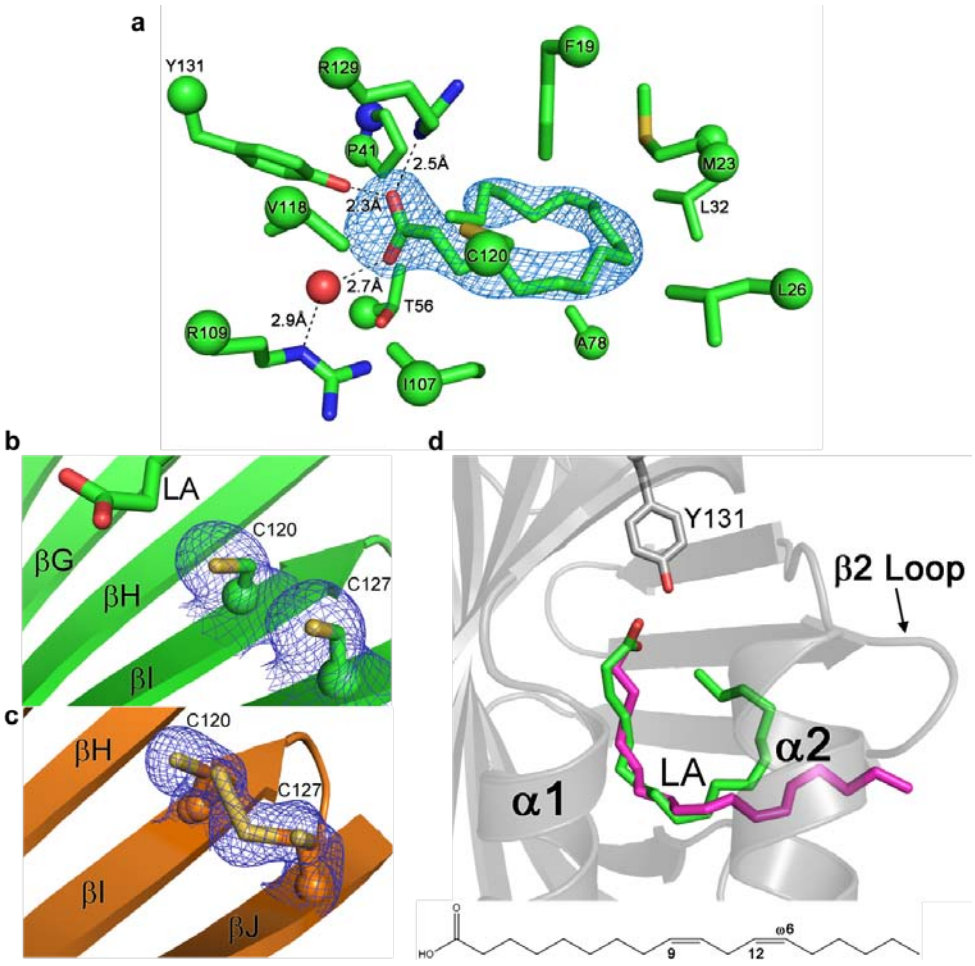

2-2. Analysis of FABP5 ligand binding pocket and LA's bound conformations

a, LA is held within FABP5 via a salt bridge and hydrogen bonding with its carboxylic headgroup, and hydrophobic interactions with its alkyl tail. *b* and *c*, C120 and C127 are unequivocally in their sulfhydryl forms in the presence of LA (*b*), yet are able to adopt either free or disulfide bond states within *apo* FABP5 (*c*). The simulated annealing $F_o - F_c$ omit map of electron density was contoured at 2.5σ for *a*, while $2F_o - F_c$ electron density maps were modeled at 1σ for *b* and *c*. *d*, conformation of LA when bound to monomers A and B (purple) vs. monomers C and D (green) in the FABP5-LA crystal structure (see Figure 2-1*b*).

between the two structures, suggesting their importance in maintaining binding pocket architecture. Conservation of such a relatively large number of FABP5's ordered waters likely reflects the protein's heavy reliance upon enthalpic versus entropic contributions in binding fatty acids, a property common to the protein class (306).

Although monomers C and D bind LA in the traditional U-conformation most commonly seen for fatty acids within the binding pockets of iLBP subfamily IV members (FABP 3-5, and 7-9), LA adopts a bent, or "L" conformation within the pockets of monomers A and B (8; 11; 280). Overlay of the two ligand configurations from monomers B and C reveal a high degree of positional similarity between the acidic headgroup and carbons 1 through 10 of the aliphatic chain. However, while the *cis*-9 and 12 double bonds of U-conformation LA provide the two turns necessary for keeping the entire ligand inside the binding cavity, the L-conformation only features the first turn, resulting in the protrusion of the fatty acid tail from the β2 portal loop of the protein (aas 58-62) into solvent (Figure 2-2d). Though electron density and isotropic B-factors indicate that the U-conformation is more highly ordered, LA is likely able to switch between the two binding states within FABP5 in solution.

2.3.3 Conformation of the Bound Fatty Acid Dictates Activation of FABP5

Studies conducted with FABP4 show that fatty acids which are presumably unable to cause its nuclear translocation bind in a manner that disrupts the protein's β2 portal loop, similar to LA's L-conformation (293; 307). Thus, it was reasoned that LA's U-conformation correlates to its FABP5 activating form, while the L-conformation represents a non-activating binding mode. Based on this rationale, FABP5-activating fatty acids could be predicted based on their propensity to adopt a similar U vs. L-

configuration when bound to the protein. To test this hypothesis, four lipids in addition to LA were selected for functional analysis: arachidonic acid (AA), a 20 carbon polyunsaturated ω-6 fatty acid known to activate PPARβ/δ (219), palmitoleic acid (PoA), a 16 carbon monounsaturated ω-7 fatty acid, sapienic acid (SpA), a 16 carbon monounsaturated ω-10 fatty acid, and the fully saturated 16 carbon palmitic acid (PA) (Table 2-2). Assuming that their ability to favor an activating binding mode within FABP5 correlates to their natural degree of conformational curvature, AA was predicted to be a FABP5-activating fatty acid, similar to LA, while PoA, SpA, and PA were predicted non-activators.

To gauge an appropriate range of ligand concentrations needed for FABP5 activation assays, we determined the affinity of FABP5 for the five fatty acid candidates by testing their ability to displace the fluorophore 1,8-ANS from the lipid binding pocket, as previously described (303). The binding constants obtained for AA, LA, PoA, and PA (Table 2-3) are somewhat higher than those calculated previously using a similar technique, falling within the range of affinities measured via the Lipidex method (264; 289). Additionally, our results indicate that FABP5 binds AA significantly worse than the other candidates, while exhibiting a relatively high affinity for PA (Figure 2-3a). Thus, in our hands, the binding preference of FABP5 approximately correlates with fatty acid aqueous solubility, a phenomenon known as the “solubility hypothesis” that has been used to characterize the ligand affinity trends of proteins throughout the group (308; 309).

We then examined the proclivity of these fatty acids to drive FABP5 nuclear localization. Endogenous FABP5 localizes primarily to the cytoplasm; however, overexpression of the protein combined with the innate ability of EGFP to partially

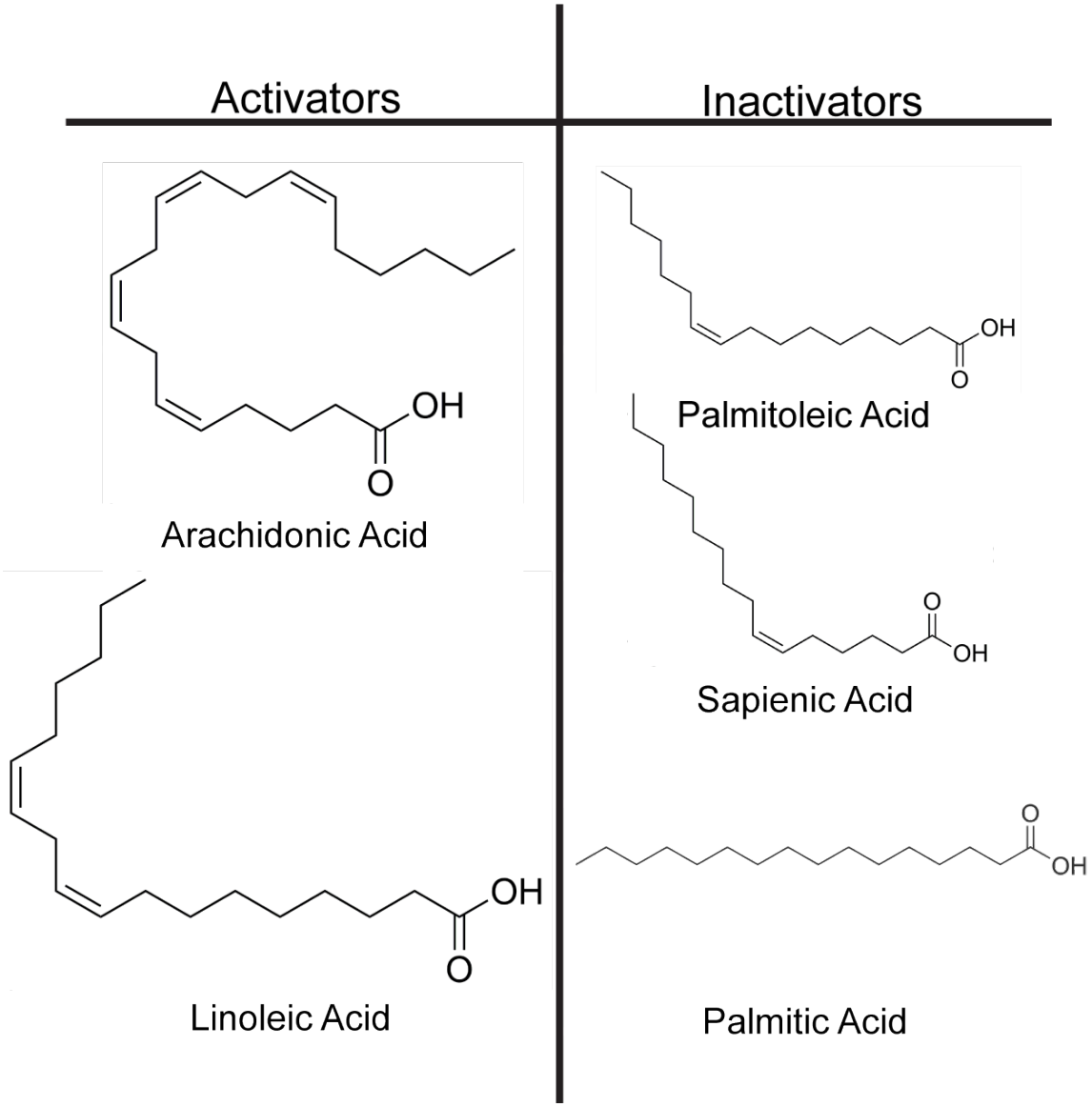

2-2. Proposed fatty acid activators and non-activators of FABP5

FABP5	Ligand	Binding Constant(μM)	95% Conf. Interval(μM)
WT	ANS	6.57 (K_D)	5.68 - 7.47
WT	AA	2.59 (K_i)	1.77 - 3.77
WT	LA	1.26 (K_i)	0.84 - 1.88
WT	PoA	1.36 (K_i)	1.12 - 1.66
WT	SpA	1.10 (K_i)	0.89 - 1.36
WT	PA	0.67 (K_i)	0.52 - 0.87
NLSm	ANS	12.64 (K_D)	11.50 - 13.78
NLSm	AA	9.37 (K_i)	7.40 - 11.86
NLSm	LA	2.17 (K_i)	1.40 - 3.37
NLSm	PoA	1.64 (K_i)	0.99 - 2.71
NLSm	SpA	1.24 (K_i)	0.66 - 2.31
NLSm	PA	3.06 (K_i)	1.74 - 5.36
DSm	ANS	6.10 (K_D)	5.53 - 6.68
DSm	AA	5.01 (K_i)	3.79 - 6.62
DSm	LA	3.47 (K_i)	1.80 - 6.69
DSm	PoA	1.78 (K_i)	0.92 - 3.45
DSm	SpA	0.70 (K_i)	0.31 - 1.61
DSm	PA	0.69 (K_i)	0.54 - 0.88

2-3. Binding constants for wild type and mutant FABP5

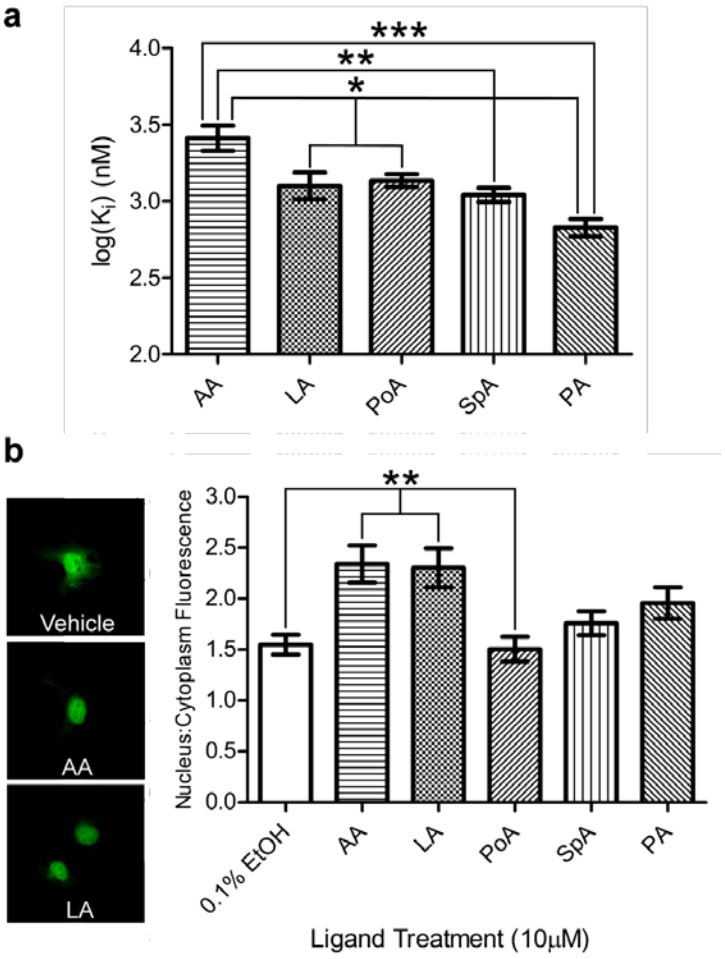

2-3. Fatty acid binding and induced nuclear localization of FABP5

a, binding of FABP5 to each fatty acid candidate was measured via 1,8-ANS displacement assay (n=6), revealing a significantly lower affinity for AA. *b*, confocal images such as those represented on left of EGFP-FABP5 expressing COS-7 cells exposed to 10 μM fatty acid or 0.1% ethanol vehicle were quantified using ImageJ (right, n=30), with LA and AA exposure resulting in higher nuclear:cytoplasmic fluorescence intensity. The mean ± S.E. is shown. Statistical analyses were performed using one-factor ANOVA, with Tukey HSD post hoc tests used for individual comparisons. *: $p \leq 0.05$, **: $p \leq 0.01$, ***: $p \leq 0.001$.

localize to the nucleus results in the presence of FABP5-EGFP construct throughout the cell, even in the absence of ligand (Figure 2-3b,Top Panel) (268; 310). Therefore, to obtain a robust measurement of ligand-induced nuclear localization, we quantified the ratio of nuclear fluorescence to cytoplasmic fluorescence, and averaged this value for 30 cells per condition. LA treatment resulted in a statistically significant increase in nuclear localization compared to 0.1% ethanol (vehicle) treatment only, thus confirming LA as an activating ligand of FABP5 (Figure 2-3b). Additionally, AA exposure led to the highest increase in nuclear:cytoplasmic average fluorescence, while PA, SpA, and especially PoA, had no significant effect. These results designate AA as a newly discovered FABP5 activator.

As FABP5 has been shown to participate in a direct signaling pathway with PPARβ/δ (25), we investigated the protein's ability to enhance AA and LA induced PPARβ/δ activation. To reduce background, assays were carried out in MCF-7 cells, which produce very low levels of endogenous FABP5. Verification of PPARβ/δ activation as a suitable metric for fatty acid signaling was first conducted in cells overexpressing receptor only. Exposure of cells to high concentrations (100 μM) of either LA or AA resulted in an increase in PPAR promoter-driven luciferase expression (2.4 and 4.7-fold, respectively), corroborating previous findings that both ligands are able to bind (215) and agonize (219) the receptor (Figure 2-4a). Surprisingly, the other unsaturated fatty acid candidates were able to activate PPARβ/δ at levels comparable to or greater than LA, allowing their signaling ability to also be measured (Figure 2-4a). FABP5 overexpression augmented AA agonism of PPARβ/δ starting at 40 μM, with the effect becoming more pronounced at higher concentrations (Figure 2-4b). PPARβ/δ activation in the presence of

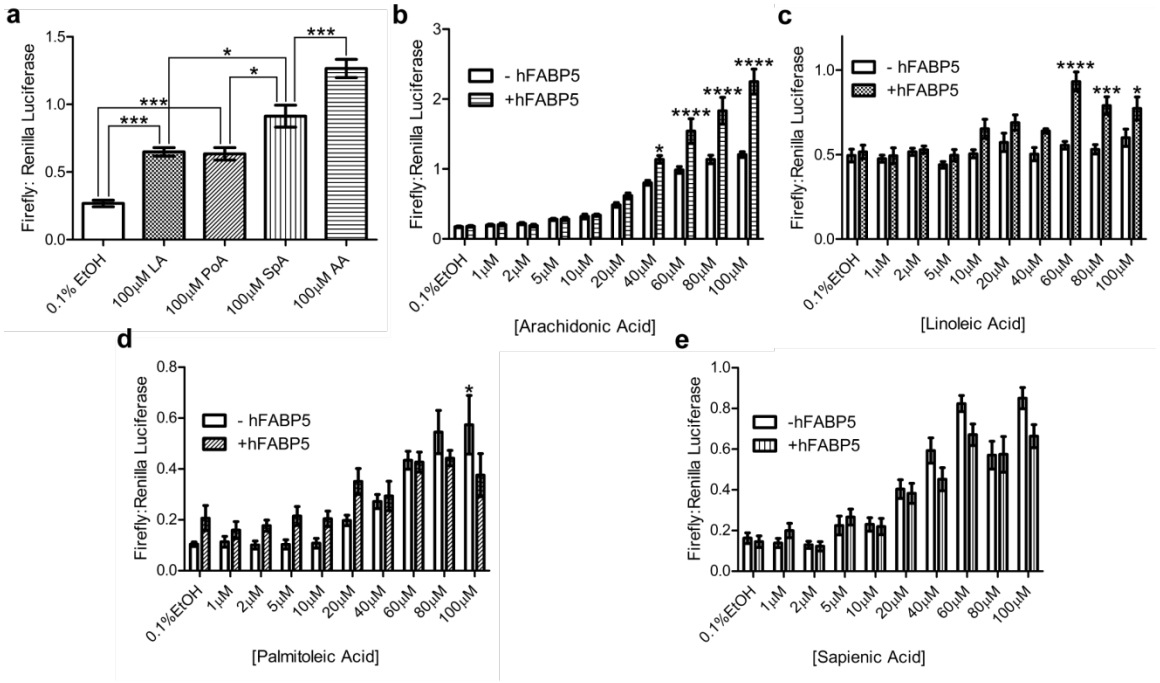

2-4. PPAR β/δ activation by fatty acids in the presence and absence of FABP5 overexpression

a, all unsaturated fatty acid candidates' exposure to MCF-7 cells in the absence of overexpressed FABP5 resulted in PPAR β/δ activation, albeit with varying efficacy, as measured by luciferase reporter assay (n=6). *b* and *c*, overexpression of FABP5 enhanced both AA and LA-induced PPAR β/δ activation at ligand concentrations of 40-100 μM and 60-100 μM, respectively (n=6). *d* and *e*, the presence of overexpressed FABP5 was unable to enhance activation of PPAR β/δ by the fatty acids PoA and SpA, with an opposing effect seen at the highest concentration of PoA tested (n=6). Statistical analysis was performed using either one-factor (*a*) or two-factor (*b*-*e*) ANOVA, with Tukey HSD (*a*) or Bonferroni (*b*- *e*) post hoc tests used for individual comparisons. *: $p \leq 0.05$, ***: $p \leq 0.001$, ****: $p \leq 0.0001$. The mean ± S.E. is shown for all data points.

LA was also enhanced by overexpression of FABP5, the effect being first observed at 60 μM fatty acid and gradually diminishing at 80 and 100 μM (Figure 2-4c). In contrast, FABP5 did not enhance PoA nor SpA induced receptor activation, even leading to a dampening of response at 100 μM PoA (Figure 2- 4d,e).

2.3.4 FABP5 Contains a Ligand-Sensitive NLS Within Its α Helical Lid

We next set out to determine the structural mechanism responsible for the ligand-specific nuclear translocation of FABP5. FABP5 does not harbor a classical NLS within its primary sequence. However, studies conducted on the iLBPs cellular retinoic acid binding protein 2 (CRABP-II) (177) and FABP4 (286) prompted us to search for a tertiary, or cryptic, NLS within the 3 dimensional structure. As the vast majority of all known NLS motifs are highly basic in nature (311), we created an electrostatic potential map of FABP5, which clearly displays a large patch of positive charge located on the surface of the protein's α helical cap. Within this region we identified two well ordered, solvent exposed lysines (Lys-24 and Lys-34) and an arginine (Arg-33), homologous to the NLS residues of CRABP-II and FABP4 (shown in overlay with monomer C of FABP5-LA) (Figure 2-5a).

To test the role of these residues in nuclear import, we created FABP5NLSm, in which Lys-24, Lys-34 and Arg-33 were substituted with alanines. The substitutions had no impact on expression, purification, or stability (data not shown). All fatty acid candidates were able to successfully compete 1,8-ANS from the protein's binding pocket, although the NLS mutant exhibited reduced binding affinity for AA and PA (Figure 2-5b,c, Table 2-3). Cell localization assays reveal that FABP5NLSm is unable to translocate

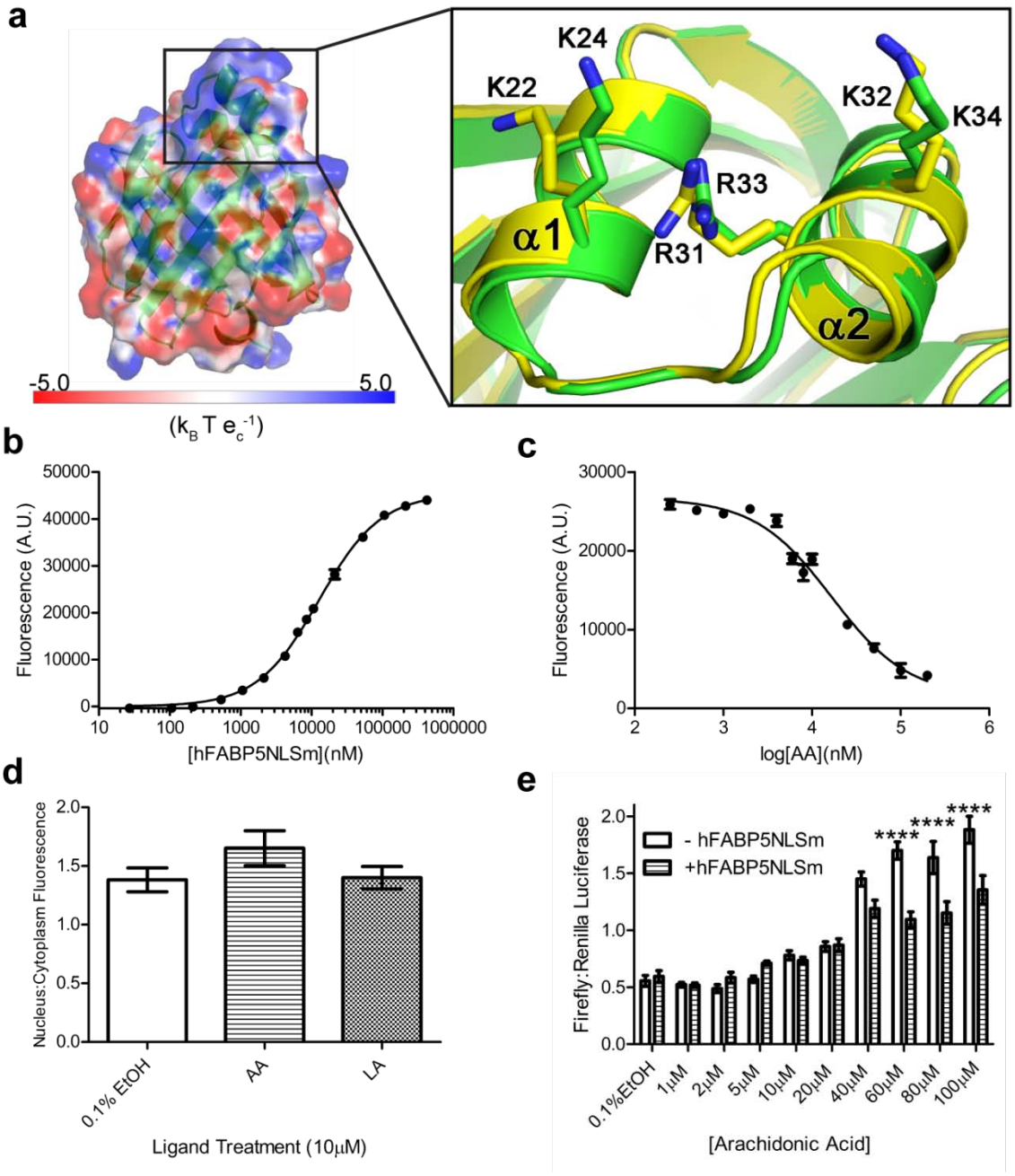

2-5. The tertiary nuclear localization signal of FABP5

a, surface potential of FABP5 bound to LA in the active "U" conformation. Units are in multiples of 26.7 mV (k_B: Boltzmann's constant, T: Temperature, e_c: Electron charge). Overlay of activated FABP5-LA (green) with FABP4 bound to 1,8-ANS (yellow, Protein

Data Bank code 2ANS) reveals FABP5's homologous tertiary NLS residues: K24, K34, and R33. *b* and *c*, FABP5NLSm was able to bind 1,8-ANS (*b*), which could be displaced from the binding pocket by all fatty acid candidates tested (only AA is shown (c)) (n=6). *d*, neither LA nor AA exposure (10 μM) resulted in significant nuclear translocation of EGFP-FABP5NLSm (n=30), as determined by one-factor ANOVA. *e*, expression of FABP5NLSm resulted in subdued PPARβ/δ activation at AA concentrations of 60, 80, and 100 μM (n=6). Statistical analysis was performed using two-factor ANOVA, with Bonferroni post hoc tests used for individual comparisons. ****: $p \leq 0.0001$. The mea n ± S.E. is shown for all data points.

to the nucleus in the presence of the activators AA or LA (Figure 2-5d). Similarly, FABP5NLSm was unable to enhance AA-induced activation of PPARβ/δ at any of the selected ligand concentrations, instead suppressing PPARβ/δ transactivation at exposure levels of 60, 80, and 100 μM (Figure 2-5e). As these concentrations are 6.4, 8.5, and 10.7-fold, respectively, over the ligand's K_i value, it is extremely unlikely that such effects are attributable to the mutant's altered AA binding ability. Collectively, these data indicate that a cryptic NLS, located on the α helical cap of the fatty acid binding pocket, is required for ligand-dependent activation.

2.3.5 FABP5's NES Equivalent Residues Are Necessary for Protein Stability

FABP4 has been shown to possess a tertiary nuclear export signal (NES) comprised of three leucine residues (Leu-67, Leu-87, and Leu-92) located at the edge of its β-barrel farthest from its α-helix lid (Figure 2-6a) (286). Given their structural similarity, we reasoned that FABP5 might also have a tertiary NES that is formed from residues equivalent to those that belong to the NES of FABP4. A structural overlay of the two proteins reveals the conservation of two of the three leucines (residues 69 and 94) with the third being Phe-89 in FABP5 (Figure 2-6b), a less common though still acceptable NES amino acid substitution owing to its ability to preserve the overall hydrophobic character of the signal (312). However, expression of EGFP tagged FABP5NESm, in which the three residues had been mutated to alanines, resulted in the presence of fluorescing puncta located within both the nuclei and cytoplasm of COS-7 cells (Figure 2-6c), suggesting that the mutations may affect structural integrity.

To address this concern, we carried out guanidinium hydrochloride (GnHCl) unfolding of both FABP5NESm and wild type protein, using maximal intrinsic

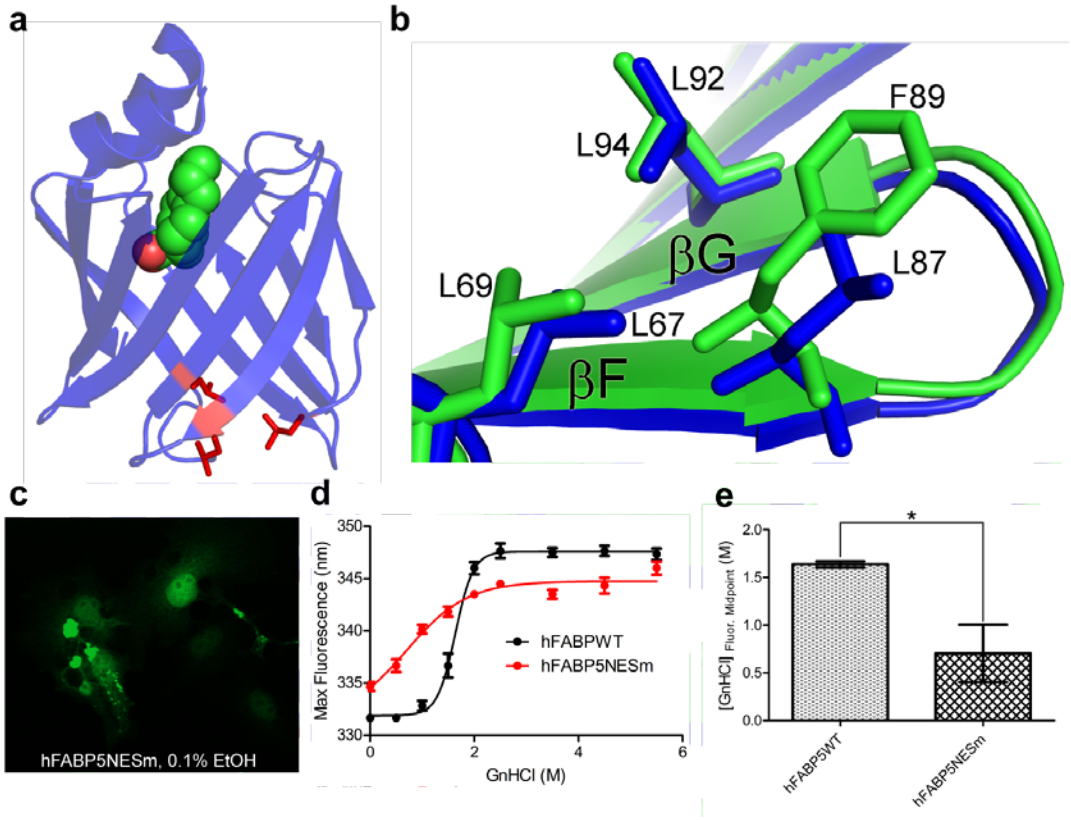

2-6. The putative nuclear export signal of FABP5

a, crystal structure of FABP4 bound to LA (Protein Data Bank code 2Q9S), with the leucine residues composing the tertiary NES shown in red. *b*, Overlay reveals strong similarity between the NES of FABP4 (blue) and the potential NES of FABP5 (green). *c*, representative confocal image of untreated COS-7 cells expressing EGFP-FABP5NESm, displaying aggregation of mutant protein. *d*, unfolding curves, as measured by protein maximum fluorescence shift, for purified FABP5WT vs. FABP5NESm in the absence of ligand addition (n=6). The mean ± S.E. is shown for all data points. *e*, comparison of the calculated fluorescence intensity shift midpoint for both proteins reveals that wild type FABP5 is significantly more resistant to chemical denaturing than the NESm construct. Statistical analysis was performed using an unpaired t-test with Welch's correction. *: $p \leq 0.05$.

fluorescence intensity wavelength as an indicator of tertiary structure. The unfolding curve of unaltered FABP5 is sigmoidal in nature with the protein exhibiting an average max fluorescence wavelength of 331 nm in the absence of denaturant. On the other hand, FABP5NESm's curve appears substantially more linear, with an average maximum fluorescence wavelength of nearly 335 nm at 0 M GnHCl, indicating a partially denatured resting state of the mutant protein (Figure 2-6d). The concentration of GnHCl necessary to induce the midpoint in maximal intensity wavelength shift varied significantly between proteins, at 1.64±0.03 M for wild type FABP5, and 0.70±0.30 M for FABP5NESm (Figure 2-6e). Therefore, since mutating residues 69, 94 and 98 reduced protein stability, we were unable to positively confirm the presence or identity of the NES.

2.3.6 Ligand-Specific Dynamics Between β2 Loop and α2 Helix Drives Tertiary NLS Formation

Having identified the cryptic NLS within FABP5, we lastly directed our efforts to elucidating a possible driving force responsible for ligand-specific NLS formation. The βC-D, or β2 loop, along with the βE-F loop and α2 helix together constitute the portal domain (21), a feature common throughout the FABPs that is hypothesized to gate ligand access to and from the binding pocket (306) and which has been shown to display structural mobility within FABP5 (265). Analysis of the backbone temperature values for *apo* FABP5 lends support for this domain's relatively more labile nature, with the average B-factors of the α2 helix (20.95 Å^2) and especially the β2 loop (28.42 Å^2) considerably higher than that for the entire protein (16.3 Å^2) (Figure 2-7a). Furthermore, overlay of FABP5-LA in its proposed activated (monomer C) vs. inactivated state (monomer B) reveals that, to avoid a collision with L-conformation LA, the backbone of residues 59-61

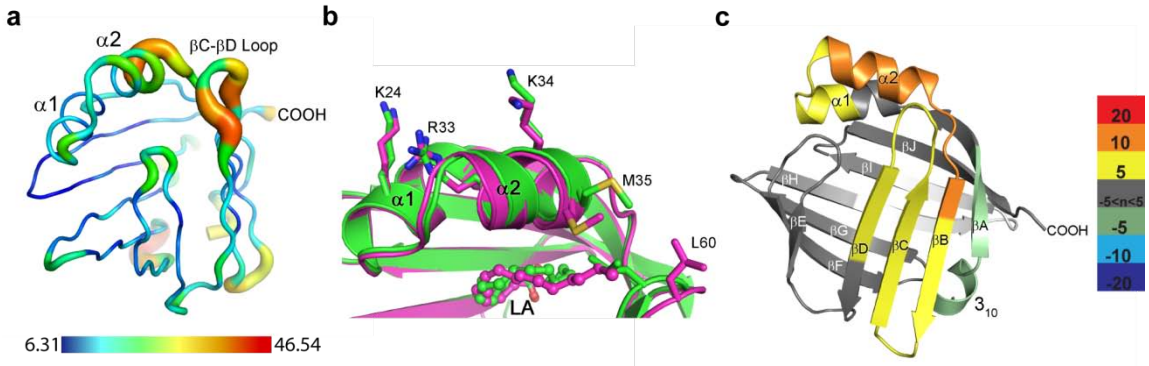

2-7. The structural mechanism driving FABP5 activation

a, putty representation of the backbone of *apo* FABP5 with B-factor color coordination displaying elevated thermal movement within α2 helix and βC-βD loop. Scale is in units of $Å^2$. *b*, the portal loop of both monomers of FABP5-LA is ordered, yet owing to the "L" conformation of LA, assumes a more open position farther from the α2 helix in its presumed inactivated (purple) vs. activated (green) state. *c*, HDX analysis difference map of FABP5WT-PoA minus FABP5WT-AA avg. percent deuterium uptake values shows loss of protection from deuterium exchange across the entire portal region of FABP5, including the βC-βD loop and α-helical cap in the presence of PoA vs. AA. Portions of the protein colored in white indicate a lack of peptide data coverage. Color bar displays cutoff values for avg. percent deuterium uptake differences.

within the β2 loop must shift away from the rest of the protein body, assuming a conformation in which there is less contact with α-helix 2 (Figure 2-7b).

To probe the dynamics of FABP5 bound to a non-activator vs. activator, we utilized HDX, which provides an unbiased assessment of backbone motion in solution. The difference in percent deuterium uptake revealed weaker protection of residues that comprise the α2 helix and β2 loop within FABP5-PoA relative to FABP5-AA, indicating decreased stabilization of these elements (Figure 2-7c). Taken together with our crystallographic data, we hypothesize that the interaction between the α2 helix and the β2 loop via residues Met-35 and Leu-60 determines the activation state of the protein (Figure 2-7b,c). When bound to a fatty acid with a solvent exposed alkyl tail, the loop must remain open. This breaks contact between Met-35 and Leu-60, destabilizing the α2 helix and thereby rendering FABP5 inactive. Conversely, binding to a more compact, sterically constrained fatty acid such as AA allows for loop closure, providing the additional hydrophobic contacts required to stabilize the α2 helix. This results in a more coalesced formation of the NLS and likely drives protein activation.

To examine the potential role of Met-35 and Leu-60 as ligand conformation sensing "activation switches," we reduced their hydrophobic interaction via mutation of both residues to alanines, creating a "double-switch" mutant of FABP5 (FABP5DSm). These mutations had no major impact on ligand binding *in vitro* (Figure 2-8a,b, Table 2-3), yet HDX analysis reveals that they decrease the stability of the α2 helix–β2 loop interface within the mutant protein bound to AA, relative to the wild type protein AA complex (Figure 2-8c). Thus FABP5DSm does not possess the allosteric coordination that senses and relays information from AA to the NLS. Additionally, comparison of

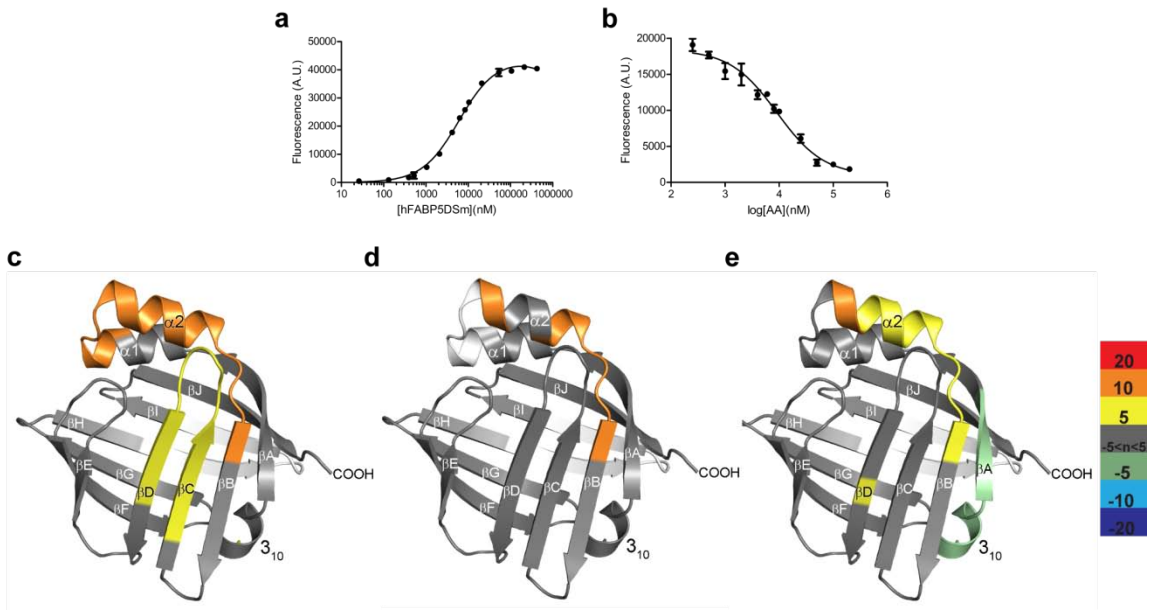

2-8. Structural determination of FABP5's activation switch residues

a and *b*, FABP5DSm was able to bind both the fluorophore 1,8-ANS (*a*) as well as all fatty acid candidates tested (only AA is shown (*b*)) (n=6). *c*-*e*, HDX analysis difference map displaying the avg. percent deuterium uptake values of FABP5DSm-AA minus FABP5WT-AA (*c*), FABP5DSm-PoA minus FABP5WT-PoA (*d*), and FABP5DSm-PoA minus FABP5DSm-AA (*e*) confirms that the mutation of residues Met-35 and Leu-60 results in perturbed βC-βD loop/α2 helix dynamics, resulting in a mutant protein less sensitive to the structural changes brought about by AA vs. PoA binding. Portions of the protein colored in white indicate a lack of peptide data coverage. Color bar displays cutoff values for avg. percent deuterium uptake differences.

mutant to wild type protein when both are bound to the non-activating PoA displays far fewer differences in subsequent deuterium exchange, indicative of largely equal states of loop/helix disruption (Figure 2-8d). This effect can also be observed in the HDX analysis of FABP5DSm-PoA relative to FABP5DSm-AA, which, when compared to Figure 2-7c, clearly illustrates the mutant's severely hampered ability to structurally distinguish activating from non-activating ligand (Figure 2-8e).

Finally, we conducted cellular assays with the double-switch mutant protein to provide biological verification of the results obtained from HDX. While LA exposure was unable to induce additional FABP5DSm nuclear localization, AA treatment actually resulted in increased cytoplasmic localization (Figure 2-9a). Reporter gene assays confirmed a loss in signaling ability of FABP5DSm, with expression of the protein resulting in diminished AA-induced PPARβ/δ activation at 60-100 μM AA (Figure 2-9b). These conclusions are further strengthened by the more striking direct comparison of normalized AA dose responses in the presence of wild type and mutant FABP5 (Figure2-9c). While overexpression of FABP5WT causes a continual increase in nuclear receptor activation with greater concentrations of AA, expression of either mutant results in a plateau of response beginning at 40 μM ligand. Such a similarity in effect between mutants underscores both the importance of the NLS as well as the switch residues Met-30 and Leu-60 in FABP5 activation.

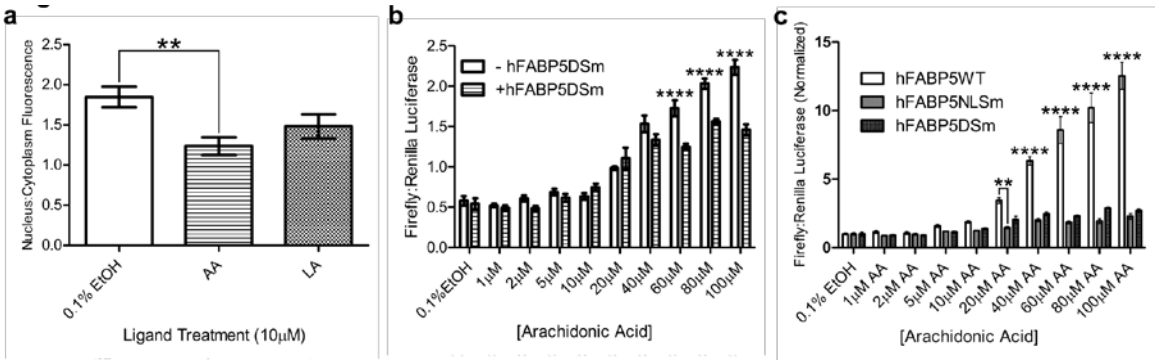

2-9. Biological verification of FABP5's activation switch residues

a, neither LA nor AA exposure induced nuclear translocation of FABP5DSm, with the presence of AA leading to significantly reduced levels of "switch mutant" protein within the nuclei vs. cytoplasm of COS-7 cells (n=30). *b*, FABP5DSm expression significantly suppressed AA-induced PPAR β/δ activation at concentrations of 60, 80, and 100 μM (n=6). *c*, direct comparison of AA dose responses of PPAR β/δ in the presence of FABP5WT, FABP5NLSm, or FABP5DSm. Data sets were taken from Figures 2-4b, 2-5e, and 2-9b, and normalized internally by dividing all replicate values by the avg. value obtained from vehicle treatment only. Statistical analyses were performed using either one-factor (*a*) or two-factor (*b*,*c*) ANOVA, with Tukey HSD (*a*) or Bonferroni (*b*,*c*) post hoc tests used for individual comparisons. **: $p \leq 0.01$, ****: $p \leq 0.0001$. The mean ± S.E. is shown for all data points.

2.4 Discussion

Since the discovery of the first FABPs by Ockner *et al*. over 40 years ago (313), a wealth of data has steadily accumulated regarding this class of proteins' structures and functions (6). While the vast majority of structural studies have focused on the determinants of stability and ligand binding, almost no attention outside of FABPs 1 and 4 has been given to the physical mechanisms driving signal propagation and protein-protein interaction (286; 293; 314-316). We have expanded understanding of FABP signaling by identifying the molecular switch that dictates fatty acid-specific activation, whereby the conformation of bound LCFA relays information from what we now term the "activation loop" (βC-D) of the portal region to the protein's tertiary NLS, consisting of Lys-24, Arg-33 and Lys-34.

In this way, FABP5 shares key mechanistic elements from both FABP4 and CRABP-II, yet ultimately undergoes a method of activation different from either. Like FABP4, only certain ligands cause nuclear localization of the protein (25; 293). However, instead of dimer rearrangement driving the cytosolic exposure of the NLS, FABP5, like CRABP-II, remains monomeric, with binding of activating ligand resulting in stabilization of the NLS that is necessary for nuclear import (177; 293). Interestingly, while this process can occur in as little as 30-60 min. for all three proteins, the ensuing enhancement of nuclear receptor driven gene transcription is most frequently tested 24 h after ligand introduction (176; 286; 317). This time difference could explain, at least in part, why 10 μM AA and LA are sufficient for our localization assays, but not for FABP5 enhanced transactivation of PPARβ/δ, as ligand degradation and metabolism become more relevant over time.

Sequence alignment in Clustal Omega (318) of all 9 human FABP members with other iLBPs known to participate in ligand mediated signaling reveals that FABP8, a major protein constituent of peripheral nervous system myelin (319), contains residues homologous to the cryptic NLS present in FABPs 4, 5 and CRABP-II, as well as to the pair of bulky/hydrophobic amino acids which constitute the ligand dependent activation switch (Figure 2-10). This raises the possibility that myelin FABP could also undergo directed nuclear localization; however, the same NLS homology is also found within the α-helices of the iLBP cellular retinol binding protein I (CRBP-I), where it governs the protein's retinol dependent interaction with the transmembrane receptor stimulated by retinoic acid 6 (STRA6) (320). Therefore, the potential of FABP8 to engage in a ligand-driven signaling pathway other than nuclear translocation cannot be discounted. Based on its predicted amino acid sequence (not shown), the same directed inquiries can also be made for the newly discovered FABP12, though its presence within cells has not been documented beyond the mRNA level (321).

Additionally, we have shown that a single fatty acid can adopt at least two unique conformations within the binding pocket of FABP5. While FABP-bound FA tail mobility has been noted previously via X-ray crystallography (322), our delineation of an active U-conformation vs. inactive L-conformer opens up exciting new possibilities for structure based drug design. The overexpression of FABP5 has been linked to insulin resistance (266), and its signaling related to cancer cell survival (268), proliferation (269; 271), and metastasis (272; 291), making the protein an ideal candidate for antagonist development. Theoretically, such compounds could exert their influence via one of several mechanisms of action. The first would be to bind and disrupt the portal region,

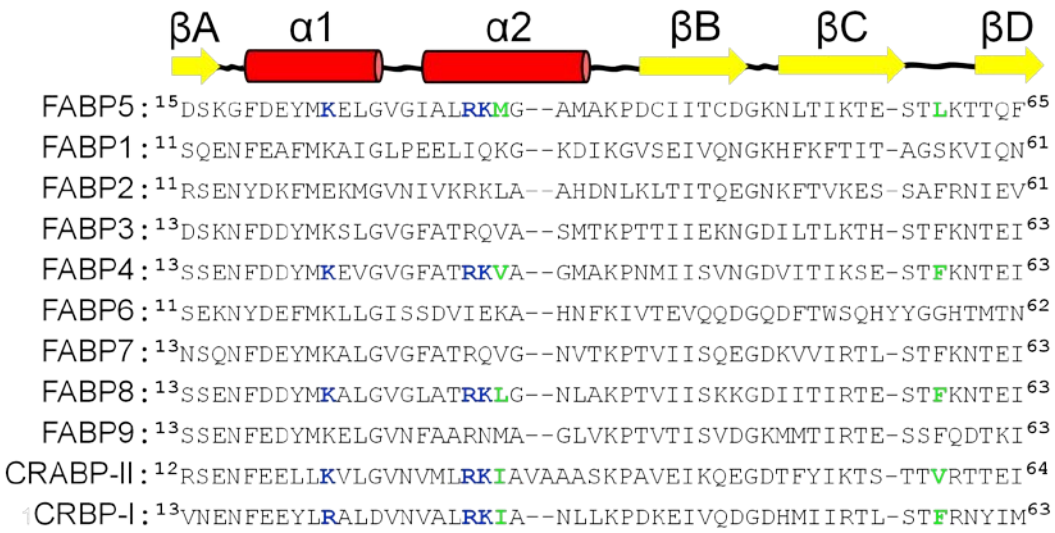

2-10. Alignment of FABP1-9 with CRABP-II and CRBP-I

Sequence alignment of the region in FABP5 shown to be most affected by ligand induced activation with that of the other human FABPs as well as CRABP-II and CRBP-I. FABP8 is the only protein in its class that harbors all three homologous NLS residues (bold, blue) and appropriately bulky/hydrophobic “switch” residues (bold, green), yet is currently untested for ligand driven nuclear translocation.

forcing the activation loop into its inactive state. The second would be to bind completely within the binding pocket, allowing closure of the activation loop and subsequent nuclear translocation of the protein, though the compound itself would be unable to bind PPARβ/δ. The third, and likely most effective, would be to improve the nuclear accumulation of current PPARβ/δ antagonists by optimizing their ability to bind and activate FABP5.

Conversely, our fatty acid binding model can be used for the prediction of additional FABP5 activators. We have demonstrated that the state of unsaturation is one of the major determinants of a fatty acid's activation potential, presumably due to its affect on U-conformation preference within the binding pocket. Judging from the configurations seen within our structures as well as that published by Hohoff *et al*. (264), the first 11-13 carbons share a remarkably close alignment regardless of fatty acid type, thereby placing a greater degree of importance for activator differentiation on the *cis* double bonds located more distal to the carboxylate head group. As both LA and AA were found to be activators, yet PoA (a ω-7 FA) was not, this suggests an intriguing role for FABP5 as a specific mediator for ω-6 and possibly ω-3 fatty acid signaling. Since all unsaturated fatty acids tested, including oleic acid (OA) (data not shown) were able to significantly activate PPARβ/δ in the absence of FABP5, the presence of such a secondary control measure likely serves to ensure preferential activation of the nuclear receptor by this or a similar subset of fatty acids.

CHAPTER 3 : VIABILITY OF A STRUCTURE BASED INVESTIGATION OF NON-CLASSICAL ALL-*TRANS* RETINOIC ACID (ATRA) SIGNALING

3.1 Introduction

For over 50 years the pleiotropic biological effects of all-*trans* retinoic acid (atRA), one of the several major retinoids resulting from the metabolism of Vitamin A, have been studied (113). Beginning in large part with its role in the regulation of teratogenesis, the list has since expanded to include a diverse array of cellular processes in both the embryo and adult organism (119; 323-325). Traditionally, such profundity of atRA-induced cellular response has been ascribed to the retinoic acid receptors (RARs) (119; 324; 326). As class II nuclear hormone receptors, RARs remain localized in the nucleus where they are bound as heterodimers with the nuclear receptor retinoid X receptor (RXR) to hormone response elements (120; 121). Therefore, their level of exposure to atRA is highly dependent on the presence of cellular retinoic acid binding protein-II (CRABP-II), an intracellular lipid binding protein (iLBP) family member located primarily within the endoplasmic reticulum of the cell in its *apo* form (176; 179). Upon binding of atRA, CRABP-II undergoes a conformational shift that results in the formation of a tertiary nuclear localization signal (NLS) in three dimensional space, thus allowing it to be recognized by the importin-α machinery (177). Ensuing nuclear translocation allows for a protein-protein interaction between atRA-bound CRABP-II and RAR, with the ligand being directly “channeled” from CRABP-II to the binding pocket of the nuclear receptor (178; 317). These studies have thus helped to illustrate the mechanism whereby atRA is able to elicit RAR activation, in effect establishing a greater understanding of the “traditional” atRA signaling pathway.

Though RARs' wide spectrum of target genes does lend proof at the molecular level of this receptor group's far reaching physiological impact, RAR signaling power alone cannot explain many of the paradoxical actions of atRA. For example, the activation of RARs by either 9-*cis* (9cRA) or atRA often results in the inhibition of cell proliferation, yet exposure of many cell types to atRA will promote their survival (119). Such a stark dichotomy of observations has eventually led to the proposal of a second and completely novel atRA signaling pathway involving the de-orphanized peroxisome proliferator-activated receptor (PPAR) β/δ.

Like the RARs, the PPARs are class II nuclear receptors (121). However, unlike RARs, which selectively bind 9cRA and atRA with nanomolar and subnanomolar affinity, respectively (327; 328), all three PPAR members are capable of binding to a wide array of hydrophobic ligands, including both saturated and unsaturated long-chain fatty acids ranging in size from 14-20 carbon units (215) as well as various fatty acid metabolites (216) and eicosanoids (217-219). Despite this degree of promiscuity, atRA not only displays binding selectivity for PPARβ/δ over PPARs α and γ, but also induces both the receptor's association with co-activator proteins as well as the expression of known PPARβ/δ downstream target genes upon exposure to keratinocytes (230; 329). Additionally, the iLBP fatty acid binding protein 5 (FABP5), a known facilitator in both polyunsaturated fatty acid (see Chapter 2) and synthetic ligand-induced PPARβ/δ signaling (25), undergoes increased nuclear localization upon atRA introduction to cell culture (268). Once inside the nucleus, FABP5, like CRABP-II, is proposed to interact with its receptor partner, allowing for direct transfer of its bound cargo into PPARβδ's ligand binding pocket. This, in turn, enhances PPARβ/δ activation and has been shown to

be responsible for the pro-survival role of Vitamin A acid in select cell types (268; 269; 329-331). Nevertheless, many key components of this novel atRA pathway remain to be elucidated, such as the possible formation of a cryptic NLS within FABP5 upon its binding to atRA, the ability of atRA to elicit an activated conformation within PPARβ/δ, and proof at the molecular level of FABP5-PPARβ/δ complex formation with subsequent ligand channeling. To test these hypotheses, we used ligand binding assays, gel filtration chromatography, isothermal titration calorimetry, protein complex crosslinking, and X-ray crystallography to assess the validity of engaging in a directed study of the atRA-FABP5-PPARβ/δ pathway from a structural perspective.

3.2 Methods

Reagents - Chemicals for buffers and atRA were purchased from Sigma. 1,8-ANS and LA were purchased from Cayman Chemical Company. The crosslinker bis(sulfosuccinimidyl)suberate (BS^3) and Spectra Multicolor Broad Range Protein Ladder were purchased from Thermo Fisher Scientific, Inc. Precision Plus Protein Kaleidoscope Standards was purchased from Bio-Rad Laboratories, Inc. Lipidex-1000 resin was purchased from PerkinElmer, Inc., while Phenyl Sepharose High Performance resin was purchased from GE Healthcare Life Sciences. Transcriptional mediators/intermediary factor 2 (TIF2) peptide (sequence: KENALLRYLLDKDD) and its longer variant (TIF2L) (sequence: PVSPKKKENALLRYLLDKDDT) were purchased from Sigma and SynBioSci, respectively. PPARγ coactivator 1α (PGC-1α) peptide (sequence: EEPSLLKKLLLAPA) was also purchased from SynBioSci. Codon optimized DNA

encoding full-length hFABP5 was purchased from GenScript Corp., while DNA constructs for full length hCRABP-II and hPPARβ/δ were purchased from QIAGEN. A vector incorporating DNA corresponding to amino acids 55-529 of human karyopherin-α2 (hKPNA2ΔIBB) was graciously provided by Noa Noy (Case Western Reserve University, Cleveland). The pMCSG7-His vector was a gift from John Sondek (UNC, Chapel Hill), and pET-30a vector harboring the DNA for amino acids 89-542 of yeast importin α (SRP1pΔIBB) was generously given by Anita Corbett (Emory University, Atlanta.)

Cloning - DNA for full length hFABP5, hCRABP-II, and hKPNA2ΔIBB (amino acids 55-529) were subcloned into the pMCSG7-His vector, while the ligand binding domain (amino acids 165-441) of hPPARβ/δ was subcloned into the pRSET-A vector.

Protein Expression and Purification - Full length recombinant hFABP5 in the pMCSG7-His vector was expressed and purified according to the procedure outlined in Chapter 2. Full length hCRABP-II, hKPNA2ΔIBB, and SRP1pΔIBB in pMCSG7-His vectors, and hPPARβ/δLBD in the pRSET-A vector were each transformed in the BL21(PLysS) strain of *E.coli*, which were then grown in 6 1.3 L flasks containing Terrific Broth (12 g L^{-1} tryptone, 24 g L^{-1} yeast extract, 55 mM glycerol, 72 mM dipotassium phosphate, 17 mM monopotassium phosphate) shaking at 210 rpm and 37 °C until a 600 nm optical density (OD_{600}) of 0.8 was reached. Cultures transformed with hCRABP-II were induced with 1 mM IPTG at 32 °C for 4 h, while those harboring the vectors containing hKPNA2ΔIBB, SRP1pΔIBB, and hPPARβ/δLBD were cooled to 20 °C for 1 h before being induced with 1 mM IPTG for 18 h. Bacterial cells were then collected via centrifugation at 5000 rpm for 15 min, lysed, and re-suspended in “Nickel A” buffer (300

mM sodium chloride, 50 mM dipotassium phosphate, 5 % (v/v) glycerol, 25 mM imidazole, pH=7.4). Having been engineered with $[His]_6$ tags, all recombinant proteins were purified via Ni^{2+}-based immobilized metal ion affinity chromatography, using 5 mL HisTrap HP columns (GE Healthcare Life Sciences) pre-equilibrated in Nickel A buffer. After the entire sample was flowed over the column, resin was washed for 3 column volumes with Nickel A, followed by 5 column volumes of 5 % (v/v) Nickel A: Nickel B (300 mM sodium chloride, 50 mM dipotassium phosphate, 5 % (v/v) glycerol, 250 mM imidazole, pH=7.4) mixture at 2 mL min^{-1}. Protein was then eluted with a 50 % (v/v) Nickel A: Nickel B mixture, concentrated, and dialyzed in PBS (137 mM sodium chloride, 2.7 mM potassium chloride, 10 mM disodium phosphate, 1.8 mM monopotassium phosphate, 10 mM β-mercaptoethanol (BME), pH=7.4) overnight. Finally, size exclusion chromatography was performed, using either a Superdex 75 16/30 or Superdex 200 26/60 HiLoad PG column (GE Healthcare Life Sciences) pre-equilibrated in PBS and run at 1 mL min^{-1}.

Electrophoretic Mobility Shift Assays - All protein sample solutions were mixed in a 1:5 ratio with Loading Buffer (50 mM Tris-Hydrochloride, pH =6.8, 100 mM dithiothreitol (DTT), 2 % sodium dodecyl sulfate (SDS), 10 % glycerol, 0.1 % Bromophenol Blue), heated to 99 °C for 1 min, and allowed to cool before being loaded onto a 12.0 % (v/v) SDS polyacrylamide gel for electrophoresis (PAGE). Gels were allowed to run for 35-60 min at 220 V in a Mini-PROTEAN Tetra Cell powered by a PowerPac Basic (Bio-Rad Laboratories, Inc.), before being stained with Coomassie Brilliant Blue G-250 at room temperature overnight, and subsequently de-stained with deionized water.

hFABP5 Delipidation - Delipidation of hFABP5 was carried out by three separate methods: Bligh and Dyer chloroform/methanol extraction (294) followed by protein refolding (see Chapter 2 for details concerning methodology), hydrophobic interaction chromatography (HIC), and Lipidex-1000 treatment. HIC was carried out in a similar fashion to that employed by Velkov et al. (332). Briefly, purified protein in PBS was concentrated to ~1.0 mg mL^{-1}, and dialyzed in PBS containing 3.0 M ammonium sulfate. Sample was then applied to a pre-equilibrated column packed with Phenyl Sepharose HP resin at a flow rate of 3.0 mL min^{-1} and temperature of 20 °C, washed with 40 mL dialysis buffer, and eluted with a 100-0 % gradient of 3.0 M ammonium sulfate over 60 mL. Eluate was once more dialyzed in PBS before being used for ligand binding assays. Additionally, Lipidex-1000 treatment was performed in a fashion similar to what has been previously described (333). In brief, purified hFABP5 in PBS was mixed with Lipidex-1000 resin to partition the bound lipids into the hydrophobic resin, and the slurry was slowly shaken at 65 rpm and 37 °C for 1.5 hrs. Sample was then removed from resin, cooled to room temperature, and filtered.

1,8-ANS Competition Binding Assays - Binding assays using the fluorophore 1,8-ANS were conducted using the procedure outlined in Chapter 2, with few modifications. Complex formation of the fluorescent probe was conducted with a constant concentration of 500 nM 1,8-ANS in PBS, pH=7.4 at 37 °C, with the concentration of purified delipidated/non-delipidated hFABP5 ranging from 10 nM – 402 μM. Blank wells containing protein only were subtracted from those with 1,8-ANS for each protein concentration tested to account for background fluorescence. Competition assays with LA and atRA were carried out by varying ligand concentration in the presence of both 500

nM 1,8-ANS and hFABP5 in PBS, pH=7.4 at 37 °C and room temperature, respectively. Blank wells consisting of ligand and 1,8-ANS only were subtracted from those with protein for each ligand concentration tested. All values were then normalized to the condition in which no competing ligand was present. Data were collected on a BioTek Synergy plate reader using an excitation filter of 380 nm with a 20 nm band pass and an emission filter of 460 nm with a 40 nm band pass, and processed in GraphPad Prism 5 using the "one site, total" binding function to calculate the K_D and K_i values.

atRA Filtration Binding Assays - Purified protein in the presence or absence of co-activator peptide was exposed to varying amounts of atRA via dimethyl sulfoxide (DMSO), ethanol, or buffer stock in either PBS, pH=7.4, pH=8.0, or Buffer E (500 mM ammonium acetate, 20 mM 4-(2-hydroxyethyl)-1-piperazineethanesulfonic acid (HEPES), 10 mM DTT, pH=7.5), the latter of which had been used by Xu et al to purify hPPARβ/δLBD prior to crystallization (215). The total volume of each condition was 35 mL, and incubation of protein and ligand was allowed to progress for 2 hrs at room temperature and in complete darkness before being passed through a 0.2 μm polyethersulfone (PES) sterile syringe filter (VWR) to remove insoluble atRA. Protein from each sample was then placed in an Amicon Ultra-15 centrifugal filter unit (Millipore) with a molecular weight cutoff of 3000 Da, and concentrated to a final volume of 1 mL via centrifugation at 4,000 g in an Allegra X-15R centrifuge with a SX4750A swinging rotor. An absorption profile across a 220-750 nm spectrum was measured from a 2 μL aliquot of concentrated sample via a ND-1000 spectrophotometer (Nanodrop), with the A_{280} and A_{350} values used to calculate the concentration of protein and atRA present, respectively. Extinction coefficients of 14,180 M^{-1} cm^{-1} for hFABP5,

19,543 M^{-1} cm^{-1} for hCRABP-II, and 24,410 M^{-1} cm^{-1} for hPPARβ/δLBD were estimated using the ProtParam tool, part of the ExPASy Bioinformatics Resource Portal, while a value of 37,600 M^{-1} cm^{-1} for atRA in aqueous solution was taken from the literature (334). Identically treated samples in which protein was absent were used as spectrophotometric blanks, and only samples with an A_{280} value 10X greater than that measured for their flow-through were used for analysis.

Crystallization, Data Collection, Structural Refinement - Purified hFABP5 that had been delipidated via the Lipidex-1000 method in PBS, pH=7.4 at a concentration of 20 μM was exposed to a 10X molar ratio of atRA in the presence of 9 % (v/v) DMSO. The resulting solution was sonicated for 40 min, covered, in a bath sonicator (Laboratory Supplies Company, Inc., model G1125PIG), and then passed through a 0.2 μm PES sterile syringe filter. The filtered sample, still observed to be yellow, was next concentrated to ~300 μL in order to achieve a protein concentration of ~15 mg mL^{-1}, and crystals were grown over a month at 4 °C in the dark via hanging drop vapor diffusion, using a mother liquor consisting of 33% (v/v) PEG 4000, 240 mM ammonium acetate, and 100 mM Na citrate, pH=5.4. Crystals were then flash cooled in liquid nitrogen, and 130° of data comprising 260 images were collected at 100 K with a 1.00 Å wavelength beam at the SER-CAT beamline (Advanced Photon Source, Argonne, IL). Data was processed with the HKL-2000 software HKL-2000 (295), and the structure was solved to a resolution of 1.95 Å by molecular replacement in PHASER (296), using our previously solved *apo* hFABP5 structure (PDB code: 4LKP) as a model. Building and refinement were conducted in iterative cycles, using the programs COOT (297) and phenix.refine (298), respectively.

Protein Complex Gel Filtration Assays - Purified hFABP5 and KPNA2ΔIBB at concentrations of 30 μM each were incubated in PBS, pH=7.4 at room temperature for 10 min in the presence of 140 μM LA. Sample (V=3 mL) was then loaded at a flow rate of 1.0 mL min^{-1} onto a Superdex 75 column kept at 12 °C and pre-equilibrated in PBS, and 25 μL aliquots from the 1 mL fractions corresponding to the highest A_{280} values for both major absorption peaks were collected and analyzed via SDS-PAGE. Similarly, purified SRP1pΔIBB and hFABP5 at concentrations of 50 μM and 400 μM, respectively, were mixed for 10 min in PBS, pH=7.4, containing 1 % (v/v) ethanol at room temperature in the presence of 100 μM LA. Sample (V=500 μL) was loaded at a flow rate of 0.4 mL min^{-1} onto a Superose 6 10/300 GL column (GE Healthcare Life Sciences) kept at 12 °C and pre-equilibrated in PBS, and the 0.4 mL fraction corresponding to the highest A_{280} value for the first major absorption peak was collected, concentrated to 50 μL, and analyzed via SDS-PAGE.

Calorimetric Binding Assay - Isothermal titration calorimetry was conducted using a MicroCal Auto-iTC_{200} (GE Healthcare Life Sciences). Both hFABP5 and hKPNA2ΔIBB were purified and dialyzed together overnight in PBS, pH=7.4 to assure exact buffer compatibility. Linoleic acid was added to a final concentration of 445 μM to both protein solutions ($[Ethanol]_{Final}$ = 0.5 % (v/v)), and hFABP5 and hKPNA2ΔIBB were adjusted to final concentrations of 401 μM and 41 μM, respectively. The hFABP5-LA stock was then injected over 35 aliquots (1 μL each) in 3 min intervals at 25 °C, until a nearly 2:1 molar ratio of hFABP5: hKPNA2ΔIBB was reached. Raw data were processed and visualized by the Origin software package supplied by the manufacturer.

hFABP5-hPPARβ/δLBD Complex Crosslinking Assay - Varying amounts of purified hFABP5 ($[hFABP5]_{Final}$ = 1, 10, 33, or 100 μM) were introduced to a fixed amount of purified hPPARβ/δLBD ($[hPPARβ/δLBD]_{Final}$ = 15 μM) in PBS, pH=7.4 with 5 mM BME at 4 °C (V_{Final} = 100 μL/condition). After a 25 min incubation, 1 μL of 25 mM BS^3 linker in PBS was added to the appropriate experiments, and the crosslinking reaction was quenched after 3, 10, or 30 min by the addition of 11 μL of a 250 mM glycine stock in PBS. Conditions in which crosslinker was not added also underwent quenching step for uniformity. A 25 μL aliquot was then taken for SDS-PAGE analysis. Negative control experiments in which maltose binding protein (MBP) was used instead of hFABP5 were conducted simultaneously and in identical fashion, with the exception that $[hPPARβ/δLBD]_{Final}$ = 9 μM and [MBP] = 55 μM.

Structure Overlays and Modeling - Overlay of the structure of atRA-exposed *apo* hFABP5 with that of hCRABP-II bound to atRA (PDB code: 2FR3) was conducted using the PyMOL Molecular Graphics System (Schrodinger, LLC), and yielded a root mean square (RMS) deviation of 1.48 Å using 109 matched homologous residue backbone atoms. Modeling of atRA into the ligand binding pocket of hPPARβ/δ was accomplished in COOT, using the protein coordinates of hPPARβ/δLBD bound to the synthetic agonist GW2433 (PDB code: 1GWX) and the ligand coordinates of atRA bound to hRARγLBD (PDB code: 2LBD). Ligand was placed such that both the orientation and hydrogen bonding distance of its carboxylate group relative to PPARβ/δ residues His-287, His-413, and Tyr-437 followed that of structures in which the nuclear receptor was shown bound to fatty acids (PDB codes: 3GWX, 2BAW, 2B50, 2AWH), and visualization of receptor

binding pocket volume for model representation was carried out with PyMOL (Schrödinger, LLC).

3.3 Results

3.3.1 hFABP5 Does Not Bind atRA at Levels Tractable for Crystallography

The first step in alternative atRA signaling is the binding of the Vitamin A metabolite to FABP5. Therefore, we set out to obtain a crystal structure of the complex, which would not only provide seminal information regarding how a member of the FABP group is able to accommodate a retinoid within its binding pocket, but also delineate the mechanism whereby atRA is able to activate the protein for nuclear translocation. In order to help guide crystallographic trials, we measured hFABP5's affinity for atRA binding via 1,8-ANS displacement, which had been employed previously for fatty acids (see Chapter 2). Since bacterially expressed hFABP5 has been shown to purify bound to various long chain fatty acids (LCFAs) from its host, we first tested whether delipidation of the protein resulted in increased affinity for fluorescent probe (264). Several delipidation methods were selected: Bligh and Dyer chloroform/methanol extraction, Lipidex-1000 chromatography, and hydrophobic interaction chromatography (HIC), a relatively newer procedure that had been used successfully on both hFABP1 and hFABP6 (332). Surprisingly, while HIC did not result in a significant difference in hFABP5 affinity for 1,8-ANS, both Bligh and Dyer treatment and Lipidex-1000 resin exposure led to a ~1.8-fold and ~2.2-fold decrease in dissociation constant compared to untreated protein (Figure 3-1a, Table 3-1). However, while HIC treated hFABP5 was still able to bind the positive control linoleic acid (LA) with low micromolar affinity, atRA displayed

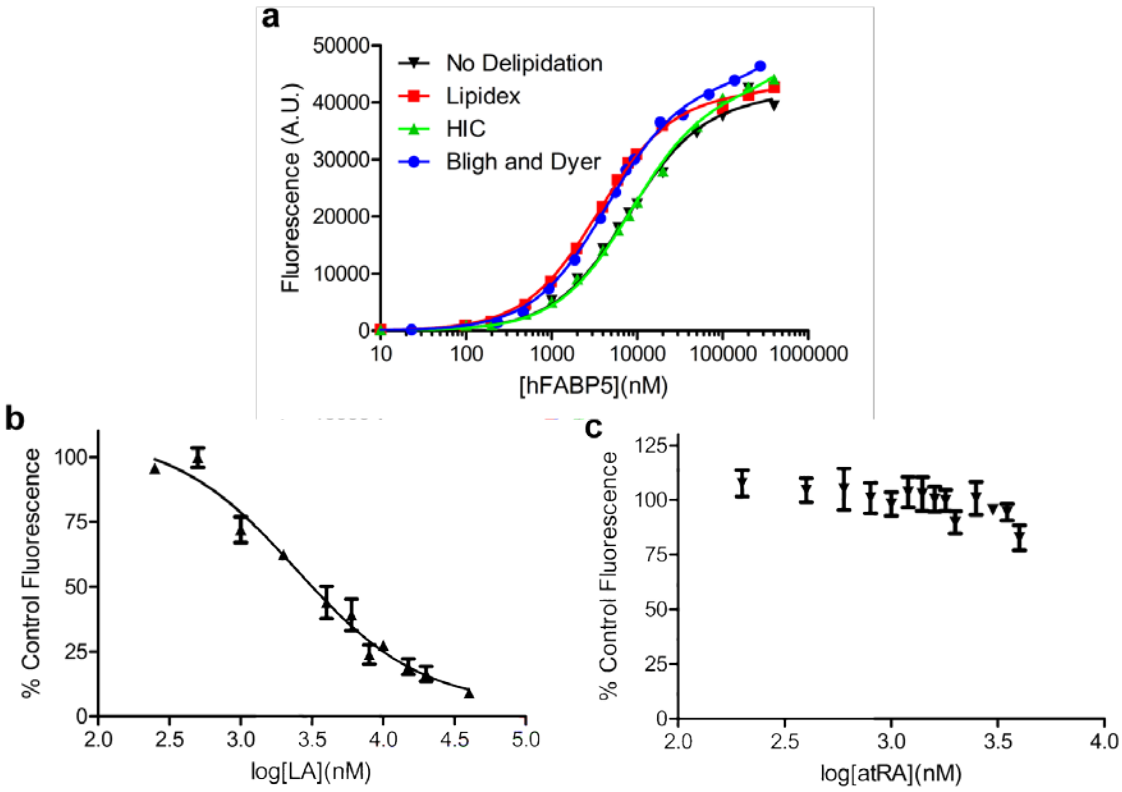

3-1. 1,8-ANS binding and displacement assays conducted on hFABP5.

a, binding of 1,8-ANS to hFABP5 reveals that, unlike with HIC (n=4), delipidation via Lipidex-1000 (n=3) as well as Bligh and Dyer treatment (n=3) results in the protein's significantly higher fluorophore binding affinity as compared to untreated control (n=3). *b* and *c*, while the polyunsaturated fatty acid LA was able to successfully compete 1,8-ANS from hFABP5's binding pocket (*b*), atRA was unable to generate a complete inhibition isotherm, even at concentrations up to 40 μM (n=3).

Delipidation Method	Ligand	Binding Constant(μM)	95% Conf. Interval(μM)	R^2
None	ANS	7.84 (K_D)	6.82-8.85	0.991
HIC	ANS	8.49 (K_D)	7.47-9.50	0.990
Bligh & Dyer	ANS	4.44 (K_D)	4.18-4.70	0.998
Lipidex-1000	ANS	3.54 (K_D)	3.29-3.79	0.998
HIC	LA	2.34 (K_i)	1.57-3.48	0.953
None	atRA	n.c.	n.c.	0.631

3-1. Calculated binding constants and isotherm fit values for hFABP5

K_D: Dissociation Constant

K_i: Inhibition Constant

n.c.: not calculated

minimal displacement of ANS from untreated protein, even at concentration levels well beyond the retinoid's solubility threshold (Figure 3-1b,c, Table 3-1) (334; 335).

Since atRA has been shown to bind FABP5 *in vitro* using 1,8-ANS displacement assays in other labs (268; 303), we decided to verify our results using a filtration based assay which directly measures complex formation by taking advantage of atRA's spectral properties. Briefly, protein was incubated with atRA either in powdered form or solubilized in organic solvent and insoluble atRA was removed via syringe filtration through a 0.2 μm filter. Ligand binding was tested by centrifuging the sample through a Millipore concentrator (MW 3000 Da) and comparing the amount of retained ligand in the supernatant versus the flow through relative to a control. An absorption spectrum was measured for the concentrated sample, using an identically prepared protein-free filtered solution as blank calibration. Absorption values at 280 nm and 350 nm, the established absorption peak wavelengths for hFABP5 (336) and atRA (337), respectively, were used to calculate the molar amounts of protein and ligand, and the ratio was taken to determine whether and to what extent a binding event had occurred. As proof of principle, we first conducted this filtration binding assay using recombinant CRABP-II, which binds atRA with high affinity and selectivity (158). Full-length hCRABP-II was first expressed in *E. coli* and purified to >95% purity (Figure 3-2a). Interestingly, while incubation of 1 μM of the protein to either 500 nM or 1 μM ethanol solubilized atRA resulted in minimal binding, concentrations of the retinoid at 2 μM and above led to completely saturated protein (Table 3-2). In contrast, ethanol mediated exposure of 1 μM hFABP5 to levels of atRA up to 10X that of protein was unable to drive efficient complex formation (Table 3-3). Introduction of 100 μM atRA to hFABP5 by DMSO resulted in a permanently yellow

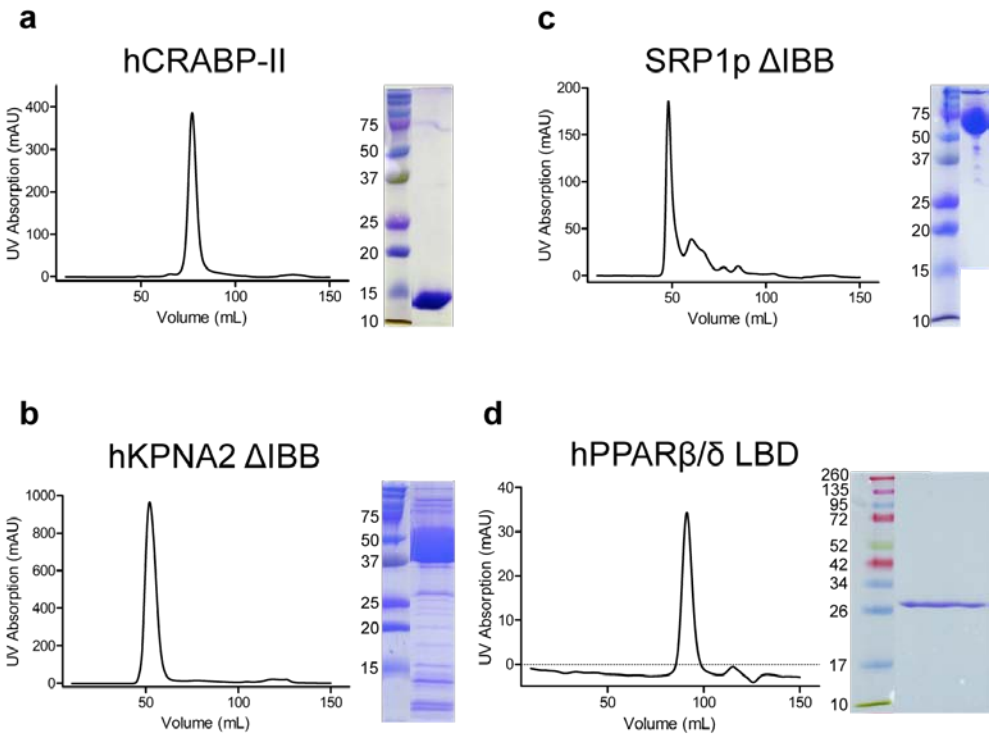

3-2. Purification of select proteins involved in RA signaling

Representative size exclusion chromatographs of hCRABP-II (*a*), hKPNA2ΔIBB (*b*), SRP1pΔIBB (*c*), and hPPARβ/δLBD (*d*), using absorption at 280 nm as readout. *a*, gel filtration of hCRABP-II yielded a single, well-defined peak, which is revealed to be highly purified protein. *b*, gel filtration of hKPNA2ΔIBB also yielded a solitary, symmetrical peak, containing recombinant protein (large, broad band shown in gel on right) along with lesser amounts of numerous impurities of both higher and lower molecular weight. *c*, SRP1p co-purified with a small assortment of mostly lower weight proteins, but could be separated by collecting samples from the earlier eluting half of its peak. *d*, hPPARβ/δLBD, much like hCRABP-II, eluted as a single protein peak of high purity. The data presented here were collected on either a Superdex 75 16/60 (*a*-*c*) or Superdex 200 26/60 (*d*) HiLoad PG column. The number demarcations for the SDS-PAGE protein ladders are in units of kDa.

hCRABP-II(nM)	atRA(nM)	Ethanol(%)	Buffer	% Protein Bound
1000	500	1	PBS, pH=7.4	3.8
1000	1000	1	PBS, pH=7.4	2.5
1000	2000	1	PBS, pH=7.4	109.1
1000	5000	1	PBS, pH=7.4	108.6
1000	10000	1	PBS, pH=7.4	109.3

3-2. Filtration binding assay conditions and values for hCRABP-II

PBS: Phosphate Buffered Saline

Percentages were calculated assuming a 1:1 hCRABP-II:atRA binding ratio

hFABP5(nM)	atRA(nM)	Solvent(%)	Buffer	% Protein Bound
1000	2000	2 (EtOH)	PBS, pH=7.4	1.8
1000	4000	2 (EtOH)	PBS, pH=7.4	2.0
1000	2000	1 (EtOH)	PBS, pH=7.4	5.7
1000	1000	0.5 (EtOH)	PBS, pH=7.4	6.9
1000	10000	1 (EtOH)	PBS, pH=7.4	7.2
1000	50000	0	PBS, pH=8.0	10.4
1000	100000	1 (DMSO)	PBS, pH=7.4	113.6*

3-3. Filtration binding conditions and values for hFABP5

EtOH: Ethanol

DMSO: Dimethyl Sulfoxide

PBS: Phosphate Buffered Saline

Percentages were calculated assuming a 1:1 hFABP5:atRA binding ratio

*Value obtained from anomalous absorption spectrum, and should be regarded with caution

solution after filtration whose color became further pronounced upon concentration, with absorption values that would indicate fully bound protein (Table 3-3). However, it was observed that the sample produced an anomalous absorption spectrum with an ill-defined peak at 280 nm and an overall absorption maximum at 400 nm, which became even more difficult to interpret after gel filtration chromatography, indicating unfolded/misfolded protein (data not shown). Therefore, our absorption binding assay corroborates the results of 1,8-ANS displacement, both of which suggest hFABP5 does not efficiently bind to atRA *in vitro*.

Attempts at crystallization of a hFABP5-atRA complex were performed concurrently to ligand binding assays. A variety of incubation procedures were carried out, in which atRA was introduced at various levels to protein via ethanol, DMSO, or phospholipid vesicles for several minutes to several hours in PBS, pH=7.4-8.0, prior to concentration. Samples were then subjected to available commercial crystallization suites, as well as more directed screens based off of published crystallant conditions for hFABP5 (264) and hCRABP-II (27). In certain instances, we were able to replicate the phenomena described above, in which the protein-ligand sample remained yellow even after filtration, with a positive correlation between color intensity and protein concentration. Crystals formed from these samples were always observed to be bipyramidal, and in the $P4_32_12$ spacegroup (Figure 3-3a). We show here a representative high quality data set collected at sub-2.0 Å resolution (Table 3-4), in which hFABP5 adopts the canonical β-clam fold with accompanying α-helix lid (Figure 3-3b)(Chapter 2) (264). Inspection of the protein's binding pocket, however, did not support the modeling of atRA. Instead, the LBP contained only unconnected, spherical electron density peaks,

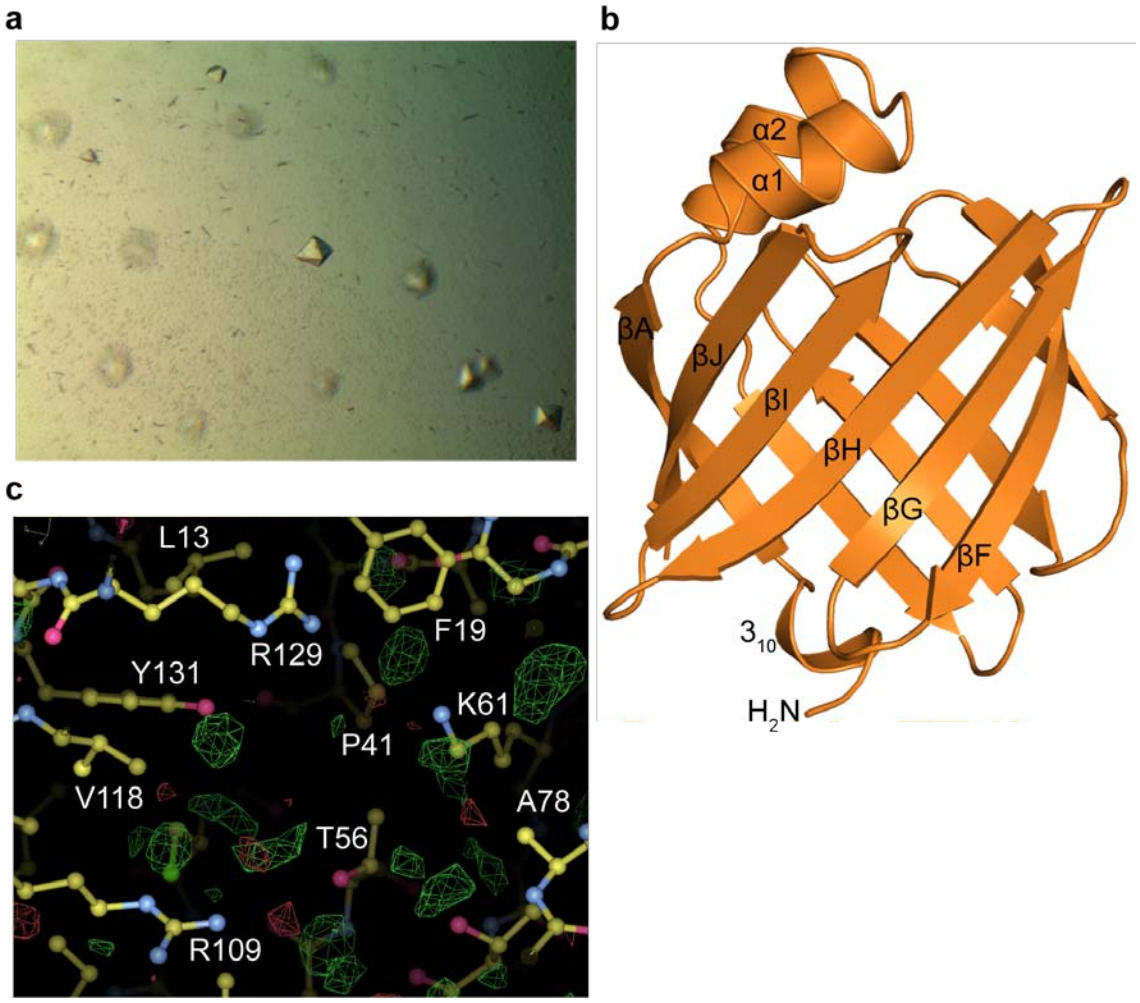

3-3. Crystallization of hFABP5 in presence of atRA

a, hFABP5 exposed to atRA formed bipyramidal crystals belonging to the $P4_32_12$ spacegroup. *b*, the asymmetric unit of atRA-exposed hFABP5 consists of a monomer, displaying the canonical iLBP fold of a 10 strand β-barrel capped by two α-helices. *c*, inspection of hFABP5's ligand binding pocket reveals only globular electron density peaks, indicative of a water network. The simulated annealing $F_o - F_c$ omit map of electron density was contoured at 3σ.

	Apo FABP5, RA Exposed
Data collection	
Space group	$P4_32_12$
Cell dimensions	
a, *b*, *c* (Å)	62.9, 62.9, 73.6
α, β, γ (°)	90.0, 90.0, 90.0
Resolution (Å)	1.95 (2.02 – 1.95)*
R_{sym} or R_{merge}	7.3 (39.7)
$I / \sigma I$	32.40 (8.74)
Completeness (%)	99.9 (100.0)
Redundancy	10.2 (10.3)
Refinement	
Resolution (Å)	1.95
No. reflections	11262
R_{work} / R_{free}	20.0 / 25.0
No. atoms	
Protein	1069
Ligand/ion	0
Water	64
B-factors	
Protein	17.6
Ligand/ion	N/A
Water	21.6
R.m.s. deviations	
Bond lengths (Å)	0.013
Bond angles (°)	1.496

3-4. Data collection and refinement statistics (molecular replacement)

* Data collected from a single crystal; values in parentheses are for highest-resolution shell.

which could be easily filled with waters (Figure 3-3c). Thus, even assuming a successful binding event between hFABP5 and atRA, crystallization selects exclusively for *apo* protein.

3.3.2 hFABP5 Interaction With Yeast Importin α Occurs With Weak Affinity

The next step in nonclassical atRA signaling is the nuclear translocation of hFABP5 in cells exposed to the retinoid. Thus, we began our investigation of this stage of the pathway by expressing a construct of human importin-α1, also known as karyopherin-α2 (hKPNA2) whose auto-inhibitory N-terminal importin β binding domain (IBB) had been truncated in order to facilitate its binding of protein in the absence of importin β (338). This particular importin α subtype was chosen not only for its ability to selectively bind CRABP-II in the presence of atRA (177), but also because it had been successfully crystallized in both its cargo bound (339) and unbound states (PDB codes: 3FEY, 4E4V). Unfortunately, we were not able to purify hKPNA2ΔIBB greater than ~80% (Figure 3-2b), even with the use of high salt buffers, due to the presence of an array of tightly bound proteins originating from the *E.coli* expression host. Since atRA did not convincingly complex with hFABP5 in our binding assays, we used the fatty acid LA, which we have shown can both bind (Figure 3-1b) and cause nuclear import of hFABP5 (Chapter 2), to facilitate protein-protein interaction. However, despite addition of 140 μM activating fatty acid, 30 μM hFABP5 did not migrate with an equimolar amount of hKPNA2ΔIBB in a size-exclusion column (Figure 3-4a). The absence of a binding event was then confirmed with isothermal titration calorimetry (ITC) (Figure 3-4b).

Since there exist multiple importin α isoforms with differing substrate specificities in eukaryotes (340), we re-ran our gel filtration binding assay with SRP1p, the only NLS

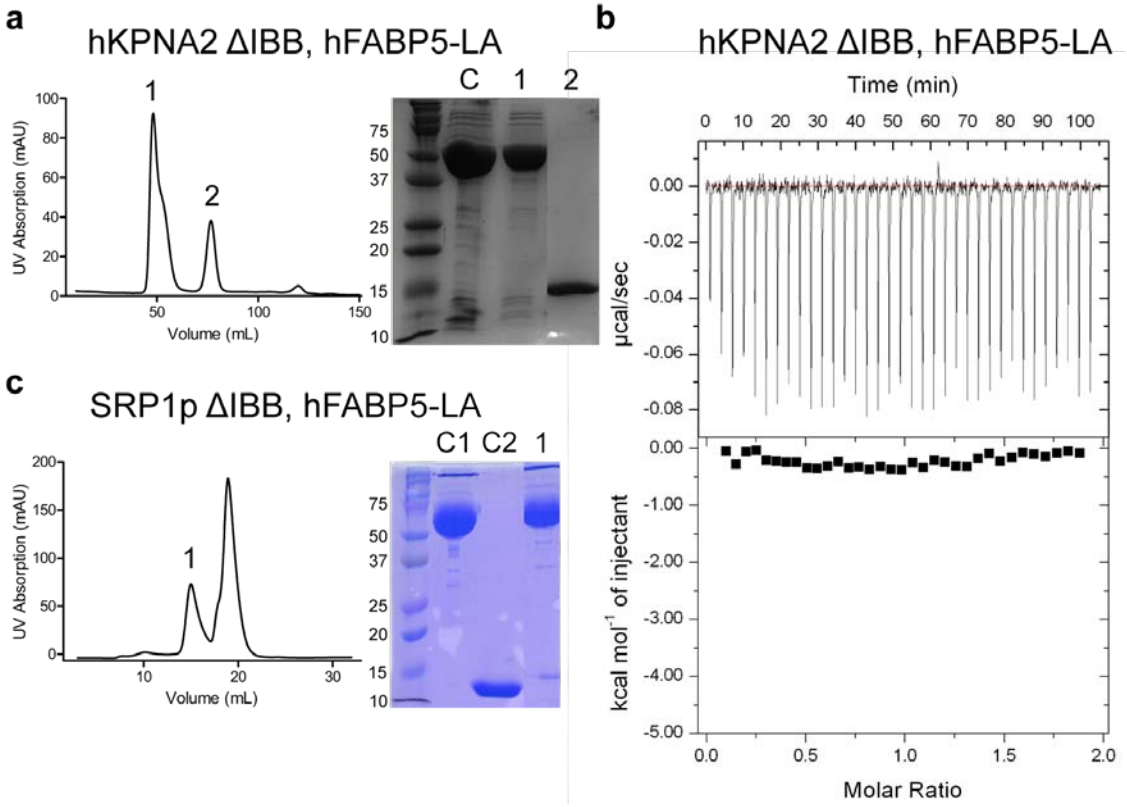

3-4. Investigation of hFABP5, importin α complex formation

a, despite its asymmetrical appearance, SDS-PAGE reveals that peak 1 does not contain a complex of hKPNA2ΔIBB bound to hFABP5-LA. C: control consisting of purified hKPNA2ΔIBB only. Peak 2 is hFABP5. Data collected on a Superdex 75 16/60 PG column. *b*, isothermal titration calorimetry conducted on hKPNA2ΔIBB and hFABP5 (injectant) results in the complete absence of a binding curve. *c*, mixture of purified SRP1pΔIBB (C1) and hFABP5-LA (C2) followed by gel filtration indicates a small degree of complex formation (Peak 1). Data collected on a Superose 6 10/300 GL column. The number demarcations for the SDS-PAGE protein ladders are in units of kDa.

receptor protein expressed in *S.cerevisiae*. SRP1pΔIBB could be purified to ~95% (Figure 3-2c), yet despite exposure of up to 50 μM yeast importin α construct with 400 μM hFABP5 in the presence of 100 μM LA, only a small proportion of purified protein was able to form a complex, whose elution peak was unable to be resolved from that of SRP1pΔIBB alone (Figure 3-4c). Taken together, these data suggest that an isoform of importin α other than karyopherin-α2 could be responsible for the nuclear translocation of activated hFABP5, although such a complex would have to show far greater stability than what was observed with the yeast homologue in order to be a viable crystallographic target.

3.3.3 The Transient hFABP5-PPARβ/δ Complex Can Be Captured With Crosslinking

The proposed penultimate process in hFABP5-mediated atRA shuttling to PPARβ/δ is the interaction between the two proteins, whereby the Vitamin A metabolite is transferred, or "channeled," directly into PPARβ/δ's ligand binding pocket. PPARβ/δ-FABP5 interaction has been shown to occur by via coprecipitation assays (25), albeit to an extent far too small for crystallographic pursuit. In light of this, we explored the effect of crosslinking on channeling complex stability. The highly purified hPPARβ/δ ligand binding domain (LBD) (Figure 3-2d) was mixed at a constant concentration of 15 μM with increasing concentrations of hFABP5 in the presence or absence of BS_3 at several time increments (Figure 3-5a). The specific linker was chosen for its water solubility, homobifunctionality, and ability to link primary amines. Our results show that covalently bonded complex formation is both time and hFABP5 concentration dependent, with the appearance of a ~45 kDa doublet at 10 minutes of hPPARβ/δLBD exposure to 33 μM hFABP5, and after only 3 minutes of 100 μM hFABP5 exposure (Figure 3-5a). An

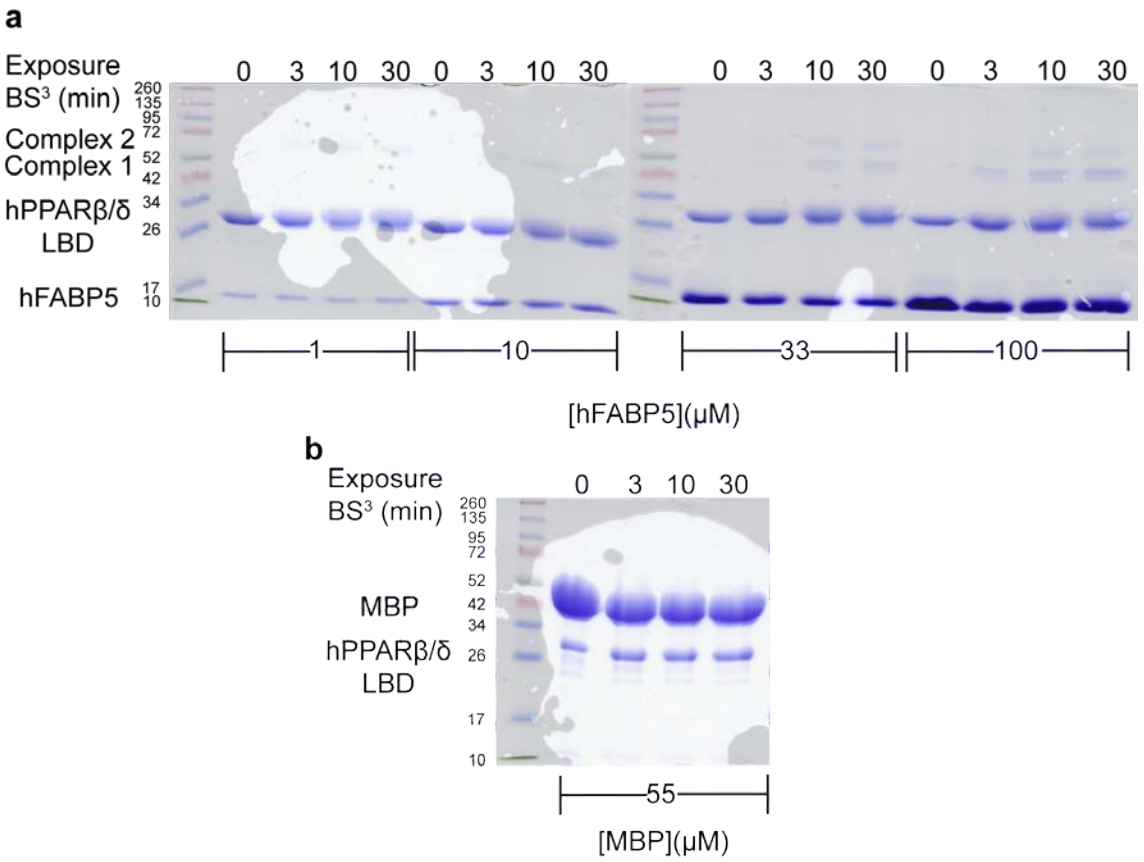

3-5. Crosslinking of hFABP5-PPARβ/δLBD complex

a, exposure of PPARβ/δLBD to hFABP5 in the presence of BS^3 leads to the hFABP5 concentration and time dependent formation of ~45 kDa (Complex 1) and ~60 kDa (Complex 2) crosslinked products. *b*, negative control showing the absence of crosslinked products between hPPARβ/δLBD and MBP across all time points. The number demarcations for the SDS-PAGE protein ladders are in units of kDa.

additional 60 kDa band is also observed, possibly the result of a trimer consisting of a 2 hFABP5: 1 hPPARβ/δLBD molecular ratio (Figure 3-5a). Since BS_3 is able to crosslink proteins both via their lysines as well as their N-termini, the specificity of complex formation was tested using MBP in place of hPPARβ/δLBD, which failed to yield higher molecular weight products (Figure 3-5b). Thus, it appears that this naturally transient process within the novel atRA signaling pathway is amenable to optimization for future structural study.

3.3.4 hPPARβ/δ Does Not Appreciably Bind atRA In Vitro

Binding of atRA to PPARβ/δ completes the FABP5-PPARβ/δ partnership, with ensuing NR activation ultimately being responsible for the pro-survival response of certain cells types to Vitamin A acid exposure (268-270; 272). A structure of the PPARβ/δ-atRA complex would likely yield novel insight into nuclear receptor-ligand interaction, as it would be the first of its kind to feature a member of the superfamily outside of RAR, RXR, and RAR-related orphan receptor (ROR) bound to a naturally occurring retinoid. Although PPARβ/δ has been previously shown to directly bind atRA via competition with 1,8-ANS (230), we decided to verify this finding using our absorption binding assay, which had proven to be a good predictor of hFABP5-atRA complex crystallization viability. Purified hPPARβ/δLBD was incubated with ligand in a variety of conditions; however, even in the presence of 100 μM atRA at a 1:100 protein: ligand ratio, only ~20% hPPARβ/δLBD was bound to atRA (Table 3-5). Surprisingly, the addition of peptide fragments containing the LxxLL motif from TIF2 or PGC-1α, coactivator proteins known to interact with PPARβ/δ in response to receptor agonism (341; 342), caused a decrease in complex formation as compared to their absence in

hPPARβ/δ LBD(nM)	atRA(nM)	Solvent(%)	Co-activator Peptide(nM)	Buffer	% Protein Bound
1000	10000	1 (EtOH)	10000 (TIF2L)	PBS, pH=7.4	n.d.
1000	50000	0	0	BE	1.4
1000	10000	1 (EtOH)	10000 (PGC-1α)	PBS, pH=7.4	1.5
1000	2000	1 (EtOH)	0	BE	1.6
1000	10000	1 (EtOH)	10000 (TIF2)	PBS, pH=7.4	2.8
1000	2000	2 (EtOH)	0	PBS, pH=8.0	3.2
1000	2000	2 (EtOH)	0	BE	4.1
1000	2000	1 (EtOH)	0	PBS, pH=7.4	4.6
1000	100000	1 (DMSO)	10000 (PGC-1α)	PBS, pH=7.4	5.4
1000	100000	1 (DMSO)	0	BE	5.9
1000	10000	1 (EtOH)	0	PBS, pH=7.4	10.5
1000	50000	0	0	PBS, pH=8.0	11.8
1000	10000	1 (EtOH)	0	BE	12.0
1000	100000	1 (DMSO)	0	PBS, pH=7.4	21.6

3-5. Absorption binding conditions and values for hPPARβ/δLBD

EtOH: Ethanol

DMSO: Dimethyl Sulfoxide

TIF2L: TIF2Long (an elongated version of TIF2 peptide)

PBS: Phosphate Buffered Saline

BE: Buffer E

n.d.: not detected

Percentages were calculated assuming a 1:1 hPPARβ/δ:atRA binding ratio

Only data was kept in which A_{280} signal in sample was at least 10X that of flow-through

identical conditions (Table 3-5). These results indicate the intractability of a structural investigation into atRA-mediated PPARβ/δ activation via X-ray crystallography.

3.4 Discussion

Despite a growing body of evidence at the cellular and whole organism level indicating that FABP5 is able to shuttle atRA to PPARβ/δ, our efforts to investigate the molecular driving forces behind this novel signaling pathway via X-ray crystallography were stymied by the inability of both participating proteins to substantially bind the retinoid ligand *in vitro*. Ironically, structural analysis provides an explanation for our results. Superposition of FABP5 and CRABP-II (RMS=1.48 Å), reveals that FABP5 possesses residues homologous to the two arginines and tyrosine used by CRABP-II to anchor the carboxylate headgroup of atRA within its binding pocket (Figure 3-6a). Moreover, these residues, which are used by FABP5 for the same purpose in fatty acid binding (Chapter 2) (264), are aligned in an identical tertiary orientation to those of CRABP-II, providing a favorable environment for a hydrogen bonding network within a hypothetical FABP5-atRA complex (Figure 3-6a). Although, unlike fatty acids, which adopt either a “U” or “L” shape within FABP5’s binding pocket (Chapter 2), the all *trans* conjugated double bonds of atRA dictate that the molecule assumes an extended, planar conformation, which would put it in direct contact with FABP5’s Leu-32, creating a steric clash (Figure 3-6b). This residue belongs to the α2 helix, which is the least aligned, especially within the N-terminal half, of all secondary structure motifs between the proteins (Figure 3-6b).

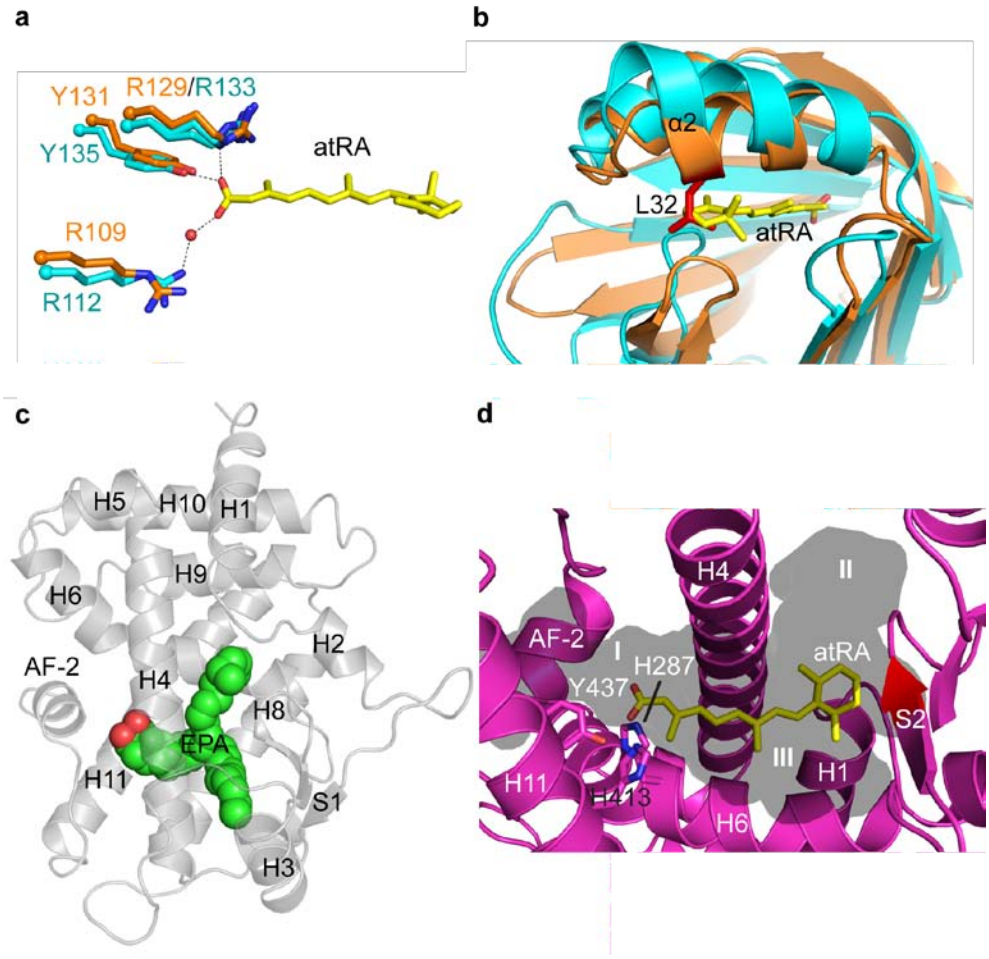

3-6. Structural modeling of hFABP5 and hPPARβ/δLBD bound to atRA

a and *b*, overlay of *apo* hFABP5 with the high resolution structure of hCRABP-II bound to atRA (PDB Code: 2FR3) reveals conservation of the residues necessary for hydrogen bond formation with atRA (*a*), however the positioning of hFABP5's α2 helix leads to a steric clash with the β-ionone ring of the ligand (*b*). *c*, structure of hPPARβ/δLBD in complex with eicosapentanoic acid (EPA) (PDB Code: 3GWX), showing alternate ligand conformations in which the alkyl tail of the fatty acid is able to fill either Arm II or III of the binding pocket. *d*, modeling of atRA into the binding site of hPPARβ/δLBD (PDB Code: 1GWX) shows the retinoid protruding from the pocket volume into S2 of the receptor. Arms I, II, and III are labeled "I", "II", and "III", respectively.

The binding pocket of PPARβ/δ, like that of FABP5, also contains three residues responsible for hydrogen bond formation with the carboxylate functional group of fatty acids (His-287, His-413, and Tyr-437) (215), with the tyrosine being especially responsible for stabilizing the activation function 2 (AF-2) helix in its activated conformation (343). In spite of its large cavity volume (~1300 $Å^3$), the tripartite nature of the "Y" shaped ligand pocket requires fatty acids, with their headgroups stabilized in Arm I, to bend the remainder of their alkyl tails either into Arm II or III (Figure 3-6c) (215; 343; 344). Placement of atRA within the binding cavity of PPARβ/δ so that its carboxylic acid head can engage in the interactions necessary for receptor activation results in protrusion of the retinoid's β-ionone ring out of the pocket edge and into close proximity with the protein's S2 β-strand (Figure 3-6d). Thus, it appears that it is not atRA's size, but the inflexibility of its isoprene chain that underlies its binding incompatibility with both FABP5 and PPARβ/δ.

In order to account for the discrepancy between our results and those published prior, we hypothesize that perhaps it is not atRA, but one or more of its stereoisomers that is responsible for the effects generated by FABP5-enhanced PPARβ/δ activation. Assuming both proteins bind RA in a similar fashion to fatty acids, *cis*-isomerism would likely have to occur at either the 9 or 11 position to provide the bend within the molecule necessary for complex formation. The presence of 9,13-di-*cis*-retinoic acid (9,13dcRA) has been confirmed across multiple tissue types in the adult mouse (123). Additionally, dysregulation of RA metabolism has been linked numerous times to various pathologies, with 9cRA and/or 11-*cis*-retinoic acid (11cRA) levels shown to be significantly altered in both breast and brain cancer as compared to healthy tissue (273; 345; 346). Undoubtedly,

further study is required to shed light on the potential role of RA diastereomers in the FABP5-PPARβ/δ signaling pathway, though progress in this regard could open up an entirely new chapter of understanding in retinoid function.

CHAPTER 4 : DISCUSSION

4.1 Summary of Results

4.1.1 Chapter 2

Of the 15 mammalian iLBPs known to be expressed at the protein level, five (CRABP-II, and FABP's 1, 3-5) have been investigated for their ability to engage in signaling with nuclear receptors – a process whereby nuclear translocation of the iLBP allows for direct channeling of cargo into the ligand binding pocket of the receptor, resulting in enhanced receptor activation and target gene transcription (25; 179; 347). However, the physical mechanisms driving these iLBPs' participation in signal transduction had thus far only been delineated for CRABP-II (176-179) and FABP4 (286; 293). Chapter 2 represents an expansion of structural understanding to include FABP5 and its role within the PPARβ/δ signaling pathway.

Residues within FABP5 homologous to those that compose the positively charged tertiary NLS of CRABP-II and FABP4, first proposed by primary sequence comparison (286), were confirmed in our study via structural overlay and electrostatic surface potential mapping. The functionality of Lys-24, Arg-33, and Lys-34 was then affirmed when a mutant harboring alanines in place of these residues (FABP5NLSm) was unable to undergo ligand-dependent nuclear localization and PPARβ/δ activation enhancement. This result could be replicated with FABP5DSm, in which Met-35 and Leu-60 were both mutated to alanines, proving that these residues, like the homologous Val-33 and Phe-58 in FABP4 (293), serve as activation switches that are able to translate information concerning the binding state of the ligand to NLS coalescence within the protein. However, while Gillilan et al. have, based on crystallographic data alone, attributed this process to the conformation of Phe-58 in FABP4, the author's HDX analysis combined

with X-ray crystallography points toward a more general interplay between the βC-D loop (ie the activation loop) and the α2 helix for FABP5.

Perhaps the most important contribution garnered by this investigation is the correlation found between bound fatty acid conformation and FABP5 activation state. Observation of the FABP5-LA structure revealed that the known activating fatty acid was able to adopt two conformations within the binding pocket: a more condense U-shape and a more elongated L-shape. Based on comparison of the activation loop between the two monomers, as well as that of the protein in its *apo* state, it was hypothesized that the U configuration allowed for compaction of the activation loop required for NLS stabilization. Therefore, it was reasoned that fatty acids whose nature and degree of unsaturation would predispose them to assuming a more condensed form would be able to activate FABP5. This allowed us not only to predict AA as a newly discovered FA activator, but to construct a working model implicating *cis* PUFAs with double bonds located distal to their carboxylic headgroup, a hallmark of ω-3 and ω-6 FAs, as an entire class of potential FABP5 activators.

4.1.2 Chapter 3

The ability of atRA to participate in FABP5-mediated PPARβ/δ signaling was first demonstrated by Schug et al. as an alternative to the CRABP-II-RAR pathway, and was proposed to account for the contradictory cell type-dependent responses to the Vitamin A metabolite (268). Though substantial evidence at the cellular level and *in vivo* continue to grow (269; 272; 348; 349), the molecular mechanisms underlying FABP5 and PPARβ/δ activation by atRA are unknown. Thus, in Chapter 3, the author approached the novel

atRA pathway from a biochemical perspective in order to ascertain its feasibility for future structural study.

Contrary to earlier studies by Kane and Berlohr, and Schug et al. that were able to measure a binding event between atRA and FABP5, albeit at affinities which differed by two orders of magnitude, the author could not detect appreciable binding using the same 1,8-ANS displacement assay (268; 303). Efforts using absorption profile comparisons to determine the percentage of bound protein across various buffer conditions and atRA concentrations (referred to above as a filtration binding assay) yielded similar results. It should be noted that the absence of complex formation between FABP5 and atRA, as measured by both absorption spectrum profile and PAGE/ radiobinding assay, was first reported as part of the protein's original purification and biochemical characterization 20 years ago (336). A similar lack of binding was observed between atRA and the purified LBD of PPARβ/δ via the filtration assay, regardless of solution environment and the presence of known receptor co-activator peptide fragments. This is in agreement with the observations made by Rieck et al. that atRA is unable to activate PPARβ/δ in cells (350). However, in the presence of LA, FABP5 was demonstrated to form a transient complex with the yeast homologue of importin α. In addition, crosslinking in the absence of ligand was shown to stabilize a FABP5-PPARβ/δ LBD complex, whose formation was protein specific as well as protein concentration and time dependent. Thus, while the data in Chapter 3 casts doubt on the validity of alternative atRA signaling, it does provide further proof for the existence of the relevant protein-protein interactions within the FABP5-PPARβ/δ pathway.

4.2 Future Directions

4.2.1 Chapter 2

As with any study that yields a model, the pertinence of future investigations lies in their capacity to confirm, refine, or discard said model in light of additional data. To this end, three routes of follow-up study are proposed. The first would test the model's predictive potential regarding certain polyunsaturated *cis* bonded LCFAs capability to elicit FABP5 activation. This could simply be achieved by conducting additional FABP5 nuclear localization as well as PPARβ/δ transactivation assays with chosen fatty acid activating candidates, such as the long-chain ω-6 or ω-3 FAs. As all of these FAs are either 18 or 20 carbon units long, and all of the non-activating FAs tested thus far span only 16 carbons, it would also be equally important to select proposed non-activators that have a length of at least 18 carbons, such as the saturated stearic acid (SA) or the more soluble monounsaturated OA, in order to assure that saturation state, not alkyl tail size, dictates activation ability. Finally, to further clarify activating criteria, polyunsaturated FAs with *cis* double bonds located nearer their headgroup should also be included. An excellent example would be meadic acid, an ω-9 20 carbon FA whose three double bonds nonetheless enable it to assume a U-like conformation in its energy minimized form.

The second avenue of study would test the validity of the model's proposed mechanics. The data presented in Chapter 2 indicates that FABP5 exists as a monomer regardless of its ligand bound state, and that it is the interaction between the complexed fatty acid tail, the activation loop, and the α2 helix that dictates NLS formation. However, Sanson et al. have recently reported that both bacterially expressed human and mouse FABP5 exists as a mixture of monomers and dimers in equilibrium in solution, the ratio

of which is unaffected by ligand (351). Moreover, they were successful in solving the structures of a domain swapped dimer of hFABP5 bound to the endocannabinoid anandamide (AEA) as well as the synthetic FABP5 AEA nuclear transport inhibitor BMS-309403 (Figure 4-1) (288). As the region of the protein that participates in dimer formation (aas 1-60) aligns remarkably well with that shown to undergo loss of protection from deuterium exchange in the presence of PoA vs. AA (Figure 2-7c), an additional study is warranted to investigate the possibility that dimerization via domain swap is not only a real physiological event, but is ligand regulated and responsible for NLS recognition and subsequent FABP5 nuclear translocation.

The third and final route for future investigation to be discussed would test the applicability of the FA U vs. L activation hypothesis established for FABP5 in relation to other FABPs that meet the precursory criteria: a homologous tertiary NLS comprised of two lysines and an arginine, along with appropriately hydrophobic and bulky amino acids homologous to FABP5's switch residues. This would be a very directed course of study, as the only two proteins to fulfill these requirements are FABP4 and FABP8. The former has already been analyzed in a similar fashion using solved crystal structures, and the analysis used to correctly predict that the synthetic fluorophore 1,8-ANS would be an FABP4 activator (293). The same guidelines also categorized SA, PA, OA, and surprisingly, AA to be non-activators, though none of these FA ligands outside of SA have been confirmed in biological assays. Therefore, as the only proven FA activator of FABP4 is LA, while the saturated SA is known to be incapable of eliciting activation, there is reason to believe that further cellular work could reveal FABP4 to have a similar, if not identical FA activator selectivity filter as FABP5. On the other hand, much less is

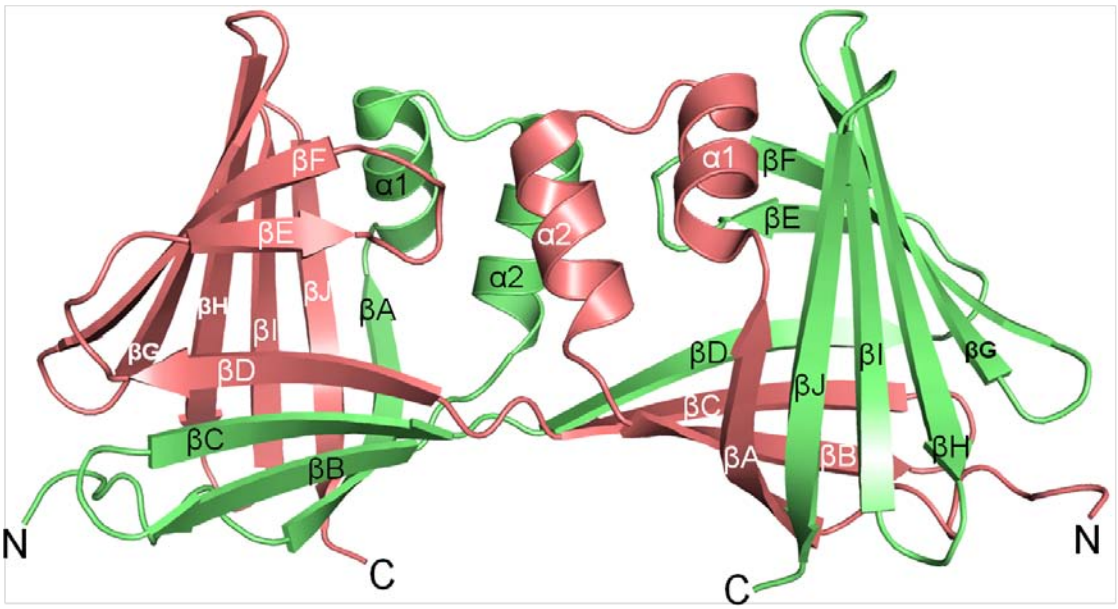

4-1. FABP5 can crystallize as a domain swapped dimer

Crystal structure of hFABP5 bound to anandamide (not shown) can undergo dimer formation via trading domains consisting of the first ~60 amino acids. Similar dimer formation also occurs within the FABP5 structure bound to the synthetic inhibitor BMS-309403. β-strands and α-helices for each protein copy have been labeled in opposing colors for clarity (PDB code: 4AZR).

known about FABP8, but its potential to engage in fatty acid signaling within Schwann cells makes it an exciting new target for pursuit.

4.2.2 Chapter 3

None of the steps crucial to the progression of the alternative atRA signaling pathway could be replicated at the basic biochemical level, yet there is an abundance of evidence in cells and animal models that both FABP5 and PPARβ/δ are involved in retinoid signal transduction. In light of this discrepancy, as well as the fact that all iLBP subfamily IV members bind fatty acids in a decidedly nonlinear fashion, the author advises that any future structural endeavors should begin by testing an array of known *cis* isomers of RA, while ignoring the major RA metabolites, which are oxidized such that the conjugated *trans* double bond system is left intact (352). Prime candidates, based on the nature of FA curvature within the FABP pocket, would be 9cRA, 9,13dcRA, and 11cRA.

4.3 Conclusion

Although 40 years have passed since the discovery of the first members of the iLBP family, new discoveries are continuing to emerge regarding their role as facilitators in the cell's ongoing ability to translate its internal lipid profile into meaningful signaling events. In this vein, the body of work presented herein not only delineates the structural mechanisms that serve as the cornerstone for fatty acid specific FABP5 nuclear translocation and PPARβ/δ signaling, but provides basic biochemical evidence favoring re-examination of the alternative atRA signal transduction pathway. It is the hope of the

author that greater understanding of the partnership between these two proteins provides a useful contribution to the greater field of lipid and structural biology.

References

1. Flower DR. 1993. Structural relationship of streptavidin to the calycin protein superfamily. *FEBS letters* 333:99-102
2. Flower DR. 1996. The lipocalin protein family: structure and function. *Biochem J* 318 (Pt 1):1-14
3. Londraville RL. 1996. Intracellular fatty acid-binding proteins: putting lower vertebrates in perspective. *Brazilian journal of medical and biological research = Revista brasileira de pesquisas medicas e biologicas / Sociedade Brasileira de Biofisica ... [et al.]* 29:707-20
4. Plenefisch J, Xiao H, Mei B, Geng J, Komuniecki PR, Komuniecki R. 2000. Secretion of a novel class of iFABPs in nematodes: coordinate use of the Ascaris/Caenorhabditis model systems. *Molecular and biochemical parasitology* 105:223-36
5. Schaap FG, van der Vusse GJ, Glatz JF. 2002. Evolution of the family of intracellular lipid binding proteins in vertebrates. *Mol Cell Biochem* 239:69-77
6. Furuhashi M, Hotamisligil GS. 2008. Fatty acid-binding proteins: role in metabolic diseases and potential as drug targets. *Nat Rev Drug Discov* 7:489-503
7. D'Ambrosio DN, Clugston RD, Blaner WS. 2011. Vitamin A metabolism: an update. *Nutrients* 3:63-103
8. Smathers RL, Petersen DR. 2011. The human fatty acid-binding protein family: evolutionary divergences and functions. *Hum Genomics* 5:170-91
9. Folli C, Calderone V, Ottonello S, Bolchi A, Zanotti G, et al. 2001. Identification, retinoid binding, and x-ray analysis of a human retinol-binding protein. *Proc Natl Acad Sci U S A* 98:3710-5
10. Folli C, Calderone V, Ramazzina I, Zanotti G, Berni R. 2002. Ligand binding and structural analysis of a human putative cellular retinol-binding protein. *J Biol Chem* 277:41970-7
11. Marcelino AM, Smock RG, Gierasch LM. 2006. Evolutionary coupling of structural and functional sequence information in the intracellular lipid-binding protein family. *Proteins* 63:373-84
12. Ong DE, Chytil F. 1978. Cellular retinoic acid-binding protein from rat testis. Purification and characterization. *J Biol Chem* 253:4551-4
13. Bailey JS, Siu CH. 1988. Purification and partial characterization of a novel binding protein for retinoic acid from neonatal rat. *J Biol Chem* 263:9326-32
14. Atshaves BP, Martin GG, Hostetler HA, McIntosh AL, Kier AB, Schroeder F. 2010. Liver fatty acid-binding protein and obesity. *The Journal of nutritional biochemistry* 21:1015-32
15. Besnard P, Niot I, Poirier H, Clement L, Bernard A. 2002. New insights into the fatty acid-binding protein (FABP) family in the small intestine. *Mol Cell Biochem* 239:139-47
16. Zimmerman AW, van Moerkerk HT, Veerkamp JH. 2001. Ligand specificity and conformational stability of human fatty acid-binding proteins. *The international journal of biochemistry & cell biology* 33:865-76
17. Vorum H, Madsen P, Svendsen I, Cells JE, Honore B. 1998. Expression of recombinant psoriasis-associated fatty acid binding protein in Escherichia coli: gel electrophoretic characterization, analysis of binding properties and comparison with human serum albumin. *Electrophoresis* 19:1793-802
18. Bennaars-Eiden A, Higgins L, Hertzel AV, Kapphahn RJ, Ferrington DA, Bernlohr DA. 2002. Covalent modification of epithelial fatty acid-binding protein by 4-hydroxynonenal in vitro and in vivo. Evidence for a role in antioxidant biology. *J Biol Chem* 277:50693-702

19. Leszczynski JF, Rose GD. 1986. Loops in globular proteins: a novel category of secondary structure. *Science* 234:849-55
20. Banaszak L, Winter N, Xu Z, Bernlohr DA, Cowan S, Jones TA. 1994. Lipid-binding proteins: a family of fatty acid and retinoid transport proteins. *Advances in protein chemistry* 45:89-151
21. Sacchettini JC, Gordon JI, Banaszak LJ. 1989. Refined apoprotein structure of rat intestinal fatty acid binding protein produced in Escherichia coli. *Proc Natl Acad Sci U S A* 86:7736-40
22. Zhang YR, Zhao YQ, Huang JF. 2012. Retinoid-binding proteins: similar protein architectures bind similar ligands via completely different ways. *PLoS One* 7:e36772
23. Blomhoff R, Blomhoff HK. 2006. Overview of retinoid metabolism and function. *Journal of neurobiology* 66:606-30
24. Noy N. 2010. Between death and survival: retinoic acid in regulation of apoptosis. *Annual review of nutrition* 30:201-17
25. Tan NS, Shaw NS, Vinckenbosch N, Liu P, Yasmin R, et al. 2002. Selective cooperation between fatty acid binding proteins and peroxisome proliferator-activated receptors in regulating transcription. *Mol Cell Biol* 22:5114-27
26. Schroeder F, Petrescu AD, Huang H, Atshaves BP, McIntosh AL, et al. 2008. Role of fatty acid binding proteins and long chain fatty acids in modulating nuclear receptors and gene transcription. *Lipids* 43:1-17
27. Vaezeslami S, Mathes E, Vasileiou C, Borhan B, Geiger JH. 2006. The structure of Apo-wild-type cellular retinoic acid binding protein II at 1.4 A and its relationship to ligand binding and nuclear translocation. *J Mol Biol* 363:687-701
28. McCollum EV, Davis M. 1913. The necessity of certain lipins in the diet during growth. *J. Biol. Chem.* 15:167-75
29. Wald G. 1968. Molecular basis of visual excitation. *Science* 162:230-9
30. Foster KW, Saranak J, Patel N, Zarilli G, Okabe M, et al. 1984. A rhodopsin is the functional photoreceptor for phototaxis in the unicellular eukaryote Chlamydomonas. *Nature* 311:756-9
31. Oesterhelt D, Stoeckenius W. 1971. Rhodopsin-like protein from the purple membrane of Halobacterium halobium. *Nature: New biology* 233:149-52
32. Beja O, Aravind L, Koonin EV, Suzuki MT, Hadd A, et al. 2000. Bacterial rhodopsin: evidence for a new type of phototrophy in the sea. *Science* 289:1902-6
33. Napoli JL. 1999. Interactions of retinoid binding proteins and enzymes in retinoid metabolism. *Biochim Biophys Acta* 1440:139-62
34. Napoli JL. 2012. Physiological insights into all-trans-retinoic acid biosynthesis. *Biochim Biophys Acta* 1821:152-67
35. Fraser PD, Bramley PM. 2004. The biosynthesis and nutritional uses of carotenoids. *Progress in lipid research* 43:228-65
36. Yamada M, Blaner WS, Soprano DR, Dixon JL, Kjeldbye HM, Goodman DS. 1987. Biochemical characteristics of isolated rat liver stellate cells. *Hepatology* 7:1224-9
37. Goodman DS, Blaner WS. 1984. Biosynthesis, absorption, and hepatic metabolism of retinol. In *The Retinoids*, ed. SM B., AB Roberts, DS Goodman, 2:1-39. New York, NY: Academic Press. Number of 1-39 pp.
38. Blomhoff R, Green MH, Green JB, Berg T, Norum KR. 1991. Vitamin A metabolism: new perspectives on absorption, transport, and storage. *Physiological reviews* 71:951-90
39. Blaner WS, Olson JA. 1994. Retinol and retinoic acid metabolism. In *The retinoids: biology, chemistry, and medicine*, ed. MB Sporn, AB Roberts, DS Goodman:229-56. New York, NY: Raven Press. Number of 229-56 pp.

40. Vogel S, Gamble MV, Blaner WS. 1999. Retinoid uptake, metabolism and transport. In *The handbook of experimental pharmacology, the retinoids*, ed. H Nau, WS Blaner:31-96. Heidelberg, Germany: Springer Verlag. Number of 31-96 pp.
41. van Bennekum A, Werder M, Thuahnai ST, Han CH, Duong P, et al. 2005. Class B scavenger receptor-mediated intestinal absorption of dietary beta-carotene and cholesterol. *Biochemistry* 44:4517-25
42. During A, Harrison EH. 2007. Mechanisms of provitamin A (carotenoid) and vitamin A (retinol) transport into and out of intestinal Caco-2 cells. *J Lipid Res* 48:2283-94
43. Lobo GP, Hessel S, Eichinger A, Noy N, Moise AR, et al. 2010. ISX is a retinoic acid-sensitive gatekeeper that controls intestinal beta,beta-carotene absorption and vitamin A production. *FASEB journal : official publication of the Federation of American Societies for Experimental Biology* 24:1656-66
44. Reboul E, Abou L, Mikail C, Ghiringhelli O, Andre M, et al. 2005. Lutein transport by Caco-2 TC-7 cells occurs partly by a facilitated process involving the scavenger receptor class B type I (SR-BI). *Biochem J* 387:455-61
45. Moussa M, Landrier JF, Reboul E, Ghiringhelli O, Comera C, et al. 2008. Lycopene absorption in human intestinal cells and in mice involves scavenger receptor class B type I but not Niemann-Pick C1-like 1. *The Journal of nutrition* 138:1432-6
46. Goodman DS, Huang HS. 1965. Biosynthesis of Vitamin a with Rat Intestinal Enzymes. *Science* 149:879-80
47. Olson JA, Hayaishi O. 1965. The enzymatic cleavage of beta-carotene into vitamin A by soluble enzymes of rat liver and intestine. *Proc Natl Acad Sci U S A* 54:1364-70
48. Hessel S, Eichinger A, Isken A, Amengual J, Hunzelmann S, et al. 2007. CMO1 deficiency abolishes vitamin A production from beta-carotene and alters lipid metabolism in mice. *J Biol Chem* 282:33553-61
49. Fierce Y, de Morais Vieira M, Piantedosi R, Wyss A, Blaner WS, Paik J. 2008. In vitro and in vivo characterization of retinoid synthesis from beta-carotene. *Archives of biochemistry and biophysics* 472:126-38
50. dela Sena C, Narayanasamy S, Riedl KM, Curley RW, Jr., Schwartz SJ, Harrison EH. 2013. Substrate specificity of purified recombinant human beta-carotene 15,15'-oxygenase (BCO1). *J Biol Chem* 288:37094-103
51. van Bennekum AM, Fisher EA, Blaner WS, Harrison EH. 2000. Hydrolysis of retinyl esters by pancreatic triglyceride lipase. *Biochemistry* 39:4900-6
52. Reboul E, Berton A, Moussa M, Kreuzer C, Crenon I, Borel P. 2006. Pancreatic lipase and pancreatic lipase-related protein 2, but not pancreatic lipase-related protein 1, hydrolyze retinyl palmitate in physiological conditions. *Biochim Biophys Acta* 1761:4-10
53. Rigtrup KM, Ong DE. 1992. A retinyl ester hydrolase activity intrinsic to the brush border membrane of rat small intestine. *Biochemistry* 31:2920-6
54. Wongsiriroj N, Piantedosi R, Palczewski K, Goldberg IJ, Johnston TP, et al. 2008. The molecular basis of retinoid absorption: a genetic dissection. *J Biol Chem* 283:13510-9
55. O'Byrne SM, Wongsiriroj N, Libien J, Vogel S, Goldberg IJ, et al. 2005. Retinoid absorption and storage is impaired in mice lacking lecithin:retinol acyltransferase (LRAT). *J Biol Chem* 280:35647-57
56. E X, Zhang L, Lu J, Tso P, Blaner WS, et al. 2002. Increased neonatal mortality in mice lacking cellular retinol-binding protein II. *J Biol Chem* 277:36617-23
57. Blomhoff R, Green MH, Berg T, Norum KR. 1990. Transport and storage of vitamin A. *Science* 250:399-404
58. Goodman DS, Huang HS, Shiritori T. 1965. Tissue distribution and metabolism of newly absorbed vitamin A in the rat. *J. Lipid Res.* 6:383-9

59. Blomhoff R, Helgerud P, Rasmussen M, Berg T, Norum KR. 1982. In vivo uptake of chylomicron [3H]retinyl ester by rat liver: evidence for retinol transfer from parenchymal to nonparenchymal cells. *Proc Natl Acad Sci U S A* 79:7326-30
60. Cooper AD. 1997. Hepatic uptake of chylomicron remnants. *J Lipid Res* 38:2173-92
61. Out R, Kruijt JK, Rensen PC, Hildebrand RB, de Vos P, et al. 2004. Scavenger receptor BI plays a role in facilitating chylomicron metabolism. *J Biol Chem* 279:18401-6
62. Harrison EH, Gad MZ, Ross AC. 1995. Hepatic uptake and metabolism of chylomicron retinyl esters: probable role of plasma membrane/endosomal retinyl ester hydrolases. *J Lipid Res* 36:1498-506
63. Boerman MH, Napoli JL. 1991. Cholate-independent retinyl ester hydrolysis. Stimulation by Apo-cellular retinol-binding protein. *J Biol Chem* 266:22273-8
64. Ghyselinck NB, Bavik C, Sapin V, Mark M, Bonnier D, et al. 1999. Cellular retinol-binding protein I is essential for vitamin A homeostasis. *The EMBO journal* 18:4903-14
65. Blomhoff R, Rasmussen M, Nilsson A, Norum KR, Berg T, et al. 1985. Hepatic retinol metabolism. Distribution of retinoids, enzymes, and binding proteins in isolated rat liver cells. *J Biol Chem* 260:13560-5
66. Senoo H. 2004. Structure and function of hepatic stellate cells. *Medical electron microscopy : official journal of the Clinical Electron Microscopy Society of Japan* 37:3-15
67. O'Byrne SM, Blaner WS. 2005. Introduction to retinoids. In *Caratenoids and retinoids: molecular aspects and health issues*, ed. L Packer, U Obermuller-Jevic, K Kraemer, H Sies:1-22. Champaign, IL: AOCS Press. Number of 1-22 pp.
68. Quadro L, Blaner WS, Salchow DJ, Vogel S, Piantedosi R, et al. 1999. Impaired retinal function and vitamin A availability in mice lacking retinol-binding protein. *The EMBO journal* 18:4633-44
69. Ronne H, Ocklind C, Wiman K, Rask L, Obrink B, Peterson PA. 1983. Ligand-dependent regulation of intracellular protein transport: effect of vitamin a on the secretion of the retinol-binding protein. *The Journal of cell biology* 96:907-10
70. Newcomer ME, Ong DE. 2000. Plasma retinol binding protein: structure and function of the prototypic lipocalin. *Biochim Biophys Acta* 1482:57-64
71. Geerts A, Bleser PD, Hautekeete ML, Niki T, Wisse E. 1994. Fat-storing (ito) cell biology. In *The liver: biology and pathobiology*, ed. IM Arias, JL Boyer, N Fausto, WB Jakoby, D Schachter, DA Shafritz:819-37. New York, NY: Raven Press. Number of 819-37 pp.
72. Geerts A. 2001. History, heterogeneity, developmental biology, and functions of quiescent hepatic stellate cells. *Seminars in liver disease* 21:311-35
73. Friedman SL. 2008. Hepatic stellate cells: protean, multifunctional, and enigmatic cells of the liver. *Physiological reviews* 88:125-72
74. Peterson PA. 1971. Studies on the interaction between prealbumin, retinol-binding protein, and vitamin A. *J Biol Chem* 246:44-9
75. van Bennekum AM, Wei S, Gamble MV, Vogel S, Piantedosi R, et al. 2001. Biochemical basis for depressed serum retinol levels in transthyretin-deficient mice. *J Biol Chem* 276:1107-13
76. Episkopou V, Maeda S, Nishiguchi S, Shimada K, Gaitanaris GA, et al. 1993. Disruption of the transthyretin gene results in mice with depressed levels of plasma retinol and thyroid hormone. *Proc Natl Acad Sci U S A* 90:2375-9
77. Wyss R, Bucheli F. 1997. Determination of endogenous levels of 13-cis-retinoic acid (isotretinoin), all-trans-retinoic acid (tretinoin) and their 4-oxo metabolites in human and animal plasma by high-performance liquid chromatography with automated column switching and ultraviolet detection. *Journal of chromatography. B, Biomedical sciences and applications* 700:31-47

78. Wassef L, Quadro L. 2011. Uptake of dietary retinoids at the maternal-fetal barrier: in vivo evidence for the role of lipoprotein lipase and alternative pathways. *J Biol Chem* 286:32198-207
79. Blaner WS, Obunike JC, Kurlandsky SB, al-Haideri M, Piantedosi R, et al. 1994. Lipoprotein lipase hydrolysis of retinyl ester. Possible implications for retinoid uptake by cells. *J Biol Chem* 269:16559-65
80. van Bennekum AM, Kako Y, Weinstock PH, Harrison EH, Deckelbaum RJ, et al. 1999. Lipoprotein lipase expression level influences tissue clearance of chylomicron retinyl ester. *J Lipid Res* 40:565-74
81. Kawaguchi R, Yu J, Honda J, Hu J, Whitelegge J, et al. 2007. A membrane receptor for retinol binding protein mediates cellular uptake of vitamin A. *Science* 315:820-5
82. Kawaguchi R, Zhong M, Kassai M, Ter-Stepanian M, Sun H. 2012. STRA6-catalyzed vitamin A influx, efflux, and exchange. *The Journal of membrane biology* 245:731-45
83. Pares X, Farres J, Kedishvili N, Duester G. 2008. Medium- and short-chain dehydrogenase/reductase gene and protein families : Medium-chain and short-chain dehydrogenases/reductases in retinoid metabolism. *Cellular and molecular life sciences : CMLS* 65:3936-49
84. Molotkov A, Deltour L, Foglio MH, Cuenca AE, Duester G. 2002. Distinct retinoid metabolic functions for alcohol dehydrogenase genes Adh1 and Adh4 in protection against vitamin A toxicity or deficiency revealed in double null mutant mice. *J Biol Chem* 277:13804-11
85. Hellgren M, Stromberg P, Gallego O, Martras S, Farres J, et al. 2007. Alcohol dehydrogenase 2 is a major hepatic enzyme for human retinol metabolism. *Cellular and molecular life sciences : CMLS* 64:498-505
86. Ang HL, Deltour L, Hayamizu TF, Zgombic-Knight M, Duester G. 1996. Retinoic acid synthesis in mouse embryos during gastrulation and craniofacial development linked to class IV alcohol dehydrogenase gene expression. *J Biol Chem* 271:9526-34
87. Molotkov A, Fan X, Deltour L, Foglio MH, Martras S, et al. 2002. Stimulation of retinoic acid production and growth by ubiquitously expressed alcohol dehydrogenase Adh3. *Proc Natl Acad Sci U S A* 99:5337-42
88. Deltour L, Foglio MH, Duester G. 1999. Impaired retinol utilization in Adh4 alcohol dehydrogenase mutant mice. *Developmental genetics* 25:1-10
89. Yamamoto H, Simon A, Eriksson U, Harris E, Berson EL, Dryja TP. 1999. Mutations in the gene encoding 11-cis retinol dehydrogenase cause delayed dark adaptation and fundus albipunctatus. *Nature genetics* 22:188-91
90. Janecke AR, Thompson DA, Utermann G, Becker C, Hubner CA, et al. 2004. Mutations in RDH12 encoding a photoreceptor cell retinol dehydrogenase cause childhood-onset severe retinal dystrophy. *Nature genetics* 36:850-4
91. Perrault I, Hanein S, Gerber S, Barbet F, Ducroq D, et al. 2004. Retinal dehydrogenase 12 (RDH12) mutations in leber congenital amaurosis. *American journal of human genetics* 75:639-46
92. Lee SA, Belyaeva OV, Popov IK, Kedishvili NY. 2007. Overproduction of bioactive retinoic acid in cells expressing disease-associated mutants of retinol dehydrogenase 12. *J Biol Chem* 282:35621-8
93. Zhang M, Hu P, Krois CR, Kane MA, Napoli JL. 2007. Altered vitamin A homeostasis and increased size and adiposity in the rdh1-null mouse. *FASEB journal : official publication of the Federation of American Societies for Experimental Biology* 21:2886-96
94. Sandell LL, Sanderson BW, Moiseyev G, Johnson T, Mushegian A, et al. 2007. RDH10 is essential for synthesis of embryonic retinoic acid and is required for limb, craniofacial, and organ development. *Genes Dev* 21:1113-24

95. Boerman MH, Napoli JL. 1995. Effects of sulfhydryl reagents, retinoids, and solubilization on the activity of microsomal retinol dehydrogenase. *Archives of biochemistry and biophysics* 321:434-41
96. Chai X, Boerman MH, Zhai Y, Napoli JL. 1995. Cloning of a cDNA for liver microsomal retinol dehydrogenase. A tissue-specific, short-chain alcohol dehydrogenase. *J Biol Chem* 270:3900-4
97. Belyaeva OV, Korkina OV, Stetsenko AV, Kim T, Nelson PS, Kedishvili NY. 2005. Biochemical properties of purified human retinol dehydrogenase 12 (RDH12): catalytic efficiency toward retinoids and C9 aldehydes and effects of cellular retinol-binding protein type I (CRBPI) and cellular retinaldehyde-binding protein (CRALBP) on the oxidation and reduction of retinoids. *Biochemistry* 44:7035-47
98. Gallego O, Belyaeva OV, Porte S, Ruiz FX, Stetsenko AV, et al. 2006. Comparative functional analysis of human medium-chain dehydrogenases, short-chain dehydrogenases/reductases and aldo-keto reductases with retinoids. *Biochem J* 399:101-9
99. Kumar S, Sandell LL, Trainor PA, Koentgen F, Duester G. 2012. Alcohol and aldehyde dehydrogenases: retinoid metabolic effects in mouse knockout models. *Biochim Biophys Acta* 1821:198-205
100. McCaffery P, Tempst P, Lara G, Drager UC. 1991. Aldehyde dehydrogenase is a positional marker in the retina. *Development* 112:693-702
101. Fan X, Molotkov A, Manabe S, Donmoyer CM, Deltour L, et al. 2003. Targeted disruption of Aldh1a1 (Raldh1) provides evidence for a complex mechanism of retinoic acid synthesis in the developing retina. *Mol Cell Biol* 23:4637-48
102. Haselbeck RJ, Hoffmann I, Duester G. 1999. Distinct functions for Aldh1 and Raldh2 in the control of ligand production for embryonic retinoid signaling pathways. *Developmental genetics* 25:353-64
103. Molotkov A, Duester G. 2003. Genetic evidence that retinaldehyde dehydrogenase Raldh1 (Aldh1a1) functions downstream of alcohol dehydrogenase Adh1 in metabolism of retinol to retinoic acid. *J Biol Chem* 278:36085-90
104. Niederreither K, Subbarayan V, Dolle P, Chambon P. 1999. Embryonic retinoic acid synthesis is essential for early mouse post-implantation development. *Nature genetics* 21:444-8
105. Mic FA, Haselbeck RJ, Cuenca AE, Duester G. 2002. Novel retinoic acid generating activities in the neural tube and heart identified by conditional rescue of Raldh2 null mutant mice. *Development* 129:2271-82
106. Li H, Wagner E, McCaffery P, Smith D, Andreadis A, Drager UC. 2000. A retinoic acid synthesizing enzyme in ventral retina and telencephalon of the embryonic mouse. *Mechanisms of development* 95:283-9
107. Mic FA, Molotkov A, Fan X, Cuenca AE, Duester G. 2000. RALDH3, a retinaldehyde dehydrogenase that generates retinoic acid, is expressed in the ventral retina, otic vesicle and olfactory pit during mouse development. *Mechanisms of development* 97:227-30
108. Molotkova N, Molotkov A, Duester G. 2007. Role of retinoic acid during forebrain development begins late when Raldh3 generates retinoic acid in the ventral subventricular zone. *Developmental biology* 303:601-10
109. Matt N, Dupe V, Garnier JM, Dennefeld C, Chambon P, et al. 2005. Retinoic acid-dependent eye morphogenesis is orchestrated by neural crest cells. *Development* 132:4789-800
110. Molotkov A, Molotkova N, Duester G. 2006. Retinoic acid guides eye morphogenetic movements via paracrine signaling but is unnecessary for retinal dorsoventral patterning. *Development* 133:1901-10
111. Rosselot C, Spraggon L, Chia I, Batourina E, Riccio P, et al. 2010. Non-cell-autonomous retinoid signaling is crucial for renal development. *Development* 137:283-92

112. Dupe V, Matt N, Garnier JM, Chambon P, Mark M, Ghyselinck NB. 2003. A newborn lethal defect due to inactivation of retinaldehyde dehydrogenase type 3 is prevented by maternal retinoic acid treatment. *Proc Natl Acad Sci U S A* 100:14036-41
113. Dowling JE, Wald G. 1960. The Biological Function of Vitamin a Acid. *Proc Natl Acad Sci U S A* 46:587-608
114. Arens JF, Van Dorp DA. 1946. Synthesis of some compounds possessing vitamin A activity. *Nature* 157:190
115. Van Dorp DA, Arens JF. 1946. Biological activity of vitamin A acid. *Nature* 158:60
116. Arens JF, Van Dorp DA. 1946. Activity of vitamin A-acid in the rat. *Nature* 158:622
117. Petkovich M, Brand NJ, Krust A, Chambon P. 1987. A human retinoic acid receptor which belongs to the family of nuclear receptors. *Nature* 330:444-50
118. Giguere V, Ong ES, Segui P, Evans RM. 1987. Identification of a receptor for the morphogen retinoic acid. *Nature* 330:624-9
119. Chambon P. 1996. A decade of molecular biology of retinoic acid receptors. *FASEB journal : official publication of the Federation of American Societies for Experimental Biology* 10:940-54
120. Kliewer SA, Umesono K, Mangelsdorf DJ, Evans RM. 1992. Retinoid X receptor interacts with nuclear receptors in retinoic acid, thyroid hormone and vitamin D3 signalling. *Nature* 355:446-9
121. Bain DL, Heneghan AF, Connaghan-Jones KD, Miura MT. 2007. Nuclear receptor structure: implications for function. *Annual review of physiology* 69:201-20
122. Mark M, Ghyselinck NB, Chambon P. 2006. Function of retinoid nuclear receptors: lessons from genetic and pharmacological dissections of the retinoic acid signaling pathway during mouse embryogenesis. *Annual review of pharmacology and toxicology* 46:451-80
123. Kane MA. 2012. Analysis, occurrence, and function of 9-cis-retinoic acid. *Biochim Biophys Acta* 1821:10-20
124. Germain P, Staels B, Dacquet C, Spedding M, Laudet V. 2006. Overview of nomenclature of nuclear receptors. *Pharmacological reviews* 58:685-704
125. Rochette-Egly C, Germain P. 2009. Dynamic and combinatorial control of gene expression by nuclear retinoic acid receptors (RARs). *Nuclear receptor signaling* 7:e005
126. Renaud JP, Rochel N, Ruff M, Vivat V, Chambon P, et al. 1995. Crystal structure of the RAR-gamma ligand-binding domain bound to all-trans retinoic acid. *Nature* 378:681-9
127. le Maire A, Teyssier C, Erb C, Grimaldi M, Alvarez S, et al. 2010. A unique secondary-structure switch controls constitutive gene repression by retinoic acid receptor. *Nature structural & molecular biology* 17:801-7
128. Hu X, Lazar MA. 1999. The CoRNR motif controls the recruitment of corepressors by nuclear hormone receptors. *Nature* 402:93-6
129. Perissi V, Staszewski LM, McInerney EM, Kurokawa R, Krones A, et al. 1999. Molecular determinants of nuclear receptor-corepressor interaction. *Genes Dev* 13:3198-208
130. Wong CW, Privalsky ML. 1998. Transcriptional silencing is defined by isoform- and heterodimer-specific interactions between nuclear hormone receptors and corepressors. *Mol Cell Biol* 18:5724-33
131. Farboud B, Hauksdottir H, Wu Y, Privalsky ML. 2003. Isotype-restricted corepressor recruitment: a constitutively closed helix 12 conformation in retinoic acid receptors beta and gamma interferes with corepressor recruitment and prevents transcriptional repression. *Mol Cell Biol* 23:2844-58
132. Hauksdottir H, Farboud B, Privalsky ML. 2003. Retinoic acid receptors beta and gamma do not repress, but instead activate target gene transcription in both the absence and presence of hormone ligand. *Molecular endocrinology* 17:373-85

133. Loudig O, Babichuk C, White J, Abu-Abed S, Mueller C, Petkovich M. 2000. Cytochrome P450RAI(CYP26) promoter: a distinct composite retinoic acid response element underlies the complex regulation of retinoic acid metabolism. *Molecular endocrinology* 14:1483-97
134. Dupe V, Davenne M, Brocard J, Dolle P, Mark M, et al. 1997. In vivo functional analysis of the Hoxa-1 3' retinoic acid response element (3'RARE). *Development* 124:399-410
135. Qian A, Cai Y, Magee TR, Wan YJ. 2000. Identification of retinoic acid-responsive elements on the HNF1alpha and HNF4alpha genes. *Biochemical and biophysical research communications* 276:837-42
136. de The H, Vivanco-Ruiz MM, Tiollais P, Stunnenberg H, Dejean A. 1990. Identification of a retinoic acid responsive element in the retinoic acid receptor beta gene. *Nature* 343:177-80
137. Smith WC, Nakshatri H, Leroy P, Rees J, Chambon P. 1991. A retinoic acid response element is present in the mouse cellular retinol binding protein I (mCRBPI) promoter. *The EMBO journal* 10:2223-30
138. Mangelsdorf DJ, Umesono K, Kliewer SA, Borgmeyer U, Ong ES, Evans RM. 1991. A direct repeat in the cellular retinol-binding protein type II gene confers differential regulation by RXR and RAR. *Cell* 66:555-61
139. Rastinejad F, Wagner T, Zhao Q, Khorasanizadeh S. 2000. Structure of the RXR-RAR DNA-binding complex on the retinoic acid response element DR1. *The EMBO journal* 19:1045-54
140. Khorasanizadeh S, Rastinejad F. 2001. Nuclear-receptor interactions on DNA-response elements. *Trends in biochemical sciences* 26:384-90
141. Bastien J, Rochette-Egly C. 2004. Nuclear retinoid receptors and the transcription of retinoid-target genes. *Gene* 328:1-16
142. Rochette-Egly C, Adam S, Rossignol M, Egly JM, Chambon P. 1997. Stimulation of RAR alpha activation function AF-1 through binding to the general transcription factor TFIIH and phosphorylation by CDK7. *Cell* 90:97-107
143. Bastien J, Adam-Stitah S, Riedl T, Egly JM, Chambon P, Rochette-Egly C. 2000. TFIIH interacts with the retinoic acid receptor gamma and phosphorylates its AF-1-activating domain through cdk7. *J Biol Chem* 275:21896-904
144. Poon MM, Chen L. 2008. Retinoic acid-gated sequence-specific translational control by RARalpha. *Proc Natl Acad Sci U S A* 105:20303-8
145. Farboud B, Privalsky ML. 2004. Retinoic acid receptor-alpha is stabilized in a repressive state by its C-terminal, isotype-specific F domain. *Molecular endocrinology* 18:2839-53
146. Leid M, Kastner P, Chambon P. 1992. Multiplicity generates diversity in the retinoic acid signalling pathways. *Trends in biochemical sciences* 17:427-33
147. Dolle P. 2009. Developmental expression of retinoic acid receptors (RARs). *Nuclear receptor signaling* 7:e006
148. Duong V, Rochette-Egly C. 2011. The molecular physiology of nuclear retinoic acid receptors. From health to disease. *Biochim Biophys Acta* 1812:1023-31
149. Kastner P, Chan S. 2001. Function of RARalpha during the maturation of neutrophils. *Oncogene* 20:7178-85
150. Samad TA, Krezel W, Chambon P, Borrelli E. 1997. Regulation of dopaminergic pathways by retinoids: activation of the D2 receptor promoter by members of the retinoic acid receptor-retinoid X receptor family. *Proc Natl Acad Sci U S A* 94:14349-54
151. Purton LE, Dworkin S, Olsen GH, Walkley CR, Fabb SA, et al. 2006. RARgamma is critical for maintaining a balance between hematopoietic stem cell self-renewal and differentiation. *The Journal of experimental medicine* 203:1283-93

152. Dzhagalov I, Chambon P, He YW. 2007. Regulation of CD8+ T lymphocyte effector function and macrophage inflammatory cytokine production by retinoic acid receptor gamma. *Journal of immunology* 178:2113-21
153. Gordy C, Dzhagalov I, He YW. 2009. Regulation of CD8(+) T cell functions by RARgamma. *Seminars in immunology* 21:2-7
154. Chapellier B, Mark M, Messaddeq N, Calleja C, Warot X, et al. 2002. Physiological and retinoid-induced proliferations of epidermis basal keratinocytes are differently controlled. *The EMBO journal* 21:3402-13
155. Sani BP, Hill DL. 1974. Retinoic acid: a binding protein in chick embryo metatarsal skin. *Biochemical and biophysical research communications* 61:1276-82
156. Ong DE, Newcomer ME, Chytil F. 1994. Cellular retinoid-binding proteins. In *The retinoids: biology, chemistry, and medicine*, ed. MB Sporn, AB Roberts, DS Goodman, 2:283-317. New York City, NY: Raven Press. Number of 283-317 pp.
157. Ong DE, Chytil F. 1975. Retinoic acid-binding protein in rat tissue. Partial purification and comparison to rat tissue retinol-binding protein. *J Biol Chem* 250:6113-7
158. Norris AW, Cheng L, Giguere V, Rosenberger M, Li E. 1994. Measurement of subnanomolar retinoic acid binding affinities for cellular retinoic acid binding proteins by fluorometric titration. *Biochim Biophys Acta* 1209:10-8
159. Fiorella PD, Giguere V, Napoli JL. 1993. Expression of cellular retinoic acid-binding protein (type II) in Escherichia coli. Characterization and comparison to cellular retinoic acid-binding protein (type I). *J Biol Chem* 268:21545-52
160. Dencker L, Annerwall E, Busch C, Eriksson U. 1990. Localization of specific retinoid-binding sites and expression of cellular retinoic-acid-binding protein (CRABP) in the early mouse embryo. *Development* 110:343-52
161. Kleywegt GJ, Bergfors T, Senn H, Le Motte P, Gsell B, et al. 1994. Crystal structures of cellular retinoic acid binding proteins I and II in complex with all-trans-retinoic acid and a synthetic retinoid. *Structure* 2:1241-58
162. Maden M. 1994. Distribution of cellular retinoic acid-binding proteins I and II in the chick embryo and their relationship to teratogenesis. *Teratology* 50:294-301
163. Giguere V, Lyn S, Yip P, Siu CH, Amin S. 1990. Molecular cloning of cDNA encoding a second cellular retinoic acid-binding protein. *Proc Natl Acad Sci U S A* 87:6233-7
164. Harnish DC, Soprano KJ, Soprano DR. 1992. Mouse conceptuses have a limited capacity to elevate the mRNA level of cellular retinoid binding proteins in response to teratogenic doses of retinoic acid. *Teratology* 46:137-46
165. Durand B, Saunders M, Leroy P, Leid M, Chambon P. 1992. All-trans and 9-cis retinoic acid induction of CRABPII transcription is mediated by RAR-RXR heterodimers bound to DR1 and DR2 repeated motifs. *Cell* 71:73-85
166. Astrom A, Pettersson U, Chambon P, Voorhees JJ. 1994. Retinoic acid induction of human cellular retinoic acid-binding protein-II gene transcription is mediated by retinoic acid receptor-retinoid X receptor heterodimers bound to one far upstream retinoic acid-responsive element with 5-base pair spacing. *J Biol Chem* 269:22334-9
167. Li E, Norris AW. 1996. Structure/function of cytoplasmic vitamin A-binding proteins. *Annual review of nutrition* 16:205-34
168. Eller MS, Harkness DD, Bhawan J, Gilchrest BA. 1994. Epidermal differentiation enhances CRABP II expression in human skin. *The Journal of investigative dermatology* 103:785-90
169. Zheng WL, Sierra-Rivera E, Luan J, Osteen KG, Ong DE. 2000. Retinoic acid synthesis and expression of cellular retinol-binding protein and cellular retinoic acid-binding protein type II are concurrent with decidualization of rat uterine stromal cells. *Endocrinology* 141:802-8

170. Bucco RA, Melner MH, Gordon DS, Leers-Sucheta S, Ong DE. 1995. Inducible expression of cellular retinoic acid-binding protein II in rat ovary: gonadotropin regulation during luteal development. *Endocrinology* 136:2730-40
171. Asson-Batres MA, Ahmad O, Smith WB. 2003. Expression of the cellular retinoic acid binding proteins, type II and type I, in mature rat olfactory epithelium. *Cell and tissue research* 312:9-19
172. Donovan M, Olofsson B, Gustafson AL, Dencker L, Eriksson U. 1995. The cellular retinoic acid binding proteins. *The Journal of steroid biochemistry and molecular biology* 53:459-65
173. Napoli JL. 1996. Biochemical pathways of retinoid transport, metabolism, and signal transduction. *Clinical immunology and immunopathology* 80:S52-62
174. Wei LN, Chang L, Hu X. 1999. Studies of the type I cellular retinoic acid-binding protein mutants and their biological activities. *Mol Cell Biochem* 200:69-76
175. Wei LN. 2012. Chromatin remodeling and epigenetic regulation of the CrabpI gene in adipocyte differentiation. *Biochim Biophys Acta* 1821:206-12
176. Majumdar A, Petrescu AD, Xiong Y, Noy N. 2011. Nuclear translocation of cellular retinoic acid-binding protein II is regulated by retinoic acid-controlled SUMOylation. *J Biol Chem* 286:42749-57
177. Sessler RJ, Noy N. 2005. A ligand-activated nuclear localization signal in cellular retinoic acid binding protein-II. *Mol Cell* 18:343-53
178. Budhu A, Gillilan R, Noy N. 2001. Localization of the RAR interaction domain of cellular retinoic acid binding protein-II. *J Mol Biol* 305:939-49
179. Dong D, Ruuska SE, Levinthal DJ, Noy N. 1999. Distinct roles for cellular retinoic acid-binding proteins I and II in regulating signaling by retinoic acid. *J Biol Chem* 274:23695-8
180. Fawcett D, Pasceri P, Fraser R, Colbert M, Rossant J, Giguere V. 1995. Postaxial polydactyly in forelimbs of CRABP-II mutant mice. *Development* 121:671-9
181. Lampron C, Rochette-Egly C, Gorry P, Dolle P, Mark M, et al. 1995. Mice deficient in cellular retinoic acid binding protein II (CRABPII) or in both CRABPI and CRABPII are essentially normal. *Development* 121:539-48
182. Elder JT, Astrom A, Pettersson U, Tavakkol A, Krust A, et al. 1992. Retinoic acid receptors and binding proteins in human skin. *The Journal of investigative dermatology* 98:36S-41S
183. Siegenthaler G, Tomatis I, Didierjean L, Jaconi S, Saurat JH. 1992. Overexpression of cellular retinoic acid-binding protein type II (CRABP-II) and down-regulation of CRABP-I in psoriatic skin. *Dermatology* 185:251-6
184. Iqbal J, Hussain MM. 2009. Intestinal lipid absorption. *American journal of physiology. Endocrinology and metabolism* 296:E1183-94
185. Young SG, Zechner R. 2013. Biochemistry and pathophysiology of intravascular and intracellular lipolysis. *Genes Dev* 27:459-84
186. McArthur MJ, Atshaves BP, Frolov A, Foxworth WD, Kier AB, Schroeder F. 1999. Cellular uptake and intracellular trafficking of long chain fatty acids. *J Lipid Res* 40:1371-83
187. Jump DB. 2002. Dietary polyunsaturated fatty acids and regulation of gene transcription. *Current opinion in lipidology* 13:155-64
188. Van der Vusse GJ, Roemen TH. 1995. Gradient of fatty acids from blood plasma to skeletal muscle in dogs. *Journal of applied physiology* 78:1839-43
189. Knudsen J, Jensen MV, Hansen JK, Faergeman NJ, Neergaard TB, Gaigg B. 1999. Role of acylCoA binding protein in acylCoA transport, metabolism and cell signaling. *Mol Cell Biochem* 192:95-103

190. Faergeman NJ, Knudsen J. 1997. Role of long-chain fatty acyl-CoA esters in the regulation of metabolism and in cell signalling. *Biochem J* 323 (Pt 1):1-12
191. Zanetti R, Catala A. 1991. Fatty acid binding protein removes fatty acids but not phospholipids from microsomes liposomes and sonicated vesicles. *Mol Cell Biochem* 100:1-8
192. Catala A, Arcemis C, Cerruti A. 1994. Interaction of rat liver microsomes containing saturated or unsaturated fatty acids with fatty acid binding protein: peroxidation effect. *Mol Cell Biochem* 137:135-9
193. Jolly CA, Hubbell T, Behnke WD, Schroeder F. 1997. Fatty acid binding protein: stimulation of microsomal phosphatidic acid formation. *Archives of biochemistry and biophysics* 341:112-21
194. Massey JB, Bick DH, Pownall HJ. 1997. Spontaneous transfer of monoacyl amphiphiles between lipid and protein surfaces. *Biophysical journal* 72:1732-43
195. Weisiger RA. 1996. When is a carrier not a membrane carrier? The cytoplasmic transport of amphipathic molecules. *Hepatology* 24:1288-95
196. Jakobsson A, Westerberg R, Jacobsson A. 2006. Fatty acid elongases in mammals: their regulation and roles in metabolism. *Progress in lipid research* 45:237-49
197. Maier T, Leibundgut M, Boehringer D, Ban N. 2010. Structure and function of eukaryotic fatty acid synthases. *Quarterly reviews of biophysics* 43:373-422
198. Chan DI, Vogel HJ. 2010. Current understanding of fatty acid biosynthesis and the acyl carrier protein. *Biochem J* 430:1-19
199. Nakamura MT, Nara TY. 2004. Structure, function, and dietary regulation of delta6, delta5, and delta9 desaturases. *Annual review of nutrition* 24:345-76
200. Meesapyodsuk D, Qiu X. 2012. The front-end desaturase: structure, function, evolution and biotechnological use. *Lipids* 47:227-37
201. Liu X, Strable MS, Ntambi JM. 2011. Stearoyl CoA desaturase 1: role in cellular inflammation and stress. *Advances in nutrition* 2:15-22
202. Nakamura MT, Yudell BE, Loor JJ. 2014. Regulation of energy metabolism by long-chain fatty acids. *Progress in lipid research* 53:124-44
203. Qi C, Zhu Y, Reddy JK. 2000. Peroxisome proliferator-activated receptors, coactivators, and downstream targets. *Cell biochemistry and biophysics* 32 Spring:187-204
204. Wanders RJ, Waterham HR. 2006. Biochemistry of mammalian peroxisomes revisited. *Annual review of biochemistry* 75:295-332
205. Reddy JK, Krishnakantha TP. 1975. Hepatic peroxisome proliferation: induction by two novel compounds structurally unrelated to clofibrate. *Science* 190:787-9
206. Reddy JK, Lalwai ND. 1983. Carcinogenesis by hepatic peroxisome proliferators: evaluation of the risk of hypolipidemic drugs and industrial plasticizers to humans. *Critical reviews in toxicology* 12:1-58
207. Reddy JK, Rao MS. 1986. Peroxisome proliferators and cancer: mechanisms and implications. *Trends Pharmacol. Sci.* 7:438-43
208. Issemann I, Green S. 1990. Activation of a member of the steroid hormone receptor superfamily by peroxisome proliferators. *Nature* 347:645-50
209. Dreyer C, Krey G, Keller H, Givel F, Helftenbein G, Wahli W. 1992. Control of the peroxisomal beta-oxidation pathway by a novel family of nuclear hormone receptors. *Cell* 68:879-87
210. Novac N, Heinzel T. 2004. Nuclear receptors: overview and classification. *Current drug targets. Inflammation and allergy* 3:335-46
211. Desvergne B, Wahli W. 1999. Peroxisome proliferator-activated receptors: nuclear control of metabolism. *Endocrine reviews* 20:649-88
212. Juge-Aubry C, Pernin A, Favez T, Burger AG, Wahli W, et al. 1997. DNA binding properties of peroxisome proliferator-activated receptor subtypes on various natural

peroxisome proliferator response elements. Importance of the 5'-flanking region. *J Biol Chem* 272:25252-9

213. Xu HE, Lambert MH, Montana VG, Plunket KD, Moore LB, et al. 2001. Structural determinants of ligand binding selectivity between the peroxisome proliferator-activated receptors. *Proc Natl Acad Sci U S A* 98:13919-24
214. Xu HE, Stanley TB, Montana VG, Lambert MH, Shearer BG, et al. 2002. Structural basis for antagonist-mediated recruitment of nuclear co-repressors by PPARalpha. *Nature* 415:813-7
215. Xu HE, Lambert MH, Montana VG, Parks DJ, Blanchard SG, et al. 1999. Molecular recognition of fatty acids by peroxisome proliferator-activated receptors. *Mol Cell* 3:397-403
216. Forman BM, Goode E, Chen J, Oro AE, Bradley DJ, et al. 1995. Identification of a nuclear receptor that is activated by farnesol metabolites. *Cell* 81:687-93
217. Yu K, Bayona W, Kallen CB, Harding HP, Ravera CP, et al. 1995. Differential activation of peroxisome proliferator-activated receptors by eicosanoids. *J Biol Chem* 270:23975-83
218. Devchand PR, Keller H, Peters JM, Vazquez M, Gonzalez FJ, Wahli W. 1996. The PPARalpha-leukotriene B4 pathway to inflammation control. *Nature* 384:39-43
219. Forman BM, Chen J, Evans RM. 1997. Hypolipidemic drugs, polyunsaturated fatty acids, and eicosanoids are ligands for peroxisome proliferator-activated receptors alpha and delta. *Proc Natl Acad Sci U S A* 94:4312-7
220. Chakravarthy MV, Lodhi IJ, Yin L, Malapaka RR, Xu HE, et al. 2009. Identification of a physiologically relevant endogenous ligand for PPARalpha in liver. *Cell* 138:476-88
221. Noy N. 2007. Ligand specificity of nuclear hormone receptors: sifting through promiscuity. *Biochemistry* 46:13461-7
222. Lehmann JM, Moore LB, Smith-Oliver TA, Wilkison WO, Willson TM, Kliewer SA. 1995. An antidiabetic thiazolidinedione is a high affinity ligand for peroxisome proliferator-activated receptor gamma (PPAR gamma). *J Biol Chem* 270:12953-6
223. Duffy D, Rader DJ. 2005. Drugs in development: targeting high-density lipoprotein metabolism and reverse cholesterol transport. *Current opinion in cardiology* 20:301-6
224. Monsalve FA, Pyarasani RD, Delgado-Lopez F, Moore-Carrasco R. 2013. Peroxisome proliferator-activated receptor targets for the treatment of metabolic diseases. *Mediators of inflammation* 2013:549627
225. Itoh T, Fairall L, Amin K, Inaba Y, Szanto A, et al. 2008. Structural basis for the activation of PPARgamma by oxidized fatty acids. *Nature structural & molecular biology* 15:924-31
226. Kliewer SA, Sundseth SS, Jones SA, Brown PJ, Wisely GB, et al. 1997. Fatty acids and eicosanoids regulate gene expression through direct interactions with peroxisome proliferator-activated receptors alpha and gamma. *Proc Natl Acad Sci U S A* 94:4318-23
227. Liliom K, Tsukahara T, Tsukahara R, Zelman-Femiak M, Swiezewska E, Tigyi G. 2006. Farnesyl phosphates are endogenous ligands of lysophosphatidic acid receptors: inhibition of LPA GPCR and activation of PPARs. *Biochim Biophys Acta* 1761:1506-14
228. Goto T, Nagai H, Egawa K, Kim YI, Kato S, et al. 2011. Farnesyl pyrophosphate regulates adipocyte functions as an endogenous PPARgamma agonist. *Biochem J* 438:111-9
229. O'Sullivan SE, Kendall DA. 2010. Cannabinoid activation of peroxisome proliferator-activated receptors: potential for modulation of inflammatory disease. *Immunobiology* 215:611-6
230. Shaw N, Elholm M, Noy N. 2003. Retinoic acid is a high affinity selective ligand for the peroxisome proliferator-activated receptor beta/delta. *J Biol Chem* 278:41589-92

231. Ferry G, Bruneau V, Beauverger P, Goussard M, Rodriguez M, et al. 2001. Binding of prostaglandins to human PPARgamma: tool assessment and new natural ligands. *European journal of pharmacology* 417:77-89
232. Katusic ZS, Santhanam AV, He T. 2012. Vascular effects of prostacyclin: does activation of PPARdelta play a role? *Trends in pharmacological sciences* 33:559-64
233. Alberti KG, Eckel RH, Grundy SM, Zimmet PZ, Cleeman JI, et al. 2009. Harmonizing the metabolic syndrome: a joint interim statement of the International Diabetes Federation Task Force on Epidemiology and Prevention; National Heart, Lung, and Blood Institute; American Heart Association; World Heart Federation; International Atherosclerosis Society; and International Association for the Study of Obesity. *Circulation* 120:1640-5
234. Leibowitz MD, Fievet C, Hennuyer N, Peinado-Onsurbe J, Duez H, et al. 2000. Activation of PPARdelta alters lipid metabolism in db/db mice. *FEBS letters* 473:333-6
235. Oliver WR, Jr., Shenk JL, Snaith MR, Russell CS, Plunket KD, et al. 2001. A selective peroxisome proliferator-activated receptor delta agonist promotes reverse cholesterol transport. *Proc Natl Acad Sci U S A* 98:5306-11
236. Barbier O, Torra IP, Duguay Y, Blanquart C, Fruchart JC, et al. 2002. Pleiotropic actions of peroxisome proliferator-activated receptors in lipid metabolism and atherosclerosis. *Arteriosclerosis, thrombosis, and vascular biology* 22:717-26
237. Barak Y, Liao D, He W, Ong ES, Nelson MC, et al. 2002. Effects of peroxisome proliferator-activated receptor delta on placentation, adiposity, and colorectal cancer. *Proc Natl Acad Sci U S A* 99:303-8
238. Akiyama TE, Lambert G, Nicol CJ, Matsusue K, Peters JM, et al. 2004. Peroxisome proliferator-activated receptor beta/delta regulates very low density lipoprotein production and catabolism in mice on a Western diet. *J Biol Chem* 279:20874-81
239. Lee CH, Olson P, Hevener A, Mehl I, Chong LW, et al. 2006. PPARdelta regulates glucose metabolism and insulin sensitivity. *Proc Natl Acad Sci U S A* 103:3444-9
240. Muoio DM, MacLean PS, Lang DB, Li S, Houmard JA, et al. 2002. Fatty acid homeostasis and induction of lipid regulatory genes in skeletal muscles of peroxisome proliferator-activated receptor (PPAR) alpha knock-out mice. Evidence for compensatory regulation by PPAR delta. *J Biol Chem* 277:26089-97
241. Wang YX, Zhang CL, Yu RT, Cho HK, Nelson MC, et al. 2004. Regulation of muscle fiber type and running endurance by PPARdelta. *PLoS biology* 2:e294
242. Grimaldi PA. 2010. Metabolic and nonmetabolic regulatory functions of peroxisome proliferator-activated receptor beta. *Current opinion in lipidology* 21:186-91
243. Schuler M, Ali F, Chambon C, Duteil D, Bornert JM, et al. 2006. PGC1alpha expression is controlled in skeletal muscles by PPARbeta, whose ablation results in fiber-type switching, obesity, and type 2 diabetes. *Cell metabolism* 4:407-14
244. Luquet S, Lopez-Soriano J, Holst D, Fredenrich A, Melki J, et al. 2003. Peroxisome proliferator-activated receptor delta controls muscle development and oxidative capability. *FASEB journal : official publication of the Federation of American Societies for Experimental Biology* 17:2299-301
245. Bishop-Bailey D, Bystrom J. 2009. Emerging roles of peroxisome proliferator-activated receptor-beta/delta in inflammation. *Pharmacology & therapeutics* 124:141-50
246. Fan Y, Wang Y, Tang Z, Zhang H, Qin X, et al. 2008. Suppression of pro-inflammatory adhesion molecules by PPAR-delta in human vascular endothelial cells. *Arteriosclerosis, thrombosis, and vascular biology* 28:315-21
247. Liang YJ, Liu YC, Chen CY, Lai LP, Shyu KG, et al. 2010. Comparison of PPARdelta and PPARgamma in inhibiting the pro-inflammatory effects of C-reactive protein in endothelial cells. *International journal of cardiology* 143:361-7

248. Piqueras L, Sanz MJ, Perretti M, Morcillo E, Norling L, et al. 2009. Activation of PPARbeta/delta inhibits leukocyte recruitment, cell adhesion molecule expression, and chemokine release. *Journal of leukocyte biology* 86:115-22
249. Minutoli L, Antonuccio P, Polito F, Bitto A, Squadrito F, et al. 2009. Peroxisome proliferator activated receptor beta/delta activation prevents extracellular regulated kinase 1/2 phosphorylation and protects the testis from ischemia and reperfusion injury. *The Journal of urology* 181:1913-21
250. Yue TL, Nerurkar SS, Bao W, Jucker BM, Sarov-Blat L, et al. 2008. In vivo activation of peroxisome proliferator-activated receptor-delta protects the heart from ischemia/reperfusion injury in Zucker fatty rats. *The Journal of pharmacology and experimental therapeutics* 325:466-74
251. Smeets PJ, Teunissen BE, Planavila A, de Vogel-van den Bosch H, Willemsen PH, et al. 2008. Inflammatory pathways are activated during cardiomyocyte hypertrophy and attenuated by peroxisome proliferator-activated receptors PPARalpha and PPARdelta. *J Biol Chem* 283:29109-18
252. Rodriguez-Calvo R, Serrano L, Coll T, Moullan N, Sanchez RM, et al. 2008. Activation of peroxisome proliferator-activated receptor beta/delta inhibits lipopolysaccharide-induced cytokine production in adipocytes by lowering nuclear factor-kappaB activity via extracellular signal-related kinase 1/2. *Diabetes* 57:2149-57
253. Defaux A, Zurich MG, Braissant O, Honegger P, Monnet-Tschudi F. 2009. Effects of the PPAR-beta agonist GW501516 in an in vitro model of brain inflammation and antibody-induced demyelination. *Journal of neuroinflammation* 6:15
254. Nadra K, Anghel SI, Joye E, Tan NS, Basu-Modak S, et al. 2006. Differentiation of trophoblast giant cells and their metabolic functions are dependent on peroxisome proliferator-activated receptor beta/delta. *Mol Cell Biol* 26:3266-81
255. Tan NS, Michalik L, Noy N, Yasmin R, Pacot C, et al. 2001. Critical roles of PPAR beta/delta in keratinocyte response to inflammation. *Genes Dev* 15:3263-77
256. Di-Poi N, Tan NS, Michalik L, Wahli W, Desvergne B. 2002. Antiapoptotic role of PPARbeta in keratinocytes via transcriptional control of the Akt1 signaling pathway. *Mol Cell* 10:721-33
257. Hall MG, Quignodon L, Desvergne B. 2008. Peroxisome Proliferator-Activated Receptor beta/delta in the Brain: Facts and Hypothesis. *PPAR Res* 2008:780452
258. Peters JM, Lee SS, Li W, Ward JM, Gavrilova O, et al. 2000. Growth, adipose, brain, and skin alterations resulting from targeted disruption of the mouse peroxisome proliferator-activated receptor beta(delta). *Mol Cell Biol* 20:5119-28
259. Rosenberger TA, Hovda JT, Peters JM. 2002. Targeted disruption of peroxisomal proliferator-activated receptor beta (delta) results in distinct gender differences in mouse brain phospholipid and esterified FA levels. *Lipids* 37:495-500
260. Raza H, Chung WL, Mukhtar H. 1991. Specific high-affinity binding of fatty acids to epidermal cytosolic proteins. *The Journal of investigative dermatology* 97:323-6
261. Madsen P, Rasmussen HH, Leffers H, Honore B, Celis JE. 1992. Molecular cloning and expression of a novel keratinocyte protein (psoriasis-associated fatty acid-binding protein [PA-FABP]) that is highly up-regulated in psoriatic skin and that shares similarity to fatty acid-binding proteins. *The Journal of investigative dermatology* 99:299-305
262. Siegenthaler G, Hotz R, Chatellard-Gruaz D, Jaconi S, Saurat JH. 1993. Characterization and expression of a novel human fatty acid-binding protein: the epidermal type (E-FABP). *Biochemical and biophysical research communications* 190:482-7
263. Lucke C, Gutierrez-Gonzalez LH, Hamilton JA. 2003. Intracellular lipid binding proteins: evolution, structure, and ligand binding. In *Cellular proteins and their fatty acids in health and disease*, ed. AK Duttaroy, F Spener:106. Weinheim, Germany: Wiley-VCH Verlag GmbH & Co. Number of 106 pp.

264. Hohoff C, Borchers T, Rustow B, Spener F, van Tilbeurgh H. 1999. Expression, purification, and crystal structure determination of recombinant human epidermal-type fatty acid binding protein. *Biochemistry* 38:12229-39
265. Gutierrez-Gonzalez LH, Ludwig C, Hohoff C, Rademacher M, Hanhoff T, et al. 2002. Solution structure and backbone dynamics of human epidermal-type fatty acid-binding protein (E-FABP). *Biochem J* 364:725-37
266. Maeda K, Uysal KT, Makowski L, Gorgun CZ, Atsumi G, et al. 2003. Role of the fatty acid binding protein mal1 in obesity and insulin resistance. *Diabetes* 52:300-7
267. Yeung DC, Wang Y, Xu A, Cheung SC, Wat NM, et al. 2008. Epidermal fatty-acid-binding protein: a new circulating biomarker associated with cardio-metabolic risk factors and carotid atherosclerosis. *Eur Heart J* 29:2156-63
268. Schug TT, Berry DC, Shaw NS, Travis SN, Noy N. 2007. Opposing effects of retinoic acid on cell growth result from alternate activation of two different nuclear receptors. *Cell* 129:723-33
269. Schug TT, Berry DC, Toshkov IA, Cheng L, Nikitin AY, Noy N. 2008. Overcoming retinoic acid-resistance of mammary carcinomas by diverting retinoic acid from PPARbeta/delta to RAR. *Proc Natl Acad Sci U S A* 105:7546-51
270. Morgan E, Kannan-Thulasiraman P, Noy N. 2010. Involvement of Fatty Acid Binding Protein 5 and PPARbeta/delta in Prostate Cancer Cell Growth. *PPAR Res* 2010
271. Kannan-Thulasiraman P, Seachrist DD, Mahabeleshwar GH, Jain MK, Noy N. 2010. Fatty acid-binding protein 5 and PPARbeta/delta are critical mediators of epidermal growth factor receptor-induced carcinoma cell growth. *J Biol Chem* 285:19106-15
272. Levi L, Lobo G, Doud MK, von Lintig J, Seachrist D, et al. 2013. Genetic ablation of the fatty acid-binding protein FABP5 suppresses HER2-induced mammary tumorigenesis. *Cancer research* 73:4770-80
273. Campos B, Centner FS, Bermejo JL, Ali R, Dorsch K, et al. 2011. Aberrant expression of retinoic acid signaling molecules influences patient survival in astrocytic gliomas. *The American journal of pathology* 178:1953-64
274. Gottlicher M, Widmark E, Li Q, Gustafsson JA. 1992. Fatty acids activate a chimera of the clofibric acid-activated receptor and the glucocorticoid receptor. *Proc Natl Acad Sci U S A* 89:4653-7
275. Banner CD, Gottlicher M, Widmark E, Sjovall J, Rafter JJ, Gustafsson JA. 1993. A systematic analytical chemistry/cell assay approach to isolate activators of orphan nuclear receptors from biological extracts: characterization of peroxisome proliferator-activated receptor activators in plasma. *J Lipid Res* 34:1583-91
276. Amri EZ, Bonino F, Ailhaud G, Abumrad NA, Grimaldi PA. 1995. Cloning of a protein that mediates transcriptional effects of fatty acids in preadipocytes. Homology to peroxisome proliferator-activated receptors. *J Biol Chem* 270:2367-71
277. Kersten S, Desvergne B, Wahli W. 2000. Roles of PPARs in health and disease. *Nature* 405:421-4
278. Willson TM, Brown PJ, Sternbach DD, Henke BR. 2000. The PPARs: from orphan receptors to drug discovery. *J Med Chem* 43:527-50
279. Storch J, McDermott L. 2009. Structural and functional analysis of fatty acid-binding proteins. *J Lipid Res* 50 Suppl:S126-31
280. Chmurzynska A. 2006. The multigene family of fatty acid-binding proteins (FABPs): function, structure and polymorphism. *J Appl Genet* 47:39-48
281. Ong DE, Newcomer, M.E., & Chytil, F. 1994. Cellular Retinoid-Binding Proteins. In *The Retinoids: Biology, Chemistry, and Medicine*, ed. MB Sporn, Roberts, A. B., Goodman, D. S.:288-317. New York: Raven Press. Number of 288-317 pp.
282. Storch J, Thumser AE. 2000. The fatty acid transport function of fatty acid-binding proteins. *Biochim Biophys Acta* 1486:28-44

283. Petrescu AD, Huang H, Martin GG, McIntosh AL, Storey SM, et al. 2013. Impact of L-FABP and glucose on polyunsaturated fatty acid induction of PPARalpha-regulated beta-oxidative enzymes. *American journal of physiology. Gastrointestinal and liver physiology* 304:G241-56
284. Petrescu AD, McIntosh AL, Storey SM, Huang H, Martin GG, et al. 2013. High glucose potentiates L-FABP mediated fibrate induction of PPARalpha in mouse hepatocytes. *Biochim Biophys Acta* 1831:1412-25
285. Hostetler HA, McIntosh AL, Atshaves BP, Storey SM, Payne HR, et al. 2009. L-FABP directly interacts with PPARalpha in cultured primary hepatocytes. *J Lipid Res* 50:1663-75
286. Ayers SD, Nedrow KL, Gillilan RE, Noy N. 2007. Continuous nucleocytoplasmic shuttling underlies transcriptional activation of PPARgamma by FABP4. *Biochemistry* 46:6744-52
287. Kaczocha M, Glaser ST, Deutsch DG. 2009. Identification of intracellular carriers for the endocannabinoid anandamide. *Proc Natl Acad Sci U S A* 106:6375-80
288. Kaczocha M, Vivieca S, Sun J, Glaser ST, Deutsch DG. 2012. Fatty acid-binding proteins transport N-acylethanolamines to nuclear receptors and are targets of endocannabinoid transport inhibitors. *J Biol Chem* 287:3415-24
289. Simpson MA, LiCata VJ, Ribarik Coe N, Bernlohr DA. 1999. Biochemical and biophysical analysis of the intracellular lipid binding proteins of adipocytes. *Mol Cell Biochem* 192:33-40
290. Hong J, Gu W, Zhang Y, Yan Q, Dai M, et al. 2011. Different association of circulating levels of adipocyte and epidermal fatty acid-binding proteins with metabolic syndrome and coronary atherosclerosis in Chinese adults. *Atherosclerosis* 217:194-200
291. Jeong CY, Hah YS, Cho BI, Lee SM, Joo YT, et al. 2012. Fatty acid-binding protein 5 promotes cell proliferation and invasion in human intrahepatic cholangiocarcinoma. *Oncol Rep* 28:1283-92
292. Cologna SM, Jiang XS, Backlund PS, Cluzeau CV, Dail MK, et al. 2012. Quantitative proteomic analysis of Niemann-Pick disease, type C1 cerebellum identifies protein biomarkers and provides pathological insight. *PLoS One* 7:e47845
293. Gillilan RE, Ayers SD, Noy N. 2007. Structural basis for activation of fatty acid-binding protein 4. *J Mol Biol* 372:1246-60
294. Bligh EG, Dyer WJ. 1959. A rapid method of total lipid extraction and purification. *Can J Biochem Physiol* 37:911-7
295. Otwinowski Z, Minor W. 1997. Processing of X-ray diffraction data collected in oscillation mode. *Methods Enzymol* 276:307-26
296. McCoy AJ, Grosse-Kunstleve RW, Adams PD, Winn MD, Storoni LC, Read RJ. 2007. Phaser crystallographic software. *J Appl Crystallogr* 40:658-74
297. Emsley P, Cowtan K. 2004. Coot: model-building tools for molecular graphics. *Acta Crystallogr D Biol Crystallogr* 60:2126-32
298. Adams PD, Afonine PV, Bunkoczi G, Chen VB, Davis IW, et al. 2010. PHENIX: a comprehensive Python-based system for macromolecular structure solution. *Acta Crystallogr D Biol Crystallogr* 66:213-21
299. Dolinsky TJ, Nielsen JE, McCammon JA, Baker NA. 2004. PDB2PQR: an automated pipeline for the setup of Poisson-Boltzmann electrostatics calculations. *Nucleic Acids Res* 32:W665-7
300. Baker NA, Sept D, Joseph S, Holst MJ, McCammon JA. 2001. Electrostatics of nanosystems: application to microtubules and the ribosome. *Proc Natl Acad Sci U S A* 98:10037-41

301. Dundas J, Ouyang Z, Tseng J, Binkowski A, Turpaz Y, Liang J. 2006. CASTp: computed atlas of surface topography of proteins with structural and topographical mapping of functionally annotated residues. *Nucleic Acids Res* 34:W116-8
302. Chen VB, Arendall WB, 3rd, Headd JJ, Keedy DA, Immormino RM, et al. 2010. MolProbity: all-atom structure validation for macromolecular crystallography. *Acta Crystallogr D Biol Crystallogr* 66:12-21
303. Kane CD, Bernlohr DA. 1996. A simple assay for intracellular lipid-binding proteins using displacement of 1-anilinonaphthalene 8-sulfonic acid. *Anal Biochem* 233:197-204
304. Chalmers MJ, Busby Sa, Pascal BD, He Y, Hendrickson CL, et al. 2006. Probing protein ligand interactions by automated hydrogen/deuterium exchange mass spectrometry. *Analytical chemistry* 78:1005-14
305. Pascal BD, Willis S, Lauer JL, Landgraf RR, West GM, et al. 2012. HDX workbench: software for the analysis of H/D exchange MS data. *Journal of the American Society for Mass Spectrometry* 23:1512-21
306. Hanhoff T, Lucke C, Spener F. 2002. Insights into binding of fatty acids by fatty acid binding proteins. *Mol Cell Biochem* 239:45-54
307. Xu Z, Bernlohr DA, Banaszak LJ. 1993. The adipocyte lipid-binding protein at 1.6-A resolution. Crystal structures of the apoprotein and with bound saturated and unsaturated fatty acids. *J Biol Chem* 268:7874-84
308. Richieri GV, Ogata RT, Kleinfeld AM. 1994. Equilibrium constants for the binding of fatty acids with fatty acid-binding proteins from adipocyte, intestine, heart, and liver measured with the fluorescent probe ADIFAB. *J Biol Chem* 269:23918-30
309. Richieri GV, Ogata RT, Zimmerman AW, Veerkamp JH, Kleinfeld AM. 2000. Fatty acid binding proteins from different tissues show distinct patterns of fatty acid interactions. *Biochemistry* 39:7197-204
310. Seibel NM, Eljouni J, Nalaskowski MM, Hampe W. 2007. Nuclear localization of enhanced green fluorescent protein homomultimers. *Anal Biochem* 368:95-9
311. McLane LM, Corbett AH. 2009. Nuclear localization signals and human disease. *IUBMB Life* 61:697-706
312. Kutay U, Guttinger S. 2005. Leucine-rich nuclear-export signals: born to be weak. *Trends Cell Biol* 15:121-4
313. Ockner RK, Manning JA, Poppenhausen RB, Ho WK. 1972. A binding protein for fatty acids in cytosol of intestinal mucosa, liver, myocardium, and other tissues. *Science* 177:56-8
314. Hertzel AV, Hellberg K, Reynolds JM, Kruse AC, Juhlmann BE, et al. 2009. Identification and characterization of a small molecule inhibitor of Fatty Acid binding proteins. *J Med Chem* 52:6024-31
315. Hostetler HA, Balanarasimha M, Huang H, Kelzer MS, Kaliappan A, et al. 2010. Glucose regulates fatty acid binding protein interaction with lipids and peroxisome proliferator-activated receptor alpha. *J Lipid Res* 51:3103-16
316. Velkov T. 2013. Interactions between Human Liver Fatty Acid Binding Protein and Peroxisome Proliferator Activated Receptor Selective Drugs. *PPAR Res* 2013:938401
317. Budhu AS, Noy N. 2002. Direct channeling of retinoic acid between cellular retinoic acid-binding protein II and retinoic acid receptor sensitizes mammary carcinoma cells to retinoic acid-induced growth arrest. *Mol Cell Biol* 22:2632-41
318. Sievers F, Wilm A, Dineen D, Gibson TJ, Karplus K, et al. 2011. Fast, scalable generation of high-quality protein multiple sequence alignments using Clustal Omega. *Molecular systems biology* 7:539
319. Greenfield S, Brostoff S, Eylar EH, Morell P. 1973. Protein composition of myelin of the peripheral nervous system. *Journal of neurochemistry* 20:1207-16

320. Berry DC, O'Byrne SM, Vreeland AC, Blaner WS, Noy N. 2012. Cross talk between signaling and vitamin A transport by the retinol-binding protein receptor STRA6. *Mol Cell Biol* 32:3164-75
321. Liu RZ, Li X, Godbout R. 2008. A novel fatty acid-binding protein (FABP) gene resulting from tandem gene duplication in mammals: transcription in rat retina and testis. *Genomics* 92:436-45
322. Angelucci F, Johnson KA, Baiocco P, Miele AE, Brunori M, et al. 2004. Schistosoma mansoni fatty acid binding protein: specificity and functional control as revealed by crystallographic structure. *Biochemistry* 43:13000-11
323. Shenefelt RE. 1972. Morphogenesis of malformations in hamsters caused by retinoic acid: relation to dose and stage at treatment. *Teratology* 5:103-18
324. Luo T, Wagner E, Drager UC. 2009. Integrating retinoic acid signaling with brain function. *Developmental psychology* 45:139-50
325. Evans TR, Kaye SB. 1999. Retinoids: present role and future potential. *British journal of cancer* 80:1-8
326. Cawley S, Bekiranov S, Ng HH, Kapranov P, Sekinger EA, et al. 2004. Unbiased mapping of transcription factor binding sites along human chromosomes 21 and 22 points to widespread regulation of noncoding RNAs. *Cell* 116:499-509
327. Allenby G, Bocquel MT, Saunders M, Kazmer S, Speck J, et al. 1993. Retinoic acid receptors and retinoid X receptors: interactions with endogenous retinoic acids. *Proc Natl Acad Sci U S A* 90:30-4
328. Sussman F, de Lera AR. 2005. Ligand recognition by RAR and RXR receptors: binding and selectivity. *J Med Chem* 48:6212-9
329. Berry DC, Noy N. 2007. Is PPARbeta/delta a Retinoid Receptor? *PPAR Res* 2007:73256
330. Wang D, Wang H, Guo Y, Ning W, Katkuri S, et al. 2006. Crosstalk between peroxisome proliferator-activated receptor delta and VEGF stimulates cancer progression. *Proc Natl Acad Sci U S A* 103:19069-74
331. Tan NS, Michalik L, Desvergne B, Wahli W. 2004. Peroxisome proliferator-activated receptor-beta as a target for wound healing drugs. *Expert opinion on therapeutic targets* 8:39-48
332. Velkov T, Lim ML, Capuano B, Prankerd R. 2008. A protocol for the combined sub-fractionation and delipidation of lipid binding proteins using hydrophobic interaction chromatography. *Journal of chromatography. B, Analytical technologies in the biomedical and life sciences* 867:238-46
333. Glatz JF, Veerkamp JH. 1983. Removal of fatty acids from serum albumin by Lipidex 1000 chromatography. *Journal of biochemical and biophysical methods* 8:57-61
334. Szuts EZ, Harosi FI. 1991. Solubility of retinoids in water. *Archives of biochemistry and biophysics* 287:297-304
335. Martindale W. 1993. *The extra pharmacopoeia*. pp 770. London: Pharmaceutical Press. 2363 pp.
336. Siegenthaler G, Hotz R, Chatellard-Gruaz D, Didierjean L, Hellman U, Saurat JH. 1994. Purification and characterization of the human epidermal fatty acid-binding protein: localization during epidermal cell differentiation in vivo and in vitro. *Biochem J* 302 (Pt 2):363-71
337. Robeson CD, Cawley JD, Weisler L, Stern MH, Eddinger CC, Chechak AJ. 1955. Chemistry of vitamin A. XXIV. The synthesis of geometric isomers of vitamin A via methyl β-methylglutaconate. *J. Am. Chem. Soc.* 77:4111-9
338. Harreman MT, Cohen PE, Hodel MR, Truscott GJ, Corbett AH, Hodel AE. 2003. Characterization of the auto-inhibitory sequence within the N-terminal domain of importin alpha. *J Biol Chem* 278:21361-9

339. Dias SM, Wilson KF, Rojas KS, Ambrosio AL, Cerione RA. 2009. The molecular basis for the regulation of the cap-binding complex by the importins. *Nature structural & molecular biology* 16:930-7
340. Kohler M, Speck C, Christiansen M, Bischoff FR, Prehn S, et al. 1999. Evidence for distinct substrate specificities of importin alpha family members in nuclear protein import. *Mol Cell Biol* 19:7782-91
341. Wang YX, Lee CH, Tiep S, Yu RT, Ham J, et al. 2003. Peroxisome-proliferator-activated receptor delta activates fat metabolism to prevent obesity. *Cell* 113:159-70
342. Kleiner S, Nguyen-Tran V, Bare O, Huang X, Spiegelman B, Wu Z. 2009. PPAR{delta} agonism activates fatty acid oxidation via PGC-1{alpha} but does not increase mitochondrial gene expression and function. *J Biol Chem* 284:18624-33
343. Fyffe SA, Alphey MS, Buetow L, Smith TK, Ferguson MA, et al. 2006. Recombinant human PPAR-beta/delta ligand-binding domain is locked in an activated conformation by endogenous fatty acids. *J Mol Biol* 356:1005-13
344. Fyffe SA, Alphey MS, Buetow L, Smith TK, Ferguson MA, et al. 2006. Reevaluation of the PPAR-beta/delta ligand binding domain model reveals why it exhibits the activated form. *Mol Cell* 21:1-2
345. Shim E, Yeum KJ, Tang G, Ahn SH, Hwang J, Lee-Kim YC. 2012. Retinoids, carotenoids, and tocopherols in breast adipose tissue and serum of benign breast disease and breast cancer patients. *Nutrition and cancer* 64:956-63
346. Ali R, Campos B, Dyckhoff G, Haefeli WE, Herold-Mende C, Burhenne J. 2012. Quantification of retinoid concentrations in human serum and brain tumor tissues. *Analytica chimica acta* 725:57-66
347. Wolfrum C, Borrmann CM, Borchers T, Spener F. 2001. Fatty acids and hypolipidemic drugs regulate peroxisome proliferator-activated receptors alpha - and gamma-mediated gene expression via liver fatty acid binding protein: a signaling path to the nucleus. *Proc Natl Acad Sci U S A* 98:2323-8
348. Berry DC, Noy N. 2009. All-trans-retinoic acid represses obesity and insulin resistance by activating both peroxisome proliferation-activated receptor beta/delta and retinoic acid receptor. *Mol Cell Biol* 29:3286-96
349. Yu S, Levi L, Siegel R, Noy N. 2012. Retinoic acid induces neurogenesis by activating both retinoic acid receptors (RARs) and peroxisome proliferator-activated receptor beta/delta (PPARbeta/delta). *J Biol Chem* 287:42195-205
350. Rieck M, Meissner W, Ries S, Muller-Brusselbach S, Muller R. 2008. Ligand-mediated regulation of peroxisome proliferator-activated receptor (PPAR) beta/delta: a comparative analysis of PPAR-selective agonists and all-trans retinoic acid. *Molecular pharmacology* 74:1269-77
351. Sanson B, Wang T, Sun J, Wang L, Kaczocha M, et al. 2014. Crystallographic study of FABP5 as an intracellular endocannabinoid transporter. *Acta Crystallogr D Biol Crystallogr* 70:290-8
352. Thatcher JE, Isoherranen N. 2009. The role of CYP26 enzymes in retinoic acid clearance. *Expert opinion on drug metabolism & toxicology* 5:875-86